

**EXCITATORY-INHIBITORY INTERACTIONS
AS THE BASIS OF WORKING MEMORY**

DISSERTATION

Presented in Partial Fulfillment of the Requirements for the Degree Doctor of
Philosophy in the Graduate School of the Ohio State University

By

Robert A. McDougal, MS
Graduate Program in Mathematics

The Ohio State University

2011

Dissertation Committee:

David H. Terman, Advisor

Edward Overman II

Joseph B. Travers

Christopher P. Fall

© Copyright by
Robert A. McDougal
2011

ABSTRACT

The working memory system provides the short-term storage facility necessary to perform complex cognitive tasks. The prefrontal cortex (PFC) plays a key role; neurons in the PFC respond to stimuli and continue to maintain elevated persistent activity after the stimulus is removed. Working memory degradation is a common symptom in neurological disease.

I propose that working memory performance is driven by interactions of excitatory and inhibitory neurons and modulated by calcium dynamics. In contrast to previous models that require a carefully constructed or adapting network architecture, this model retains novel stimuli using a fixed network of neurons connected with probabilities only depending on the cell type. Persistent activity is irregular, with the coefficient of variation of the interspike intervals exceeding 0.5. Patterns are robustly maintained even in the presence of distracting stimuli, yet the network switches to new, strongly presented “urgent” patterns. The field potential of the excitatory cells exhibits a gamma rhythm. Statistical properties of the network and the role of key parameters are considered.

I consider the role of subcellular calcium and how the chemical dynamics are affected by electrical activity and dendritic geometry. The role of chemical and electrical feedback is examined, and I conclude with a description of the novel features of a custom simulation tool I wrote to perform this study.

ACKNOWLEDGMENTS

As the saying goes, “we are the sum of all the people we ever met.” Chance, initially inconsequential-seeming interactions have shaped my life and my work in profound ways. My thanks go to all the people who have played a role in my journey. In particular, I wish to thank: My parents, for instilling in me the belief in the value of an education. Sandra Stamer, Karen Melhunek, and Dr. Arthur Pittenger, for introducing me to the study of mathematics. My advisor, for his patience and guidance. Dr. Casey O. Diekman and Kyle Lyman, for valuable feedback on early versions of my simulator, `snet`. The Ohio Supercomputing Center for a grant of processor time. Finally, the math department, for making this possible.

VITA

2004	B.S. in Mathematics, University of Maryland, Baltimore County
2004 - Present	Graduate Associate, The Ohio State University
2006	M.S. in Mathematics, The Ohio State University

FIELDS OF STUDY

Major Field: Mathematics

Specialization: Mathematical Neuroscience

TABLE OF CONTENTS

Abstract	ii
Acknowledgments	iii
Vita	iv
List of Figures	ix
List of Tables	xii
List of Abbreviations	xiii

CHAPTER	PAGE
1 Introduction	1
2 Background	5
2.1 Neural Biology	5
2.1.1 Action Potentials	6
2.1.2 Synapses	10
2.1.3 Irregularity	11
2.1.4 Calcium Waves	12
2.2 Neural Modeling	13
2.2.1 Differential Equations	14
2.2.2 Types of Neuron Models	17
2.2.3 Hodgkin-Huxley Model	17
2.2.4 Simplifications	18
2.2.5 Synapses	22
2.2.6 Calcium Waves	23
2.3 Working Memory	24
2.3.1 Biology	27
2.3.2 Modeling	29
3 Model	32
3.1 Overview	32

3.2	Excitatory Cells	34
3.3	Inhibitory Cells	36
3.4	The Rest of the Brain	37
4	Results	39
4.1	Basic Results	39
4.2	Network Size Independence	44
4.3	Pattern Independence	45
4.4	Robust to Heterogeneities	47
4.5	Dopamine and Performance	47
5	Analysis	51
5.1	Simplified Single Cell Model	51
5.1.1	Excitation	53
5.1.2	Sag Current	55
5.2	Noisy Inputs	57
5.2.1	Calculation of Average Noise Input	60
5.2.2	Numerical Comparison	61
5.3	Small Networks	63
5.3.1	Two Cell Network	63
5.3.2	Three Cell Networks	65
5.4	Calcium and State Discrimination	67
5.5	Excitatory-Inhibitory Interactions	72
5.5.1	Firing Rate	73
5.5.2	Connection Probabilities in Networks	75
5.5.3	Rebound	77
5.6	Rhythmicity and Irregularity	77
6	Calcium Waves	82
6.1	Active Dendrites and Calcium Wave Initiation	82
6.2	Role of Geometry	86
6.2.1	Straight and Curved Dendrites	89
6.2.2	Abrupt Opening	90
6.2.3	Gradual Widening	95
6.2.4	Branch Points	97
6.3	Future Directions	99
7	Interaction with Other Brain Systems	100
7.1	Dopamine	100
7.2	Electrical Modulation	103

8	Simulating the Model	106
	8.1 Overview of Standard Tools	107
	8.2 Snnet	108
	8.2.1 Dynamics Specification	109
	8.2.2 Protocol Specification	110
	8.2.3 Integrator Independence	112
	8.2.4 Data Storage	112
	8.2.5 Data Analysis	112
	Bibliography	114

CHAPTER		PAGE
A	Model Equations	131
	A.1 Hodgkin-Huxley Cells	131
	A.1.1 State Variables	131
	A.1.2 Currents	132
	A.1.3 Miscellaneous Equations	132
	A.2 Simplified Model	133
	A.2.1 State Variables	133
	A.2.2 Currents	133
	A.2.3 Miscellaneous Equations	134
	A.3 Excitatory Cells	134
	A.3.1 State Variables	134
	A.3.2 Currents	135
	A.3.3 Miscellaneous Equations	135
	A.4 Inhibitory Cells	136
	A.4.1 State Variables	136
	A.4.2 Currents	137
	A.4.3 Miscellaneous Equations	137
	A.5 Calcium Waves	137
	A.5.1 State Variables	139
	A.5.2 Fluxes	139
	A.5.3 Miscellaneous Equations	139
	A.6 Noise	140
B	Parameter Selection	141
	B.1 Excitatory Cells	141
	B.2 Inhibitory Cells	143
C	On Interpreting Neuron Morphology	147

D	Derivation of the Reaction-Diffusion Equation	150
---	---	-----

LIST OF FIGURES

FIGURE		PAGE
2.1	Reconstructed CA1 pyramidal neuron morphology.	8
2.2	Schematic diagram of a neuron, showing dendrites, axon, synapses, and the ER.	9
2.3	Action potentials in the Hodgkin-Huxley model triggered by excitation and by post-inhibitory rebound.	19
2.4	Sodium inactivation and potassium activation probabilities obey a nearly linear relationship in the Hodgkin-Huxley model.	20
2.5	Comparison of action potentials under Hodgkin-Huxley model and under the simplified model.	21
2.6	Behaviors of the ER-calcium point model.	25
2.7	Cytosolic calcium limit behavior as a function of the combined effects of InsP_3 concentration and maximum InsP_3 receptor conductance.	26
3.1	Schematic diagram of a two-population model for working memory.	33
4.1	Multiphase simulation of the full network.	40
4.2	Sample calcium time course.	41
4.3	Irregular firing in the full network.	42
4.4	The local field potential exhibits a gamma rhythm during persistent activity.	43
4.5	The ability to maintain persistent activity is preserved across multiple network sizes.	45
4.6	Pattern retention is largely independent of size or pattern choice.	46
4.7	Heterogeneities in synaptic conductances are well-tolerated.	48

4.8	Inverted-U-shaped dopamine-performance curve.	49
5.1	Phase plane for the simplified single cell model.	52
5.2	The effect of raising I_{app} on the phase plane.	54
5.3	Elevated I_{app} leads to periodic firing.	56
5.4	The role of the sag current.	58
5.5	Calcium dependence of θ_h	59
5.6	High values of θ_h lead to periodic firing.	59
5.7	Comparison of noise synapse with modeled excitatory synapse.	60
5.8	Behavior in the absence of external excitatory noise.	62
5.9	Example small network architectures.	63
5.10	Two cell network performance during persistence.	64
5.11	Three cell network traces.	66
5.12	Example calcium time courses for cells in the baseline state and the persistent state.	67
5.13	Excitatory cell response to 50 mA, 0.2 ms square-wave pulse and 70 mA, 0.2 ms square-wave pulse.	68
5.14	Average cytosolic calcium concentration in an excitatory cell in arbitrary units as a function of firing rate and calcium decay, k_{Ca}	70
5.15	Probability of activation as a function of initial calcium concentration.	71
5.16	Switching effectiveness as a function of signal duration.	72
5.17	Firing rates and duration of persistent activity are functions of inhibitory input.	74
5.18	Network statistics as functions of connectivity.	76
5.19	Spike-triggered averages reveal the role of inhibition coincidence in triggering activity.	78
5.20	Network performance in a noiseless simulation, as a function of I_{app}	79
5.21	Scatter plots of performance metrics, showing least squares solution and r^2 values.	81

6.1	Dendrite cutting, showing its location on the CA1 pyramidal neuron of Poirazi et al.	84
6.2	High firing rates lead to elevated internal calcium concentrations. . .	85
6.3	Electrical activity facilitates calcium wave initiation.	87
6.4	Two dimensional dendritic-like geometries.	88
6.5	A close inspection of a stalled bistable wave reveals the nature of the stationary solution.	91
6.6	Minimum source width to propagate into half-plane.	93
6.7	Threshold source radii in the gradually widening geometry.	96
6.8	Propagation across orthogonal branches.	98
6.9	Branch angle affects wave propagation.	99
7.1	Dopamine modulation of synaptic transmission improves working memory performance.	102
7.2	Comparison of dopamine models.	103
7.3	External modulation can selectively deactivate excitatory cells. . . .	104
B.1	Example excitatory cell parameter search results, showing baseline, persistence, and distractor.	144
B.2	Example inhibitory cell parameter search results, showing baseline and persistence.	146
C.1	Frustum description of dendrite geometry creates gaps and overlaps. .	147
C.2	Cross-section of a capped frustum, showing axis and original frustum edges.	148
C.3	Portion of a neuron rendered using capped frustums.	149

LIST OF TABLES

TABLE		PAGE
A.1	Parameters for the Hodgkin-Huxley model.	132
A.2	Parameters for the simplified model, unless otherwise indicated. . . .	133
A.3	Standard parameters for the excitatory cell model.	135
A.4	Standard parameters for the inhibitory cell model.	138
A.5	Parameters for the calcium model, unless otherwise indicated.	138
A.6	Parameters for noise, except where otherwise noted.	140

LIST OF ABBREVIATIONS

AHP	After hyperpolarization current
AIS	Axon initial segment
AMPA	2-amino-3-(5-methyl-3-oxo-1,2-oxazol-4-yl)propanoic acid
BPAP	Back propagating action potential
Ca ²⁺	Calcium
CA1	Cornu Ammonis area 1
Cl ⁻	Chloride
CV	Coefficient of variation
DNA	Deoxyribonucleic acid
ER	Endoplasmic reticulum
GABA	γ -aminobutyric acid
Hz	Hertz
InsP ₃	Inositol-1, 4, 5-triphosphate
ISI	Interspike interval
K	Potassium

mGluR5	Metabotropic glutamate receptor 5
mV	Millivolts
Na	Sodium
NMDA	N-Methyl-D-aspartic acid
ODE	Ordinary differential equation
PDE	Partial differential equation
PFC	Prefrontal cortex
SERCA	Sarco/endoplasmic reticulum Ca^{2+} -ATPase
SNIC	Saddle-node bifurcation on invariant circle

CHAPTER 1

INTRODUCTION

The working memory system endows the brain with the ability to temporarily store and manipulate information needed for the performance of complex cognitive tasks [Baddeley 94]. It has been suggested that the pattern of activity in this system indicates a choice of what neural pathways should be active [Miller 01]. This mechanism is impaired in numerous neurological diseases, including Alzheimer's disease [Baddeley 91, Kensinger 03], multiple sclerosis [D'Esposito 96, Grigsby 94, Pelosi 97], Parkinson's disease [Gabrieli 96, Kensinger 03, Owen 97], and schizophrenia [Driesen 08, Silver 03, Tanaka 06].

A functioning working memory system must be able to remember novel stimuli. It should be robust to distractors – that is, presentation of a second stimulus should not necessarily disrupt the original memory – but it should be flexible and able to switch to remembering a new pattern when necessary [Miller 01].

The prefrontal cortex (PFC) appears to contain the seat of the working memory system [Curtis 03, Fuster 73, Jonides 93, Lewinsohn 72, Petrides 95], although other brain regions have also been implicated in the performance of working memory tasks [Constantinidis 96, Miller 96, Quintana 99]. The PFC is highly connected [Fuster 08, Miller 01] and responds to both sensory and cortical input. When a cue stimulus of whatever modality is presented to initiate a working memory task, neurons within the PFC respond with elevated activity that persists after the stimulus is

removed [Funahashi 94]. The activity is presumably a consequence of the interaction of pyramidal cells and inhibitory interneurons, two dominant classes of neurons in the PFC [Gabbott 05, Mountcastle 69, Wilson 94], and it is believed that this activity encodes a memory [Curtis 03, Goldman-Rakic 95]. Several mathematical models have been proposed to explain this persistent activity, although they are typically driven by one of two phenomenon: recurrent excitation or intrinsic cellular bistability.

In the recurrent excitation based models, pyramidal cells coding for a particular pattern are connected together via excitatory synapses formed by a Hebb-like learning rule [Hebb 49], commonly summarized as “neurons that fire together wire together” [Buzsák 98, Keysers 04, Lakoff 08]. Some models are able to retain novel patterns by using an attractor network that dynamically adjusts synaptic connectivity during a working memory task [Amit 97, Hopfield 82], but it is not clear that synaptic rewiring works on a sufficiently fast timescale [Durstewitz 00, Zucker 02]. A careful balance of inhibitory input is required to prevent runaway excitation while still permitting a low level of background activity [Barbieri 08].

In the models driven by cellular bistability, pyramidal cells fire at a low rate in the off state and at a high rate in the on state. This firing rate bistability has been experimentally demonstrated in isolated neurons [Egorov 02]. Many of these models [Fall 05, Guigon 95] incorporate special network architecture, such as so-called “Mexican-hat” connectivity where nearby neurons are coupled with excitatory connections and far-away neurons are coupled with inhibitory connections. This architecture helps the models to be robust to distractors and noise and is a common modeling assumption [Camperi 98, Oster 06, Somers 95]. It requires that active cells be physically located near each other, so these models are typically presented as encoding spatial location.

I present a new type of working memory model: a Hodgkin-Huxley-type

[Hodgkin 52] channel-based model driven by excitatory-inhibitory interactions modulated by calcium dynamics. Like the cellular bistable models, the neuron's state – represented here by its cytosolic calcium concentration – modulates its activity. Like the attractor networks, my model is able to retain novel patterns, but it does so without requiring modifications to the network architecture.

Persistent activity in the model's pyramidal cells is driven by inhibitory input. A calcium-modulated sag current [Hagiwara 89, Lirk 08, Pan 03, Schwindt 92] – that is, a depolarizing current that is activated in response to inhibition – controls the response of the excitatory cells to inhibitory input. Cells with high calcium respond to inhibition by becoming more likely to fire an action potential; cells with low calcium respond by becoming less likely to fire. Each action potential admits calcium, thereby making subsequent action potentials more likely. Since inhibition increases with network activity, distracting patterns of the same strength as the initial cue are unable to trigger persistent activity. Strongly presented distractors trigger extra inhibition, which shuts down the original pattern, and allows the new pattern to activate.

I consider the implications of this model on both the single cell and network level. The model is robust; it maintains persistent activity corresponding to a randomly chosen cue pattern for a wide range of connectivity patterns. It exhibits a gamma rhythm – a strong signal in the 30 - 80 Hz range – during persistent activity, which is observed experimentally during working memory tasks [Pesaran 00, Tallon-Baudry 98] and known to be disrupted in schizophrenia [Spencer 03]. Dopamine modulation of GABA_A conductances is considered and shown to lead to an inverted U-shaped performance curve, consistent with [Vijayraghavan 07, Zahrt 97]. I present evidence that dendritic geometry may affect intracellular calcium dynamics and thereby working memory. Finally, I consider the role of feedback from the rest of the brain.

Since calcium plays a key role in this model, I consider a more detailed spatially extended model of intracellular dynamics based on an extension to the classic model of Li and Rinzel [Li 94] by Wagner et al [Wagner 04]. I consider the role of back-propagating action potentials (BPAPs) in triggering calcium waves, and then I use a scalar bistable equation to consider the effects of dendritic geometry on wave propagation.

To facilitate this study of random networks of heterogeneous neurons, I developed a custom software package called `snnet`. Except where otherwise noted, all simulations were specified using the `snnet` framework, which then automatically integrated them in XPPAUT [Ermentrout 02] using the “qualrk” method, an adaptive Runge-Kutta integrator.

CHAPTER 2

BACKGROUND

The human brain serves as the seat of consciousness and is responsible for processing sensory input and regulating behavior. Disorders of the brain, like schizophrenia or Parkinson's disease, can substantially affect quality of life. Since the brain plays such a key role, researchers from a wide range of fields – including but by no means limited to biology, computer science, mathematics, medicine, and psychology – study it to understand how it works and what causes it to fail.

2.1 Neural Biology

Structurally, as with all other organs, the brain is composed of a collection of cells. A cell consists of a distinct finite volume enclosed by a plasma membrane. The specific volume may change over time, but as long as the cell is alive, it will always be bounded by a membrane. Diffusion across the membrane is restricted, allowing the inside of the cell to be chemically distinct from the outside of the cell. This distinction applies not just to large organic molecules like DNA but also to charged ions like sodium (Na^+), potassium (K^+), calcium (Ca^{2+}), and chloride (Cl^-). These local variations play a key role in brain function.

Approximately 86.1 ± 8.1 billion of the cells of a human brain are classified as neurons, described below; the remaining 84.6 ± 9.8 billion cells are primarily glial

cells [Azevedo 09]. Originally viewed as structural elements, glia are now recognized as having an active role in modulating neuronal activity; see [Araque 99] for a review. Nonetheless, the following focuses solely on the role of neurons. Most of the material in this section can be found in any standard introductory neuroscience text, such as [Kandel 00].

2.1.1 Action Potentials

At the simplest level, a neuron is an electrically excitable cell. When presented with sufficient electrical input, neurons respond with an action potential, a short term electrical spike. This spike manifests itself as a change in the electrical potential across the plasma membrane caused by a change in ionic concentrations inside and outside the neuron. Since matter is neither created nor destroyed, these changes occur because ions are selectively permitted to pass through openings or channels in the membrane.

At rest, a neuron contains a higher concentration of potassium and a lower concentration of sodium and calcium than the extracellular medium. When an action potential is initiated, the activation gate on certain sodium channels opens, allowing sodium to enter the cell. Sodium enters rather than leaves because of both the concentration gradient (around 440 mM in the extracellular space vs only 50 mM in the cytosol for the squid giant axon [Kandel 00]) and because of the potential gradient. As the membrane potential rises, the potential gradient reverses, but sodium ions continue to enter until the two forces cancel each other out at a membrane potential of around 55 mV [Kandel 00].

As the membrane potential rises, the probability of sodium channel inactivation gates closing increases, thus stopping the flow of sodium ions. Simultaneously, the

probability of potassium channels being open increases with the membrane potential, leading to potassium flow out of the neuron thereby lowering its membrane potential.

The net effect is that sodium channels activate when the membrane potential is sufficiently elevated, thereby raising the membrane potential, causing the sodium channels to inactivate and potassium channels to activate, ultimately restoring the potential to its original value. A sodium-potassium exchanger restores the chemical concentrations [Skou 65, Dahl 74], however the actual number of ions moved is small relative to the total and is typically ignored in modeling studies.

Once the membrane potential is lowered, the sodium inactivation gate opens and the potassium activation gate slows, resetting the neuron to its initial state. This resetting process takes time, and until it is mostly complete, the neuron is in a refractory state where it will typically not respond to external stimuli.

Depending on the type of neuron, other channels may be present as well. Hippocampal interneurons and pyramidal neurons both have voltage gated calcium channels [Rozsa 04, Takahashi 89]. Unlike sodium and potassium, which are maintained at concentrations of around 50 and 400 mM, respectively, cytosolic calcium is maintained at a concentration of around 0.3 μM [Lodish 00]. This baseline is low enough that the activation of voltage gated calcium channels makes a measurable difference in cytosolic calcium concentration [Miyakawa 92]. Both hippocampal interneurons and pyramidal neurons have calcium-activated potassium channels [Aoki 00, Lancaster 86, Wilson 06] that respond to these fluctuations. Pyramidal neurons also have sag currents [Magee 98], which are currents that activate when the membrane potential is below its rest state and act to raise it. In some cell types, sag currents are known to be modulated by calcium [Hagiwara 89], and it has been proposed that this modulation also occurs in pyramidal cells [Winograd 08].

Ion channels are not uniformly distributed across a neuron's membrane. Neurons



Figure 2.1: Reconstructed CA1 pyramidal neuron morphology. Data from ModelDB entry for [Poirazi 03]. Custom renderer.

have a complicated geometry, as illustrated in Figure 2.1, but can be divided into three major functionally-distinct components: an axon, dendrites, and a soma. Each of these parts contain other structures; a schematic is given in Figure 2.2. The soma is the large cell body; the axon and the dendrites are connected to it. Dendrites primarily receive input. The sodium and potassium dynamics described above primarily occur along the axon, however in some cells – including pyramidal cells – the dendrites also contain voltage gated ion channels and are thus capable of supporting back-propagating action potentials [Johnston 96].

Even along the axon, variations exist. Membrane potential and channel activation

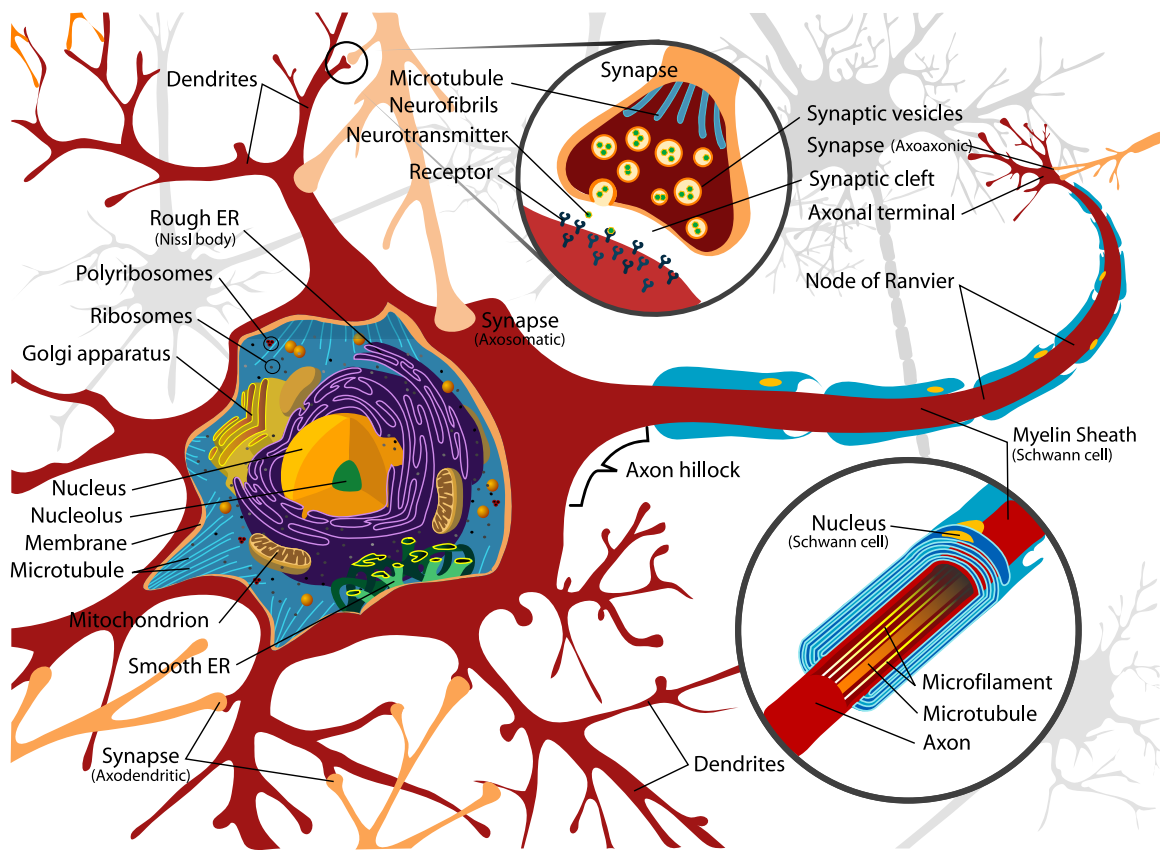


Figure 2.2: Schematic diagram of a neuron, showing dendrites, axon, synapses, and the ER. Image from the public domain, downloaded from commons.wikimedia.org/wiki/File:Complete_neuron_cell_diagram_en.svg.

are local phenomena. Action potentials typically originate on the axon initial segment (AIS), a region of axon with high sodium channel concentration and therefore more susceptible to having sufficient sodium flow to trigger an action potential [Kole 08].

As the local membrane potential rises, electrical charge diffuses to neighboring regions of the axon. Regions further out on the axon respond to the elevated potential by activating their sodium channels, thereby raising their local potential, thus propagating the wave. Regions closer to the soma will not have fully reset and thus do not respond to this charge diffusion. Note that propagation along an axon takes time and thereby introduces a delay.

2.1.2 Synapses

Neurons signal their activity to other neurons at synapses, specialized regions where the axon of the transmitting, or presynaptic, cell has grown close to a receiving, or postsynaptic, neuron. Many synapses are from axons to dendrites, although some, especially inhibitory, are from axons to the soma [Delaney 01]. Synapses whose activation leads to an increase in the post-synaptic cell's membrane potential are called excitatory, while those whose activation decreases the post-synaptic cell's membrane potential are called inhibitory.

Each synapse contains a number of synaptic vesicles laden with neurotransmitters, like glutamate (used in some excitatory synapses) and γ -aminobutyric acid (GABA) (used in some inhibitory synapses). When an action potential in the presynaptic cell reaches a synapse, it triggers release of neurotransmitters into the synaptic cleft, the small gap between the cells. The neurotransmitters bind with receptors on the postsynaptic cell.

In some receptors, known as ionotropic receptors, this binding directly causes ion channels to open, creating a postsynaptic potential, a variation in the membrane

potential. The postsynaptic potentials diffuse throughout the postsynaptic cell, combining in a nonlinear way, ultimately leading to changes in the membrane potential near the axon initial segment, potentially triggering an action potential.

Other receptors, known as metabotropic receptors, respond to bound neurotransmitter by initiating an intracellular chemical cascade. This is a slower process than opening ion channels and typically leads to longer lasting changes in neuron behavior.

The density of receptors governs the strength of the postsynaptic potential and therefore the likelihood that the post-synaptic cell will fire an action potential. This density is not fixed; in some synapses it can change with a time constant of 100 ms [Zucker 02]. Over time, neurons may form new connections or destroy old synapses.

2.1.3 Irregularity

Biological neurons fire neither regularly nor synchronously. As Stevens and Zador put it, “cortical neurons in the waking brain fire highly irregular spike trains that have more in common with the ticking of a Geiger counter than of a clock” [Stevens 98].

This irregularity has important theoretical and medical implications. Information theory [Rieke 99, Shannon 48] defines a concept of signal entropy. In essence, irregular desynchronized signals can encode more information. A neuron that always either fires regularly at 3 Hz or regularly at 15 Hz only encodes one bit of information: whether or not it is firing at the high rate. If 30 additional neurons always fire synchronously with that initial neuron, their output provides no additional information; the full state of the system could be determined by observing the first neuron. Medically, excessive synchrony of neurons is associated with diseases of the brain, like Parkinson’s [Goldberg 02, Hurtado 99, Levy 00, Raz 96].

The coefficient of variation (CV) of the interspike intervals – the ratio of the standard deviation to the mean – is one measure of the irregularity of a network.

If the firing times were distributed according to a Poisson process, the interspike intervals would have an exponential distribution, which has a coefficient of variation of 1, which is approximately the observed rate in the prefrontal cortex [Compte 03].

2.1.4 Calcium Waves

Metabotropic glutamate (mGlu) receptors – metabotropic receptors that respond to glutamate – are especially relevant to the current study, because the activation of certain types of mGlu receptors is associated with changes in internal calcium concentration. Fall et al proposed that this process plays a role in cellular bistability in the working memory system [Fall 06].

Like membrane potential and neurotransmitters, elevated calcium can open certain classes of ion channels on the cell membrane. In addition, calcium serves as a second messenger signal in most types of cells, with roles from the moment of fertilization [Busa 85] to regulating gene expression [West 01] to cell death by apoptosis [Orrenius 03]. As such, a typical cell possesses a number of means to regulate its cytosolic calcium concentration, including buffers [Stern 92] and sequestering by the mitochondria [Gunter 04] or endoplasmic reticulum (ER) [Pozzo-Miller 97]. These control mechanisms are present and used in neurons as well [Berridge 98], with the addition that in neurons, sequestering may be modulated by activity [Pozzo-Miller 97].

The activation of certain mGlu receptors initiates a sequence of events wherein phospholipase C cleaves $\text{PtdIns}(4, 5)\text{P}_2$, a phospholipid embedded in the plasma membrane, into InsP_3 and diacylglycerol. The InsP_3 then diffuses into the cytosol, the fluid in the cell interior. Some of the InsP_3 binds to receptors on the ER that trigger it to release some of its calcium store into the cytosol. This calcium then diffuses through the cytosol.

The same receptor on the ER that triggered the calcium release is also activated

by calcium. Thus as the calcium diffuses through the dendrite, it may bind to other receptors, triggering further local elevations in calcium concentration. This process can lead to a region of elevated calcium concentration spreading throughout a portion of the dendritic tree [Jaffe 94, Ross 05].

The receptor actually contains a second calcium binding site, where the binding and unbinding happens at a slower rate. When calcium is bound to this site, the corresponding ion channel on the ER membrane closes. SERCA pumps then extract calcium from the cytosol, resequestering it in the ER.

2.2 Neural Modeling

Confronted with a permanent state of having imperfect knowledge, as a species, we cope by abstracting literally everything we encounter. No two pieces of paper are truly identical; they will be composed of different numbers of atoms, and yet we routinely think of an abstract concept – a mental model – that we call a piece of paper. This mental model lets us predict the behavior of a specific piece of paper to a large degree of accuracy, but it is, out of necessity, an incomplete representation of reality. As George E. P. Box explained, “models, of course, are never true, but fortunately it is only necessary that they be useful” [Box 79].

Experimental biologists sometimes work with animal models for human systems. For example, a rat may be altered in such a way that it exhibits symptoms of schizophrenia [Häfner 91, Sams-Dodd 96]. The altered rats then serve as an animal model for the disease and can be studied to understand possible causes and treatments.

More abstractly, models need not have a physical manifestation. A purely abstract model is a set of (possibly probabilistic) rules governing the approximate behavior

of the system. These models may then be studied using mathematics, which can be viewed as the logical study of the implications of an arbitrary rule set.

In principle, depending on the problem, the rules for mathematical models may be expressed in the language of any branch of mathematics. Polynomials over finite fields have been used to study gene regulatory networks [Laubenbacher 04]. Cellular automata are a common tool in modeling biological systems [Ermentrout 93]. This study uses differential equation based models, another common technique.

2.2.1 Differential Equations

The field of differential equations is the branch of mathematics that studies how states change, be it over time, space, or both. All of the differential equations in this study can be written in one of two forms:

$$\frac{du}{dt} = f(\dots) \tag{2.2.1}$$

or

$$\frac{\partial u}{\partial t} = D \Delta u + f(\dots), \tag{2.2.2}$$

where D is a constant or constant diagonal matrix and $f(\dots)$ is some function of time and the modeled state variables, the vector u .

Equation (2.2.1) is a type of ordinary differential equation. By definition, $\frac{du}{dt}$ is the instantaneous rate of change of the state variable u as time t changes. Instantaneous here is in the sense that while a car may average a certain velocity over a trip, at every point in time, it is traveling at a specific instantaneous velocity estimated and displayed on the speedometer. Thus (2.2.1) states that the state variable changes at a rate described by the function f .

Equation (2.2.2) is a reaction-diffusion equation. Analogously to the above, $\frac{\partial u}{\partial t}$ is the instantaneous rate of change of u over time t , however here u is distributed

throughout space and has different values at different locations. The function f is the reaction term; it describes the contributions of local dynamics to the variable's change. The term $D \Delta u$ is the diffusion term, where Δ is the Laplacian operator. The proof that this term corresponds to the contribution from diffusion is given in Appendix D, but for now note that D is proportional to the rate of diffusion.

For example, the calcium waves of Section 2.1.4 will be modeled using reaction-diffusion equations, because cytosolic calcium changes over time, is at different concentrations at different locations, diffuses throughout space, but also has local dynamics where SERCA pumps and InsP_3 receptors respond to the local chemical concentrations.

Numerically Solving Differential Equations

While techniques exist for analytically solving certain differential equations, there is no general technique. Furthermore, there cannot be a general technique because many differential equations do not have a solution that can be expressed in terms of elementary functions. Even in equations that cannot be solved exactly, there are often analytic or geometric techniques for extracting some information about the dynamics from the equations; see [Strogatz 94] for an introduction.

While explicit analytic solutions often cannot be found, it is still possible to compute solutions to (2.2.1) and (2.2.2) numerically. Here I present a simple technique known as Euler's method for approximating solutions of the form (2.2.1), introduced in many introductory differential equations texts (e.g. [Boyce 92, Nagle 00]). The Crank-Nicolson method [Crank 47] is a related but more complicated technique suitable for numerically solving the reaction-diffusion equation (2.2.2).

Suppose the value of the state variables is known at time t_0 . Pick additional times t_i , $i = 1, 2, \dots$, with $t_{i-1} < t_i$. The state variables will be estimated at these times.

The method produces the least error if the difference between consecutive time points, known as the time step, is small.

The primary observation behind Euler's method is that the instantaneous rate of change is approximately equal to the average rate of change. Thus we approximate $\frac{du}{dt} = f(t, u)$ as

$$\frac{u(t_{i+1}) - u(t_i)}{t_{i+1} - t_i} = f(t_{i+1}, u(t_i)). \quad (2.2.3)$$

Rearranging terms, we find

$$u(t_{i+1}) = u(t_i) + f(t_{i+1}, u(t_i)) (t_{i+1} - t_i) \quad (2.2.4)$$

When $i = 0$, (2.2.4) becomes

$$u(t_1) = u(t_0) + f(t_1, u(t_0)) (t_1 - t_0). \quad (2.2.5)$$

Note that everything on the right hand side of (2.2.5) is known. Thus $u(t_1)$ is known. Similarly plugging in $i = 1$ to (2.2.4) and using the value for $u(t_1)$ just found, we find a value for $u(t_2)$. Continuing in this manner, we find values for the state variable u at all time points.

If the model has more than one differential equation, then Euler's method requires updating each state variable at each time point in the same manner as above.

While it is an intuitive strategy, Euler's method is impractical because it requires very small time steps to get good results, and because it is potentially numerically unstable. Thus, for the network simulations, I use an adaptive Runge-Kutta algorithm instead. Runge-Kutta algorithms are more complicated, but they have the advantage that they can produce good results using much larger time steps than Euler's method. Adaptive here means the algorithm chooses the step size at each step based on estimates of the error. This allows the use of large time steps when the network is being quiet, further reducing computational load.

2.2.2 Types of Neuron Models

There are several categories of differential equation based models for neuronal activity. Firing rate models, perhaps the most abstract, are common (e.g. [Fall 05], [Fall 06], [Tanaka 06], [Verduzco-Flores 09]). These models calculate the average firing rate of a neuron but do not attempt to capture individual action potential events. Integrate and fire models (e.g. [Brunel 01]) consider the dynamics of a cell up until a certain event occurs, interpreted to indicate that the cell will then fire an action potential. The action potential is assumed to happen instantaneously, and the neuron’s state variables are returned to rest. Unlike firing rate models, integrate and fire models give specific times for action potentials, so irregularity can be studied, but they still do not model the time course of the action potential itself.

This study instead uses a third type of model, one based on a Hodgkin-Huxley-type formalism. This class of models offers a strong correspondence to the biology, because it explicitly considers the probabilities that ion channels are open or closed, and because it offers full time courses for all the state variables.

2.2.3 Hodgkin-Huxley Model

The classic 1952 model [Hodgkin 52] of action potentials in the squid giant axon by Alan Lloyd Hodgkin and Andrew Huxley forms the basis of my model. The notation that follows is not their own, but the equations are equivalent. Their model considered the effect of two specific types of ion channels – sodium and potassium – as well as a third, general channel, dubbed “leak.” The change in membrane potential v is a result of the summed ionic currents, I_{ion} , and any applied current I_{app} :

$$C_m \frac{dv}{dt} = -I_{\text{Na}} - I_{\text{K}} - I_{\ell} + I_{\text{app}}, \quad (2.2.6)$$

where the signs follow the standard convention in the literature that positive ionic current (I_{Na} , I_{K} , and I_{ℓ}) decreases the cell's membrane potential, while positive applied current I_{app} increases the potential. Here $I_{\text{Na}} = g_{\text{Na}} m^3 h (v - v_{\text{Na}})$, $I_{\text{K}} = g_{\text{K}} n^4 (v - v_{\text{K}})$, and $I_{\ell} = g_{\ell} (v - v_{\ell})$ are the ionic currents flowing through sodium, potassium, and leak channels, respectively. Other channel types besides sodium and potassium are present in a cell; the leak current offers an approximation of their combined effects.

The variables m , h , and n are gating variables, representing the proportion of sodium activation, sodium inactivation, and potassium activation gates, respectively, on the ion channels that are open. Each gating variable is governed by an equation of the form

$$\frac{dx}{dt} = \frac{x_{\infty}(v) - x}{\tau_x(v)}, \quad (2.2.7)$$

where each instance of x is either m , h , or n . This equation implies that for a given gating variable x , the probability that the corresponding gate will be open tends to a level $x_{\infty}(v)$, depending on the membrane potential in an exponential way with time constant $\tau_x(v)$, also depending on the membrane potential. The full set of equations and parameter values are listed in Appendix A.1.

An action potential may be triggered in the Hodgkin-Huxley model by either a brief depolarizing current – that is, a current that raises the membrane potential – or following release from a longer hyperpolarizing current. This last phenomenon is known as post-inhibitory rebound. Figure 2.3 shows an example of each type.

2.2.4 Simplifications

Unfortunately, the four state variables of the Hodgkin-Huxley equations are still too complex for study by certain mathematical tools, such as phase-plane analysis [Strogatz 94]. Many simplified models were developed from the Hodgkin-Huxley framework, including [Abbott 90, Borg-Graham 87, Rinzel 85].

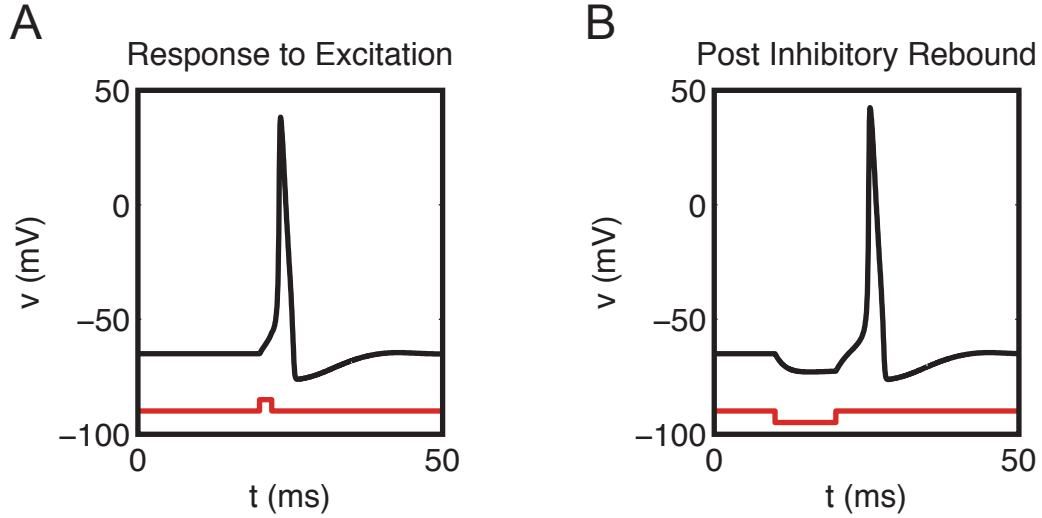


Figure 2.3: Action potentials (black) in the Hodgkin-Huxley model triggered by excitation (A) and by post-inhibitory rebound (B). The red lines indicate relative change in applied current.

Rinzel noted that sodium activation m was the fastest gate, so its dynamics could be replaced with its quasi-steady-state approximation $m = m_\infty(v)$. Furthermore, he noted that sodium inactivation probability n and potassium activation probability h share an approximately linear relationship, as illustrated in Figure 2.4 [Rinzel 85]. Thus the differential equation for h may be replaced with a linear algebraic equation. Rinzel used the line of best fit [Rinzel 85], but even $h = 1 - n$ preserves the qualitative behavior and keeps the gating variables bound between 0 and 1.

Only two state variables remain in the model: v and n . The sodium current equation is now $I_{\text{Na}} = g_{\text{Na}} (m_\infty(v))^3 (1 - n) (v - v_{\text{Na}})$. It is a standard result that no autonomous (time invariant) one-dimensional differential equation model can exhibit non-monotonic behavior [Strogatz 94], so a two-state model is the simplest possible form.

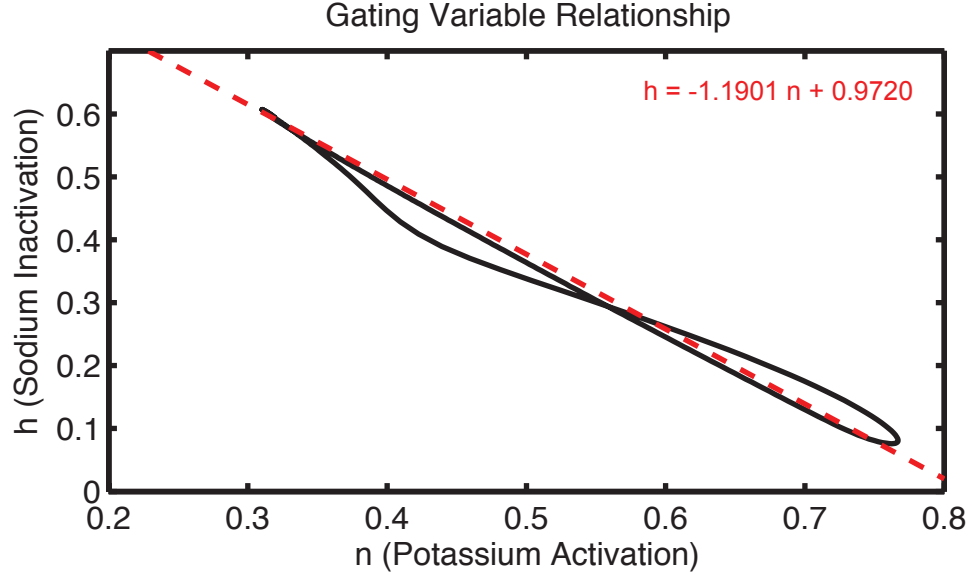


Figure 2.4: Sodium inactivation and potassium activation probabilities obey a nearly linear relationship in the Hodgkin-Huxley model. The dotted line is the line of best fit, $h = -1.1901n + 0.9720$.

Borg-Graham observed that the carefully fit functions for channel opening and closing chosen by Hodgkin and Huxley are not essential to the qualitative behavior. Instead, each limiting value could be defined as $x_\infty(v) = \Gamma(v; \theta_x, \sigma_x)$, where x is replaced by each gating variable, which in this case is only n . Here

$$\Gamma(v; \theta, \sigma) = \frac{1}{1 + \exp(-(v - \theta) / \sigma)}, \quad (2.2.8)$$

a sigmoidal function. Note that for positive σ , if $v \gg \theta$ then Γ will be near 1. Conversely, if $v \ll \theta$, then Γ will be near 0. The magnitude of σ determines the steepness of the transition. Finally, if $v = \theta$, then $\gamma = \frac{1}{2}$; that is, θ is the half-activation potential.

Figure 2.5 compares the Hodgkin-Huxley model with the simplified model described here, whose full equations are listed in Appendix A.2.

Comparison of Action Potential Models

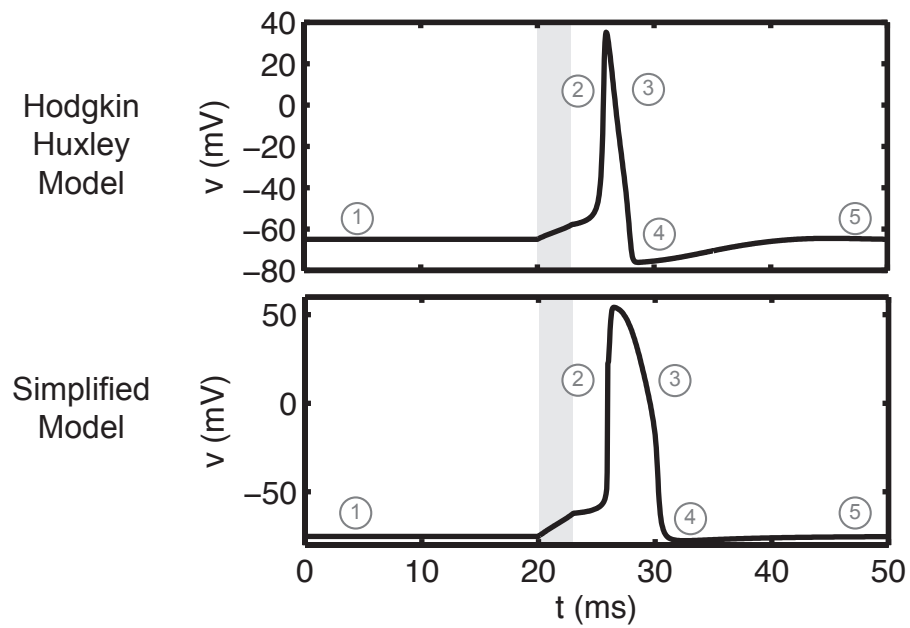


Figure 2.5: Comparison of action potentials under Hodgkin-Huxley model and under the simplified model. Both go through similar phases: (1) rest, (2) rising phase, (3) falling phase, (4) afterhyperpolarization, (5) return to rest. The action potentials were initiated by an applied current from $t = 20$ to $t = 23$ ms, the shaded time period.

2.2.5 Synapses

Synapses are places where two neurons communicate. In the case of chemical synapses, this communication is one-way, with the postsynaptic cell receiving input from the presynaptic cell. Since two cells are involved, in this Section instead of writing v for membrane potential, v_{post} will represent the membrane potential of the postsynaptic cell and v_{pre} will represent the membrane potential of the presynaptic cell.

In the simplest case, an ionotropic synapse, synaptic transmission works by opening an ion channel in the post-synaptic cell. These channels are modeled identically to any other gated ion channel [Destexhe 94b], namely

$$I_{\text{syn}} = g_{\text{syn}} s (v_{\text{post}} - v_{\text{syn}}), \quad (2.2.9)$$

where s denotes the extent to which the channel is open, which depends on the amount of neurotransmitter released by the presynaptic cell. When multiple synapses are present, the total synaptic current is the sum of terms of the form (2.2.9), one for each synapse.

It remains for the presynaptic cell to specify the channel-open probability. One typical model [Destexhe 94b] is to suppose that the synaptic gate open probability exponentially tends toward 1 when the presynaptic cell's membrane potential is elevated, then exponentially decays to 0. Mathematically, this is expressed by

$$\frac{ds}{dt} = \alpha (1 - s) s_{\infty} - \beta s, \quad (2.2.10)$$

where α and β are constants and $s_{\infty}(v_{\text{pre}}) = \Gamma(v_{\text{pre}}; \theta_{\text{syn}}, \sigma_{\text{syn}})$. Delays due to signal propagation down an axon can be explicitly incorporated into the model without modeling the spatial extent of the axon; simply replace s in (2.2.9) with $s(t - \tau_{\text{delay}})$, the value of s at a time τ_{delay} before the current time.

2.2.6 Calcium Waves

ER-based calcium dynamics were first modeled by De Young and Keizer in 1992 [De Young 92]. Since the InsP_3 receptor has three binding sites, each one of which is either bound to a molecule or not, it has $2^3 = 8$ possible states, and their model considered the proportion of InsP_3 receptors in each of these states. Note that this only requires seven state variables, since the total probability is always 1.

As with the Hodgkin-Huxley equations, Rinzel – this time working with Li – showed by a time-scale analysis that the qualitative dynamics could be preserved by simply considering the slow calcium inactivation binding site state [Li 94]. Their work formed the basis of much subsequent work in intracellular calcium dynamics [Fall 06, Fall 04, Hartsfield 05, Percy 08, Wagner 04]; the model presented here is a variant of [Wagner 04] that neglects dynamic InsP_3 production.

The ER is distributed throughout the cytosol in a connected way, through the dendrites and even dendritic spines [Harris 94, Spacek 97]. Suppose for a given cell volume, f_e denotes the fraction occupied by the ER, and f_c denotes the fraction occupied by the cytosol. Necessarily $f_c + f_e \leq 1$. The inequality is strict if other structures are present, such as mitochondria.

Recall that the ER calcium story involved InsP_3 receptors and SERCA pumps. As with the Hodgkin-Huxley equations, combine the net effects of all other channels on the ER into a leak channel. Denote by J_{IP_3} , J_{SERCA} , and J_{leak} the mass flux per unit volume due to the InsP_3 receptor, SERCA pump, and leak channels. Dividing the mass flux by the volume fraction gives the change in concentration.

Thus, if C_c and C_e represent the cytosolic and ER calcium concentration, respectively, we have

$$\frac{\partial C_c}{\partial t} = d_c \Delta C_c + \frac{J_{\text{IP}_3} + J_{\text{SERCA}} + J_{\text{leak}}}{f_c} + c_{\text{ionic}} \quad (2.2.11)$$

$$\frac{\partial C_e}{\partial t} = d_e \Delta C_e - \frac{J_{IP3} + J_{SERCA} + J_{leak}}{f_e} \quad (2.2.12)$$

where c_{ionic} denotes the net flux into the cytosol due to ion channels on the cell membrane and depends on both space and time. The first terms of the right hand sides is the contribution from diffusion, as derived in Appendix D.

The form of the fluxes J_{IP3} and J_{leak} parallels the forms for ion channels in the Hodgkin-Huxley equations: $J_{IP3} = v_{ip3r} m^3 n^3 h^3 (C_e - C_c)$ and $J_{leak} = v_{leak} (C_e - C_c)$. The SERCA pump is a pump not a channel and so has a different form, modeled with Hill-type dynamics: $J_{SERCA} = -\frac{v_{serca} C_c^2}{k_{serca}^2 + C_c^2}$. More biophysically detailed models of the SERCA pump have also been developed [Baker 02, Higgins 06]. Here m and n are fast gating variables depending on InsP₃ and calcium, respectively. The final gating variable h is for the slow calcium inactivation gate.

This model supports both bistable and excitable waves. The non-spatial dynamics are illustrated in Figure 2.6. Both types of waves have been observed in the *Xenopus* oocyte, which state depending on the oocyte's development [Fontanilla 98, Lechleiter 91].

In particular, the model can transition from excitable, to bistable, to monostable with high calcium concentration by increasing the InsP₃ concentration, see Figure 2.7.

2.3 Working Memory

The brain's short-term storage and processing capabilities are provided by the working memory system [Baddeley 94]. When a cue signal is presented that needs to be remembered, some subset of the cells in the prefrontal cortex (PFC) begin to fire more rapidly and maintain this elevated firing rate after the signal is removed. When the information is no longer relevant, the memory is discarded. In some experiments

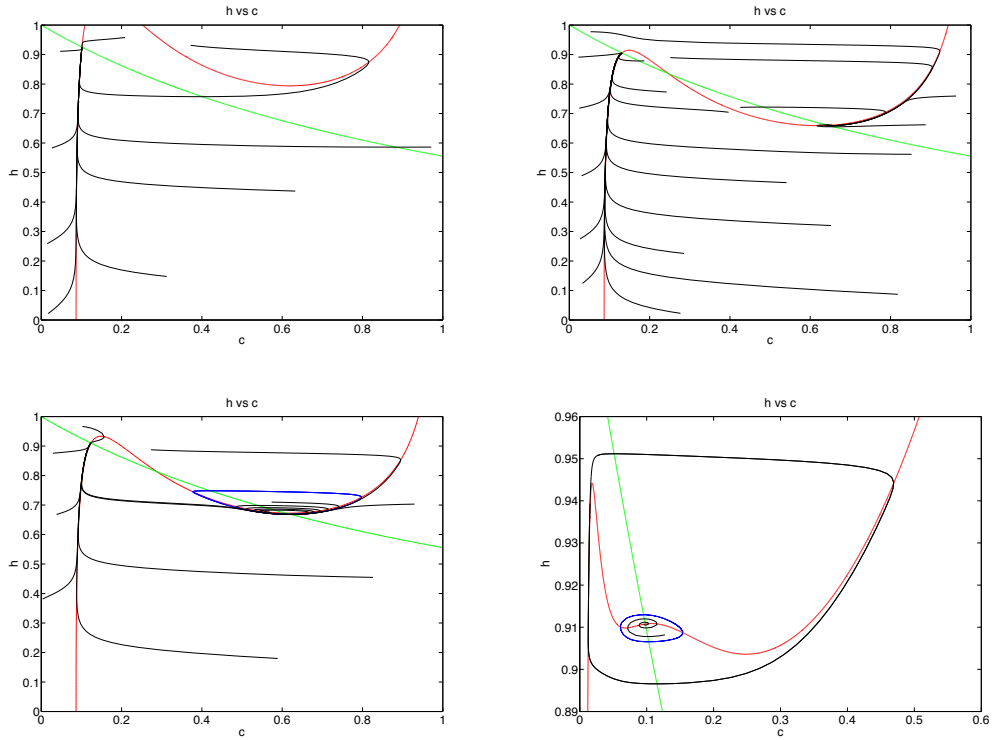


Figure 2.6: Behaviors of the ER-calcium point model. From left-to-right then top-to-bottom: excitable, bistable, bistable with unstable limit cycle, one stable fixed point with an unstable and a stable limit cycle.

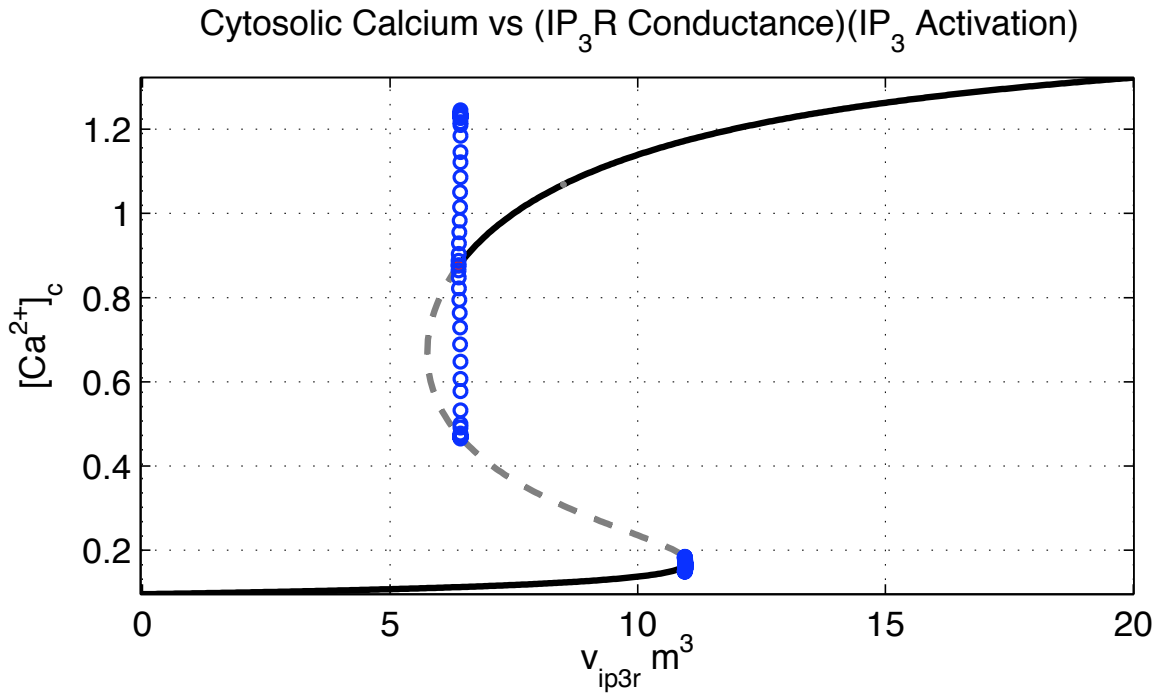


Figure 2.7: Cytosolic calcium limit behavior as a function of the combined effects of InsP_3 concentration and maximum InsP_3 receptor conductance. The bifurcation diagram was computed using XPPAUT [Ermentrout 02] and rendered using plotxppaut by Mohammad Imtiaz, which no longer seems to be available online. Solid lines denote stable limit points, dotted lines denote unstable limit points, and circles denote the extreme values of limit cycles.

[Funahashi 89, Jonides 93], this entire process occurs over just a few seconds. Presentation of the same cue again will activate the same cells, while presentation of a different cue will activate different cells. Thus the pattern of activity corresponds to the information encoded [Funahashi 89, Funahashi 94].

2.3.1 Biology

Location

Key aspects of the working memory system lie within the PFC, although other brain regions are also involved [Constantinidis 96, Jonides 93, Miller 96, Quintana 99]. Tests on brain-damaged patients, PET scans on the healthy, and direct electrical recordings from animals all testify to the PFC's important role.

Delay tasks have been used to test both human [Lewinsohn 72, Verin 93] and monkey [Funahashi 89] working memory performance. In these tests, a stimulus is presented – Lewinsohn et al tested humans using visual, auditory, and kinesthetic stimuli – and then the subject is asked to identify or reproduce the stimulus after a short delay (10 seconds in [Lewinsohn 72]). Patients with dorsolateral prefrontal lesions have a higher error rate than control individuals. Working memory deficits have also been observed in recency tests of lesion patients, wherein the subject has been shown a series of pictures or asked to say a series of words and asked to report which of two options were presented more recently [Milner 82].

Healthy subjects show increased activity in the PFC during the performance of working memory tasks as measured by positive emission tomography (PET). Jonides et al tested this by scanning volunteers who were briefly presented with a set of three spatial locations, waiting three seconds, and then asking them if a specific location was one of the original three [Jonides 93]. A similar protocol was used in

[Petrides 93], and the basic results have been confirmed using functional magnetic resonance imaging (fMRI) as well [D’Esposito 95].

Funahashi et al trained monkeys to remember the spatial location of a signal and then look in that direction after a delay. They implanted electrodes in the monkey PFC to record the electrical activity of individual neurons during this task. They found that different groups of neurons would activate in response to different locations, that these neurons would remain active during the delay period, and quickly deactivate after the task was complete [Funahashi 89].

Architecture and Connectivity

There are two dominant classes of neurons in the PFC: excitatory pyramidal cells and inhibitory GABAergic interneurons [Gabbott 05, Mountcastle 69, Wilson 94]. The exact ratios vary by region, but in the rat, typically about 85% of PFC neurons are pyramidal cells; the remaining 15% are mostly GABAergic interneurons with many subtypes [Gabbott 05]. Many of these pyramidal cells project to other brain systems; in the rat about 37% of PFC layer 6 pyramidal cells project to the mediodorsal thalamus [Gabbott 05]. The PFC is bidirectionally connected to the sensor and motor cortices. It also transmits to the basal ganglia and receives input from the thalamus and amygdala [Fuster 08, Miller 01].

Modulation

Local concentrations of the neuromodulator dopamine are known to rise during the performance of working memory tasks [Watanabe 97]. Experiments have found working memory performance has an inverted-U-shaped relationship with dopamine; performance is impaired if dopamine is too high or too low [Zahrt 97]. Disregulation of the dopamine levels [Swerdlow 87] and impairment of working memory performance [Driesen 08, Gonzalez-Burgos 08, Silver 03] are both associated with schizophrenia.

2.3.2 Modeling

Many models have been proposed for the maintenance of persistent activity. Many of these models are based on either recurrent excitation [Brunel 01, Amit 97, Hopfield 82, Mongillo 08] or cellular bistability [Fall 06, Fall 05, Guigon 95]. Both approaches are based on experimental observations: recurrent excitatory connections have been identified within the prefrontal cortex [Kritzer 95, Melchitzky 98], and intracellular calcium – often considered a measure of recent neuronal activity – has been shown to modulate a neuron’s electrical response [Fransén 06, Moore 09, Sidiropoulou 09].

Recurrent excitatory networks rely on some form of synaptic adaptation to respond to novel stimuli. Traditionally this adaptation was modeled as long-term potentiation in the synapses between neurons belonging to the same pattern [Hopfield 82, Amit 97], but while synaptic facilitation has been observed between pyramidal cells in the PFC [Wang 06] Short-term synaptic plasticity occurs with a time constant of around 100 ms [Zucker 02], so it is not clear if this mechanism is fast enough to support novel patterns in working memory. These attractor models converge on a stable network, making them robust to noise. Retained patterns may be switched by momentarily shutting down the network then introducing a new pattern [Brunel 01].

More recent work by Mongillo et al [Mongillo 08] suggests that synaptic adaptation due to changing calcium concentration at the synapses could be sufficient to maintain persistent activity. The authors propose that this chemical change is long lasting, on the order of one second, allowing the network to conserve energy by briefly stopping persistent activity while still maintaining the pattern encoded in the synapses.

Other models suppose that the response properties of the cell itself change over

time. While a traditional Hodgkin-Huxley neuron does not change over time, an actual biological neuron – a living cell – does change. These models harness this change to endow the neuron with a “memory” of its own, possibly in the form of a change in cytosolic calcium concentration [Fall 06]. To provide robustness to noise and prevent “drift” where the active cells change over time, these models often implement Mexican-hat-like synaptic distributions [Fall 06] whereby nearby cells have excitatory connections and far away cells have inhibitory connections; they are therefore limited to encoding patterns of contiguous groups of cells [Camperi 98, Fall 06]. Some [Guigon 95] also incorporate synaptic plasticity. These models typically do not consider pattern switching or robustness to a full strength distractor.

While inhibition is expressed with significant power in the PFC [Hasenstaub 05, Rudolph 07], in the recurrent excitatory models, it often serves primarily to slow down the excitatory cells [Amit 94, Brunel 01]. They typically require a careful balance of inhibition and excitation [Barbieri 08].

Both of these approaches have difficulty reproducing the irregular firing patterns seen in experiment [Barbieri 08]. The coefficient of variation – the ratio of the standard deviation to the mean – of the interspike intervals of prefrontal cortex neurons during working memory tasks has been measured to be about one [Compte 03], whereas it tends to be lower in recurrent networks and especially bistable networks [Barbieri 08]. The model of [Brunel 01], however, achieves a nearly exponential interspike-interval distribution, thanks in part to the balance of inhibition and the strong noise signal.

In the following chapters, I show that an excitatory-inhibitory network where the excitatory cells possess a calcium-modulated sag current can form the basis of a robust working memory system. The only assumptions I make on connectivity are that it is sufficiently high and that the connection probabilities between cells only depend on

their cell types. This model exhibits irregular activity even in the absence of noise from other brain regions. It maintains persistent activity, is robust to distractors, and can switch to new patterns for a wide range of connection probabilities; no careful balancing is required.

CHAPTER 3

MODEL

I propose a new model, driven by calcium-modulated interactions between excitatory and inhibitory neurons in the PFC. This structure is motivated by the observations that inhibitory connections are dominant in the PFC [Hasenstaub 05, Rudolph 07] and sag currents – currents activated by hyperpolarization – are known to increase activity in some PFC neurons [Magee 98, Winograd 08] and are themselves possibly modulated by intracellular calcium concentration [Hagiwara 89, Lirk 08, Pan 03, Schwindt 92]. Recent experiments have examined the link between intracellular calcium concentration and neuronal activity [Moore 09, Sidiropoulou 09] and provided further evidence of an association.

3.1 Overview

The model consists of two pools of neurons: excitatory cells and inhibitory cells, interpreted to correspond to pyramidal neurons and GABAergic interneurons, respectively. I seek a minimal model with as few assumptions as possible, so I neglect variations between the subtypes of each of the two major classes of neurons in the PFC. Neurons are connected at random with probability based solely on the cell types involved. While excitatory to excitatory connections are known to be present, they are not necessary for the basic performance of the model; I propose that they

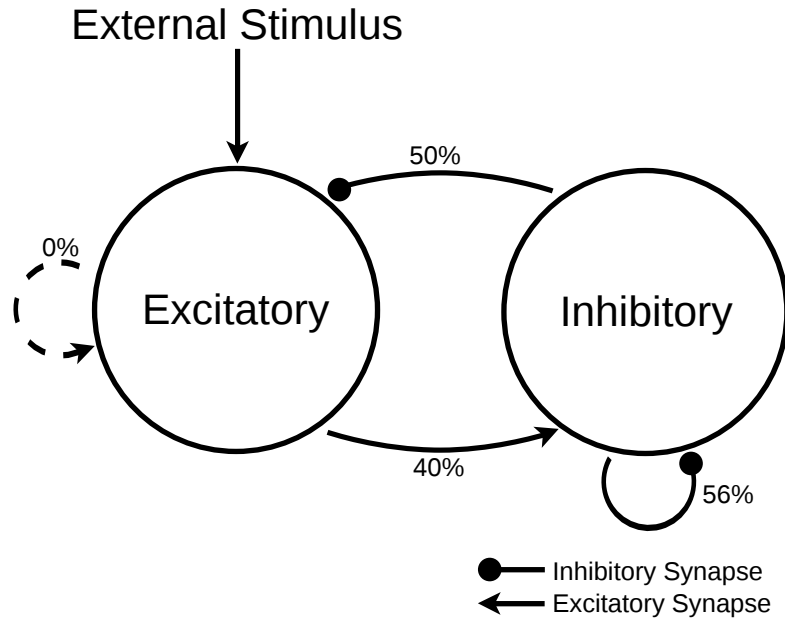


Figure 3.1: Schematic diagram of a two-population model for working memory. Connection probabilities are as shown, except where otherwise indicated.

act to improve performance with learned patterns. Most of the simulations involved networks of 80 excitatory cells and 30 inhibitory cells. This choice of network size is largely arbitrary, although the excitatory cells are known to be more numerous than the inhibitory cells in the PFC [Gabbott 05]. The basic working memory behaviors are robust across a range of network sizes. A schematic for the usual architecture is shown in Figure 3.1.

Each cell is modeled as a single compartment using the conductance-based Hodgkin-Huxley formalism [Hodgkin 52]. Delays due to spatial propagation of action potentials are modeled using delay-differential equations. Propagation delays from excitatory to inhibitory synapses are chosen from a normal distribution with mean 10 ms and standard deviation 3 ms.

Patterns to be retained are presented to the model in the form of an applied

current to a corresponding subset of the excitatory neurons. The choice of pattern is in no way linked to the particular network architecture.

The corresponding excitatory cells respond to the applied current by firing rapidly, thereby elevating their internal calcium concentration. This activity excites the inhibitory cells, which then deliver inhibition to all the excitatory cells. In excitatory neurons with a high level of calcium, the sag current then activates, depolarizing the cell, potentially raising it above threshold, triggering an action potential, thereby maintaining persistent activity. The cytosolic calcium in the quiescent cells is insufficient to activate the sag current to a level strong enough to trigger an action potential, so they remain silent.

3.2 Excitatory Cells

The excitatory cells are modeled similarly to the simplified Hodgkin-Huxley model introduced in Section 2.2.4, except they contain two additional ion channels: calcium and sag.

The membrane potential is governed by the equation

$$C_m \frac{dv}{dt} = -(I_{\text{Na}} + I_{\text{K}} + I_{\text{Ca}} + I_{\text{h}} + I_{\ell} + I_{\text{syn}} + I_{\text{noise}}) + I_{\text{app}}, \quad (3.2.1)$$

where $I_{\text{Na}} = g_{\text{Na}} m_{\infty}^3 (1 - n)(v - v_{\text{Na}})$, $I_{\text{K}} = g_{\text{K}} n^4 (v - v_{\text{K}})$, $I_{\text{Ca}} = g_{\text{Ca}} y_{\infty}^2 (v - v_{\text{Ca}})$, $I_{\text{h}} = g_{\text{h}} m_{\text{h}} (v - v_{\text{h}})$, and $I_{\ell} = g_{\ell} (v - v_{\ell})$. The choice of name I_{h} refers to the h-current, another name for the sag current. The slow gating variables n and m_{h} are governed by equations of the form given in equation (2.2.7), where x is replaced by n and m_{h} , respectively. I suppose calcium modulation of the sag current is indirect and works by modulating the half-activation variable:

$$\theta_{\text{h}} = \theta_{\text{h,min}} + (\theta_{\text{h,max}} - \theta_{\text{h,min}}) \frac{c^2}{k_{\text{h}}^2 + c^2}, \quad (3.2.2)$$

where c represents the concentration of calcium in the cytoplasm. Note that if calcium is high, i.e. $c \gg k_h$, then θ_h is near $\theta_{h,\max}$. That is, the half-activation potential for sag current is near its highest, therefore making it the easiest to switch on. Conversely, if $c \ll k_h$, then θ_h will be near $\theta_{h,\min}$, and the neuron would have to be very hyperpolarized to activate the sag current. An alternative indirect model, based on explicit binding reactions, has been proposed in [Winograd 08].

Cytoplasmic calcium, c , increases at a rate proportional to the calcium current and is cleared by mass-action kinetics, with potential additional contributions c_{internal} from the ER and c_{NMDA} from NMDA receptors:

$$\frac{dc}{dt} = \varepsilon (-I_{\text{Ca}} - k_{\text{Ca}} c) + c_{\text{internal}} + c_{\text{NMDA}}, \quad (3.2.3)$$

Recall that for historical reasons the sign convention is such that a negative current is the flow of positive charge (here calcium cations) into the cell; this convention is the reason for the initial negative sign in (3.2.3). Since most admitted calcium is quickly buffered, the change in cytosolic calcium concentration due to fluxes across the cell membrane is scaled by ε , a small constant.

Excitatory to inhibitory communication is assumed to occur via AMPA synapses, which decay quickly, with time constant about 2 ms. Excitatory to excitatory synapses, if any, are assumed to be mediated by NMDA, which has longer lasting effects [Ermentrout 10].

The full set of equations is listed in Appendix A.3. Initial parameters were chosen by a Monte Carlo search, as explained in Appendix B.1 and listed in Table A.3.

3.3 Inhibitory Cells

As with the excitatory cells, the inhibitory cells are modeled based on the simplified Hodgkin-Huxley model of Section 2.2.4, except these cells contain three additional currents: calcium I_{Ca} , an A current I_{A} , and an AHP current I_{AHP} .

It follows that the membrane potential v is governed by

$$C_m \frac{dv}{dt} = -(I_{\text{Na}} + I_{\text{K}} + I_{\text{Ca}} + I_{\text{A}} + I_{\text{AHP}} + I_{\ell} + I_{\text{syn}}) + I_{\text{app}}, \quad (3.3.1)$$

where $I_{\text{Na}} = g_{\text{Na}} m_{\infty}^3 (1 - n)(v - v_{\text{Na}})$, $I_{\text{K}} = g_{\text{K}} n^4 (v - v_{\text{K}})$, $I_{\text{Ca}} = g_{\text{Ca}} y_{\infty}^2 (v - v_{\text{Ca}})$, $I_{\text{A}} = g_{\text{A}} a^3 b (v - v_{\text{K}})$, $I_{\text{AHP}} = g_{\text{AHP}} \left(\frac{c^2}{c^2 + k_1^2} \right)^2 (v - v_{\text{K}})$, and $I_{\ell} = g_{\ell} (v - v_{\ell})$. The slow gating variables a , b , and n are governed by equations of the form (2.2.7), where x is replaced by a , b , or n , respectively.

Calcium is modeled as in (3.2.3), with $c_{\text{NMDA}} = c_{\text{internal}} = 0$. The A current, I_{A} , is a slow inactivating potassium current associated with delays [Ermentrout 10, Storm 88]. The model follows [Connor 71], with some parameter values from [Golomb 07].

The after-hyperpolarization-current is a potassium current that activates in the presence of high calcium, thereby hyperpolarizing the cell and reducing the firing rate [Abel 04]. The model used is an instantaneous variant of [Destexhe 94a]. Note that if $0 \leq c \ll k_1$, then $\frac{c^2}{c^2 + k_1^2}$ will be small, so there will be very little AHP current. Recall that calcium c is small when the cell has not fired recently. If on the other hand, $c \gg k_1$, then $\frac{c^2}{c^2 + k_1^2}$ will be near 1, and the AHP current will be near its maximum strength, exerting a hyperpolarizing influence on the membrane potential, limiting its firing rate.

Appendix A.4 lists the full set of equations. All inhibitory synapses are assumed to be mediated by GABA_{A} . A Monte Carlo search, this time based on the combined

behavior of a group of inhibitory cells, was used to pick the initial parameters, as explained in Appendix B.2. These parameter values are listed in Table A.4.

3.4 The Rest of the Brain

The working memory system does not exist in isolation; the neurons involved constantly exchange signals with the rest of the brain. As introduced in Section 2.3.1, the PFC is bidirectionally connected with the sensory systems, receives input from the thalamus and amygdala, and sends output to the basal ganglia [Fuster 08].

To simulate synaptic input from neurons not being explicitly modeled, I suppose that they fire according to a Poisson process at some known frequency. Recall that a Poisson process is a sequence of events where the delays are exponential random variables. That is, the probability that the inter-event delay X is bigger than Δt is

$$P(X > t) = e^{-\lambda \Delta t}, \quad (3.4.1)$$

where λ is the reciprocal of the average delay. Thus if the firing rate f is measured in Hz and time is measured in milliseconds, the average delay is $\frac{1000}{f}$, so $\lambda = \frac{f}{1000}$. The standard deviation and the mean of an exponential random variable are identical, so these artificial neurons fire with coefficient of variation equal to 1.

If t_i denotes the time of the i th spike for a particular non-explicitly modeled neuron, then the synaptic output for that neuron is modeled according to the form

$$s(t) = \begin{cases} 1 & \text{if } t_i \leq t < t_i + \tau_{\text{delay}} \\ \exp((t_i + \tau_{\text{delay}} - t)/\tau_{\text{decay}}) & \text{if } t_i + \tau_{\text{delay}} \leq t < t_{i+1} \end{cases}$$

That is, the synaptic output is 1 for a duration of τ_{delay} , then decays exponentially with time constant τ_{decay} until the next spike time.

In the case of full network simulations, I consider a pool of 300 background neurons, each firing according to a Poisson process at 5 Hz. Each excitatory cell receives

input from a random sample of 50 background neurons from the pool. The current from input from synaptic input from background neurons follows the same form as all the other synaptic currents, namely

$$I_{\text{noise}} = \sum_{i \in \text{presyn noise}} g_{\text{noise}} s_i (v - v_{\text{noise}}). \quad (3.4.2)$$

The parameters used for noise are as in Table A.6, except where otherwise noted.

CHAPTER 4

RESULTS

For the full network simulations, I connect 80 excitatory cells to 30 inhibitory cells using the connection probabilities and parameters as determined in Appendix B. Patterns are presented to the network in the form of an applied current administered to a subset of the excitatory cells. An alternate strategy would be to increase the firing rate of the noise sources that target the neurons belonging to the pattern; this second approach was used in [Brunel 01].

4.1 Basic Results

Figure 4.1 shows an example multiphase simulation.

During the initial phase – (i) in the Figure – no cue has been presented. The excitatory cells fire at a low rate driven by background noise from outside the model. The cells fire infrequently enough that their calcium concentration remains low, so the response of the inhibitory cells does not trigger persistent activity.

In stage (ii) in the Figure, a cue is presented to the first 30 excitatory cells. The numbering has no intrinsic meaning in the model; any group of 30 excitatory cells gives similar results. A contiguous block of cells was chosen solely as a visualization aid. The extra applied current increases the firing rate of the stimulated cells, causing their calcium concentrations to increase, as shown in Figure 4.2. This increased firing

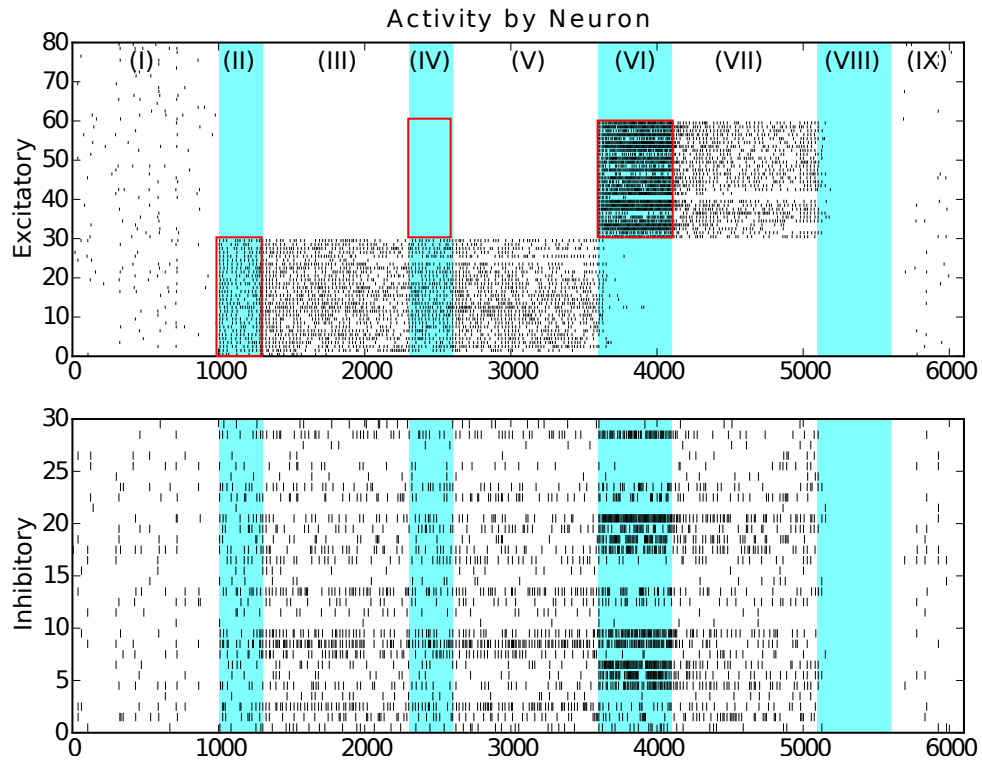


Figure 4.1: Multiphase simulation of the full network, showing baseline activity (i) and (ix), cue period (ii), persistent activity (iii), (v), and (vii), ignoring a weak distractor (iv), switching in response to a strong distractor (vi), and resetting (viii). This simulation included dopamine modulation of the inhibitory to excitatory synapses.

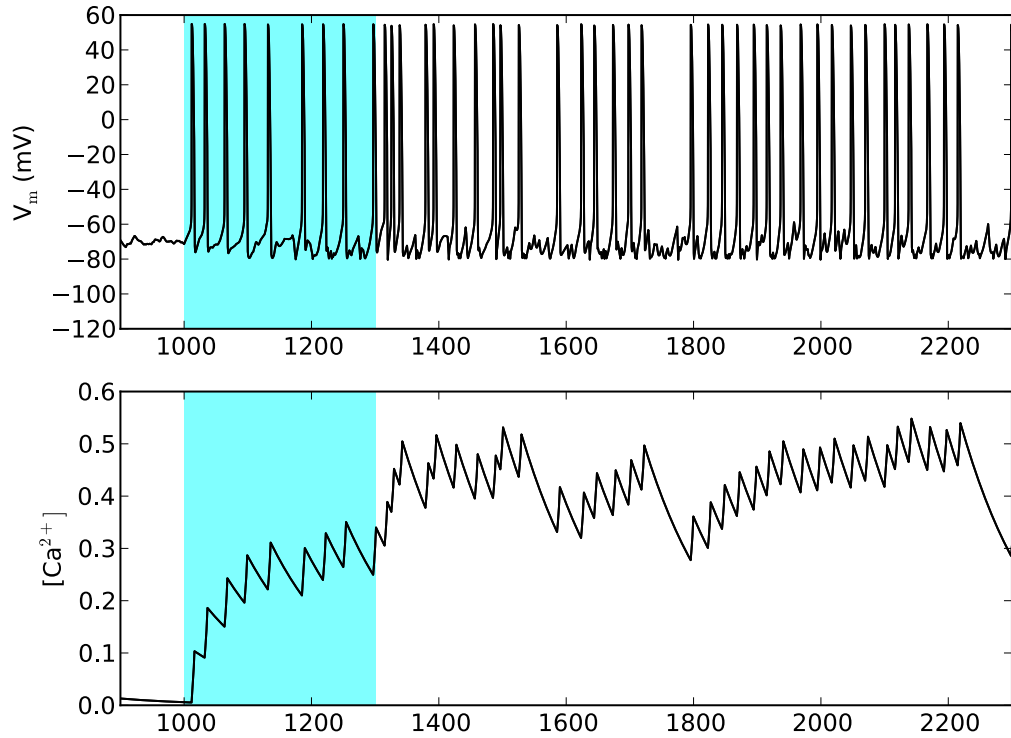


Figure 4.2: Sample calcium time course. Each action potential admits calcium, which is then cleared by a process obeying mass-action dynamics. The shaded region indicates presentation of a cue stimulus to the cell.

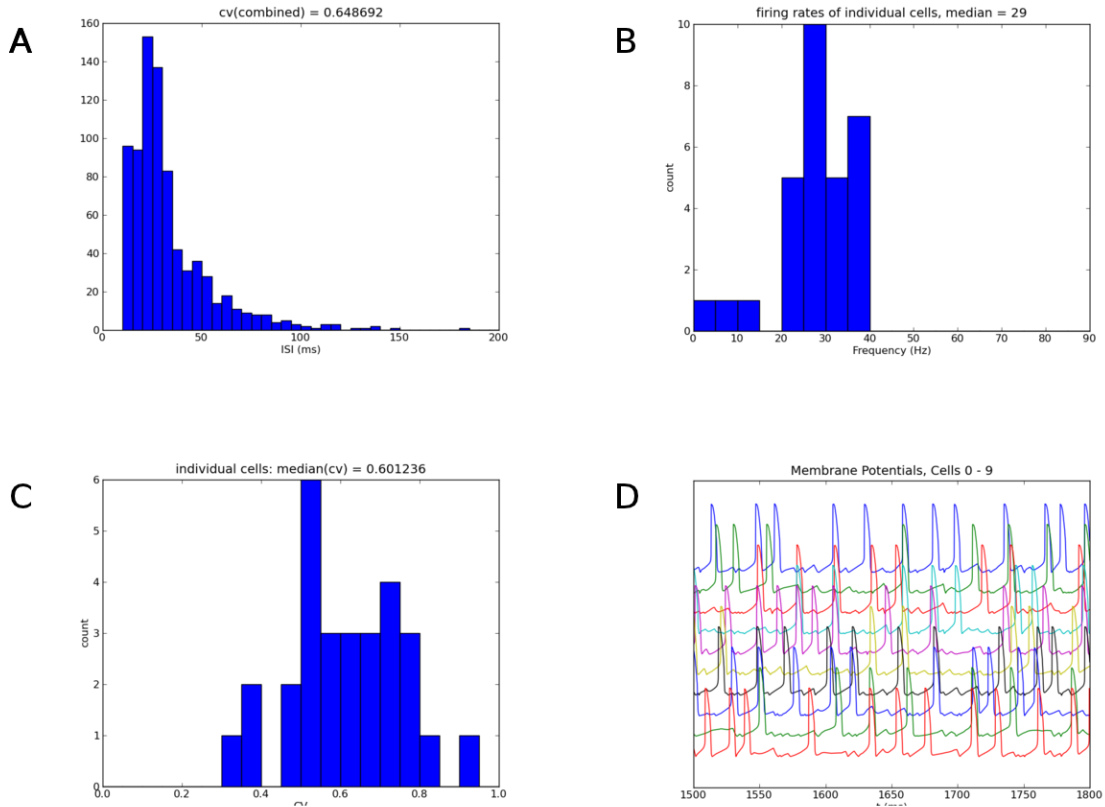


Figure 4.3: Irregular firing in the full network. (A) shows the distribution of interspike intervals, (B) the firing rates of individual cells, (C) the coefficient of variation of ISIs on a per-cell basis, and (D) membrane potential traces for 10 excitatory cells. A single simulation is shown.

rate drives the inhibitory cells faster, providing more inhibition to the excitatory cells, suppressing the activity of the non-stimulated neurons. The cue signal was maintained for 300 ms, which is the same duration used in [Verduzco-Flores 09].

During phase (iii), the cue stimulus is removed. Excitatory cells with elevated calcium concentrations respond to input from inhibitory cells by activating the h-current thereby firing more action potentials and maintaining elevated calcium levels. This

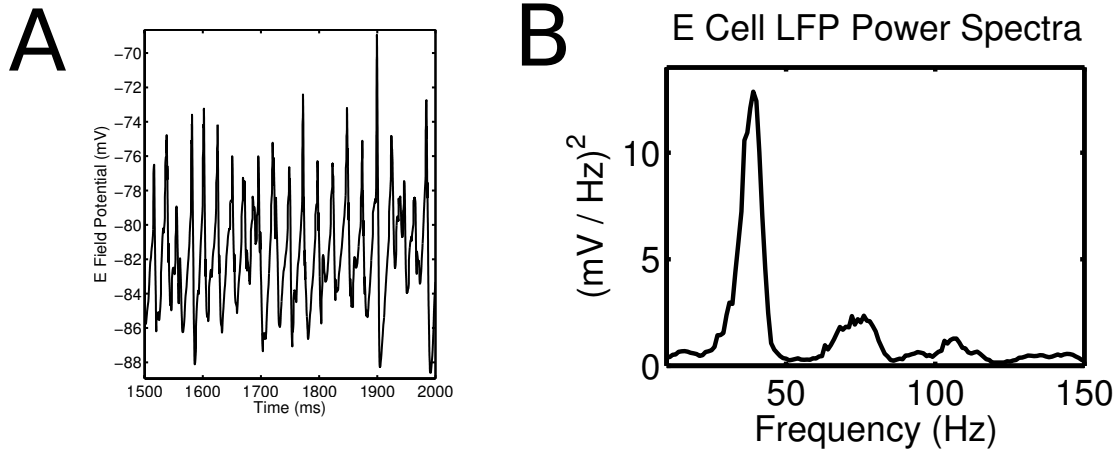


Figure 4.4: The local field potential exhibits a gamma rhythm during persistent activity. (A) shows a trace of the field potential vs time. (B) shows a periodogram of the field potential, illustrating the strengths of the component frequencies.

persistent activity is not uniform. The time between spikes varies and different neurons fire at different average rates. Nonetheless, an overarching rhythm is preserved, in the sense that the excitatory cells exhibit dynamic clustering: cells that are not firing synchronously will occasionally have action potentials at approximately the same time, see Figure 4.3.

This clustering effect causes the local field potential – here interpreted to be the average of the excitatory cell membrane potentials – to exhibit a gamma rhythm, consistent with the experimental observation in [Pesaran 00]. See Figure 4.6.

In phase (iv), a distractor of the same strength as the initial cue is presented to a different subset of the excitatory cells. The inhibitory cells, however, are now firing at a higher frequency than they were during the cue period due to the activity in the rest of the network. This additional inhibitory activity counteracts the distracting stimulus, preventing it from activating any new cells.

In phase (v), the distracting cue is removed, and the network continues to maintain persistent activity corresponding to the initial pattern.

In phase (vi), a new pattern is presented very strongly. This is simulated by applying a large applied current to the corresponding cells. This applied current is strong enough to activate the corresponding cells despite the increased inhibitory cell activity. The inhibitory cells fire more rapidly in response to the increased excitatory cell activity. This extra inhibition overcomes the sag current and prevents the cells in the original pattern from firing. By the end of this phase, the strong pattern has been presented for long enough that the calcium has built up in the new pattern but decayed in the old.

Once the strong distractor is released – phase (vii) – the network again maintains persistent activity in the cells with elevated calcium; the main difference from before is that now a different set of cells has elevated calcium.

In phase (viii) excitatory cell activity is suppressed. This may be done by either applying a hyperpolarizing applied current directly to the excitatory cells, or by applying a depolarizing applied current to the inhibitory cells, causing them to fire more rapidly and again increase the inhibition of the excitatory cells.

In phase (ix), suppression is removed. Assuming the suppression was maintained long enough, the calcium will have decayed in all of the excitatory cells to the point where the sag current will not activate, and thus the network returns to its initial baseline activity.

4.2 Network Size Independence

The basic properties identified in Section 4.1 are scalable to a variety of network sizes. Figure 4.5 illustrates that networks of various sizes can maintain persistent activity.

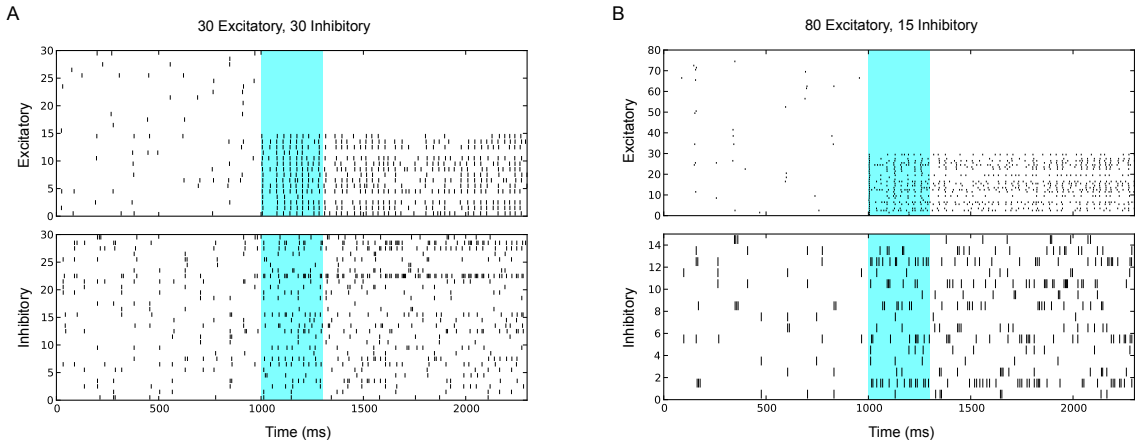


Figure 4.5: The ability to maintain persistent activity is preserved across multiple network sizes. (A) 30 Excitatory, 30 Inhibitory. (B) 80 Excitatory, 15 Inhibitory. Connection strengths are altered to preserve the total amount of synaptic input.

These scalings were achieved by altering the synaptic weights to maintain the total level of synaptic input.

4.3 Pattern Independence

The network architecture supports the retention of arbitrary patterns beyond a certain size. Randomly chosen patterns are likely to be well retained.

To quantify this, define an active cell as a cell that has fired an action potential within the past 100 ms, and consider the percentage of pattern cells active over time. Each of eight pattern sizes was tested against ten randomly chosen networks. Note that since each network is randomly connected, there is no need to randomly choose the presented patterns. Simulations were run without external excitatory input to prevent an inaccurate active count. With the exception of the smallest two

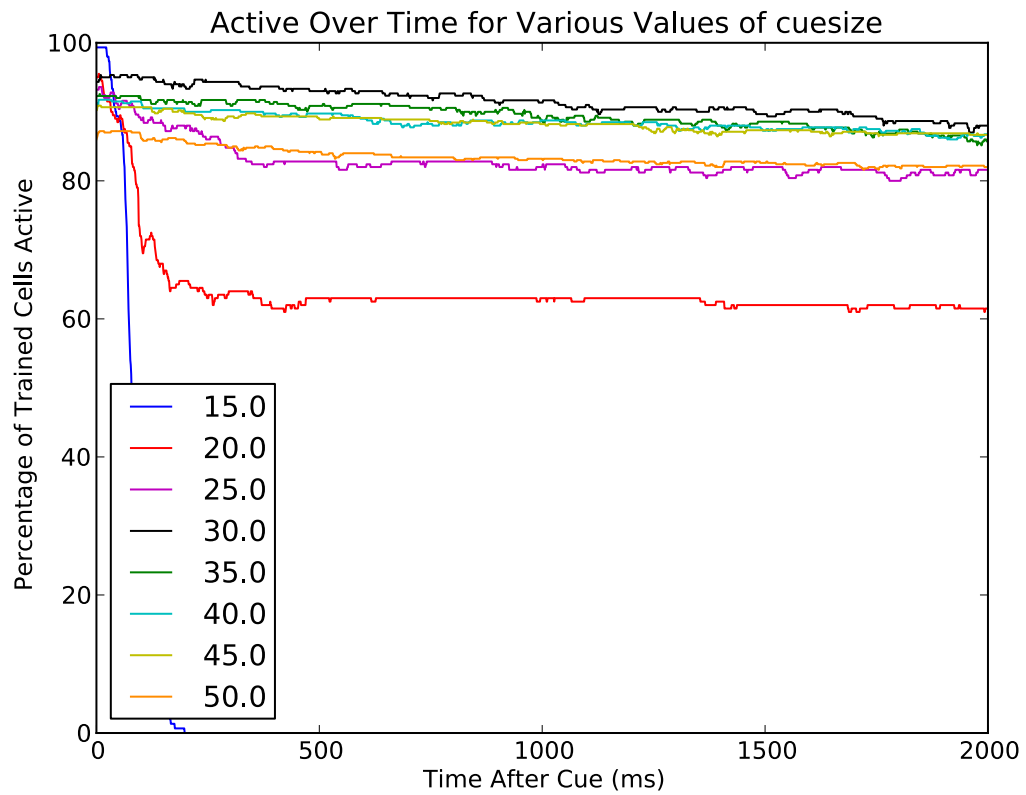


Figure 4.6: Pattern retention is largely independent of size – beyond a minimum – or pattern choice. The average percentage of pattern cells active at a given time t after the removal of cue for randomly chosen patterns of various sizes on randomly connected networks is shown. $n = 10$ simulations.

pattern sizes, on average over eighty percent of each pattern was retained for over 2000 milliseconds.

4.4 Robust to Heterogeneities

No two cells are exactly alike, so I considered the robustness of the model to heterogeneous cells, where the impact of excitatory and/or inhibitory connections varied between each cell. I compared the average performance of each cell over $n = 10$ simulations as before, except this time conductances were chosen from a normal distribution with fixed mean and a standard deviation that varied as a percentage of the mean. Network performance as measured by average fraction of active cells, average firing rates, and average coefficient of variation of the interspike intervals (a measure of the irregularity), was minimally affected for conductance standard deviation varied between zero and twenty percent of the mean, as shown in Figure 4.7.

4.5 Dopamine and Performance

Dopamine performs many roles in the brain, including modulating GABAergic synapses [Seamans 01] and sodium channel activation [Cantrell 97]. Experiments have demonstrated an inverted-U-shaped relationship between dopamine concentration and working memory performance; that is, too much or too little dopamine degrades working memory performance [Zahrt 97].

The model reproduces this behavior. If dopamine is low, GABAergic synapses are weakened, while if dopamine is high, GABAergic synapses are strengthened [Seamans 01], so I take the effective strength g_{syn} of the inhibitory to excitatory concentration as a proxy for dopamine tone and neglect temporal variations of dopamine concentration. If dopamine, and thus g_{syn} is low, then little inhibition reaches the

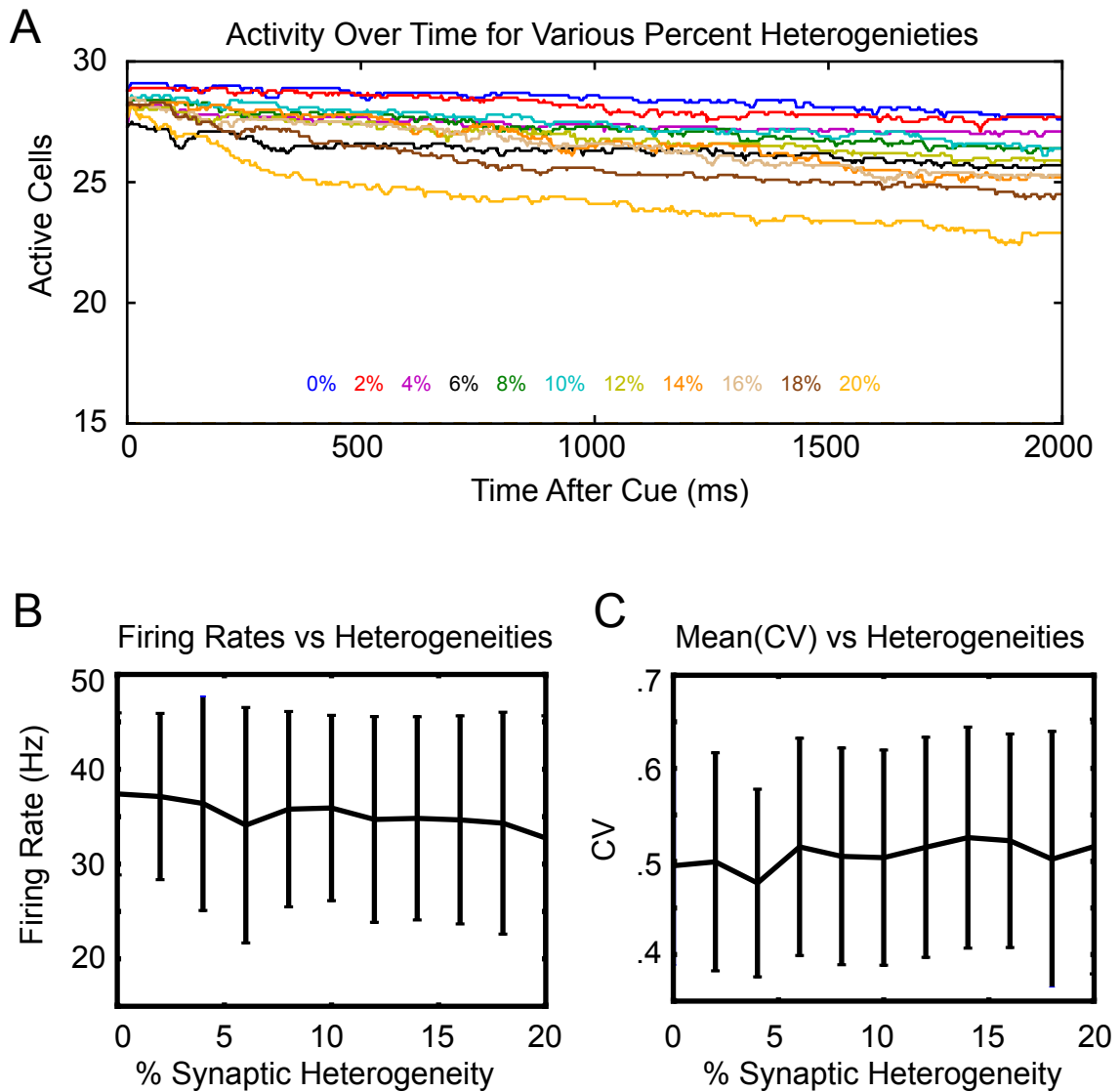


Figure 4.7: Heterogeneities in synaptic conductances are well-tolerated. Every instance of each of the three types of synaptic conductances was chosen from a normal distribution with fixed mean and standard deviation the percentage of heterogeneity shown in the graphs. This source of heterogeneity had minimal effect of persistence (A), firing rate (B), or coefficient of variation of the interspike intervals (C). Error bars denote one standard deviation. $n = 10$ simulations per data point.

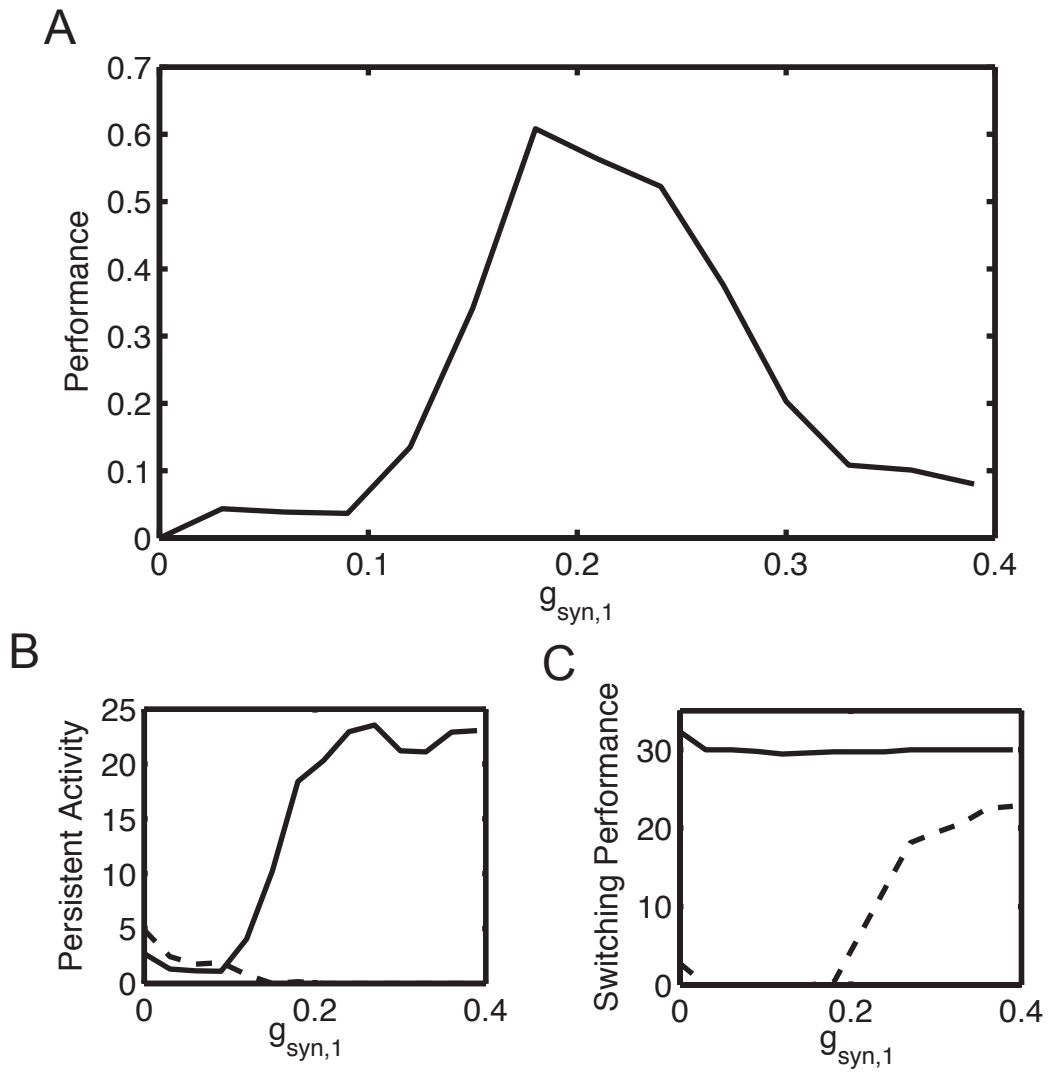


Figure 4.8: Inverted-U-shaped dopamine-performance curve: too much or too little dopamine (measured by effective strength of inhibition) degrades working memory performance (A). Persistence (B) and switching performance (C) as functions of inhibition strength are also shown. Solid lines represent the number of active cells (out of 30) in the current pattern; dotted lines represent the number of active cells outside of the pattern.

excitatory cells, so the h-current does not activate, and persistent activity fails. If dopamine is high, the excitatory cells receive too much input, causing them to fire faster, enabling them to maintain persistent activity after a distracting signal.

Define the performance of the network to be the geometric mean (square root of the product) of the number of cells that maintain persistent activity for 2500 ms after the cue is removed and the number of cells that would have maintained persistent activity but were turned off by the switching event, normalized such that maximum possible score is 1. Using this metric, network performance as a function of dopamine concentration (where the dopamine effect is indirect by way of its effect on $GABA_A$) exhibits an inverted-U shaped relation, as illustrated in Figure 4.8.

CHAPTER 5

ANALYSIS

To understand the model's behavior, I consider both the properties of the individual cells and the network level effects. Since the simplified single cell model, introduced in Section 2.2.4 with equations in Appendix A.2 forms the basis for both the excitatory and inhibitory cells, I begin by studying that model.

5.1 Simplified Single Cell Model

The simplified single cell model only has two state variables – v and n – and so can be studied via phase plane analysis. Its phase plane is shown in Figure 5.1. Trajectories starting in the shaded region will never cross $v = 0$; thus the shading can roughly be thought of as the points that fail to trigger an action potential, but note that this is not necessarily meaningful if v is initially large. The red curve is the v -nullcline, the set of points where $\frac{dv}{dt} = 0$. If the current state is below the v -nullcline, $\frac{dv}{dt} > 0$, and thus v is increasing, so the state will move to the right on the diagram. Conversely, above the v -nullcline, $\frac{dv}{dt} < 0$, so v is decreasing, and the state moves left. The blue curve is the n -nullcline. To its right, $\frac{dn}{dt} > 0$, so n is increasing and states will move upward on the diagram. To the left, $\frac{dn}{dt} < 0$, so states move downward on the diagram. At the points where the two curves intersect, $\frac{dv}{dt} = \frac{dn}{dt} = 0$, so neither

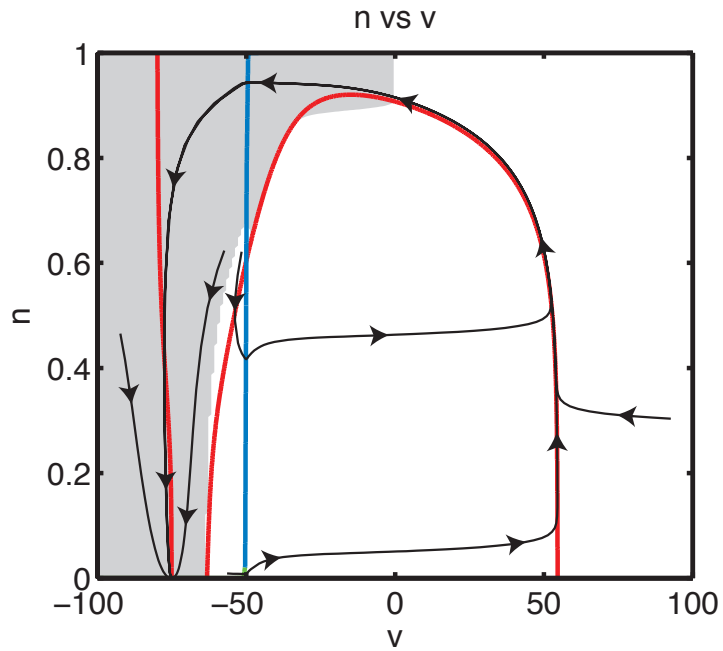


Figure 5.1: Phase plane for the simplified single cell model. The v -nullcline is in red, the n -nullcline is in blue. Sample trajectories are shown in black. The arrows indicate the direction of movement along the trajectory; note that each trajectory approaches the fixed point. The shaded region is the set of initial conditions from which v will never cross 0.

state variable changes over time; these are known as fixed points, steady states, or equilibria.

The stability of this fixed point depends on the nature of the eigenvalues to the Jacobian

$$J = \begin{pmatrix} \partial f / \partial v & \partial f / \partial n \\ \partial g / \partial v & \partial g / \partial n \end{pmatrix} \quad (5.1.1)$$

evaluated at the fixed point (v^*, n^*) , with $f = \frac{dv}{dt}$ and $g = \frac{dn}{dt}$. Numerically, I find that the left-most fixed point of the system is approximately $(v^*, n^*) \approx (-75.116, 1.9278 \times 10^{-14})$ and the eigenvalues of $J|_{(v^*, n^*)}$ are approximately $-.157165$ and $-.359540$. Since both eigenvalues have negative real part, this fixed point is stable; nearby trajectories will approach the fixed point, as illustrated in the phase plane diagram. The other two fixed points are at $(-63.182, 1.4235 \times 10^{-18})$ and $(-49.957, 0.60474)$. The first has eigenvalues $.428964$ and $-.373251$, so it is an unstable fixed point. The second has eigenvalues $2.175835 \pm 13.111964i$, so it is also unstable. (All numbers here are numerical approximations.) Since the last two fixed points are unstable, in practice they will never be observed, so the resting potential of the neuron is $v^* \approx -75.116$ mV.

5.1.1 Excitation

Recall that $C_m \frac{dv}{dt} = -I_{\text{ion}} + I_{\text{app}}$, where I_{ion} is the sum of the ion channel currents. Thus increasing I_{app} raises the value of $\frac{dv}{dt}$ at each point, so the new v -nullcline is at a place where $\frac{dv}{dt}$ was previously negative; that is, somewhere above the old nullcline; see Figure 5.2. If I_{app} is abruptly increased, for example, as the result of receiving excitatory synaptic activity, a state that was at the fixed point is now below v -nullcline, so it begins to move to the right in the diagram. With the slightest movement to the right, it becomes below the n -nullcline and therefore starts to move

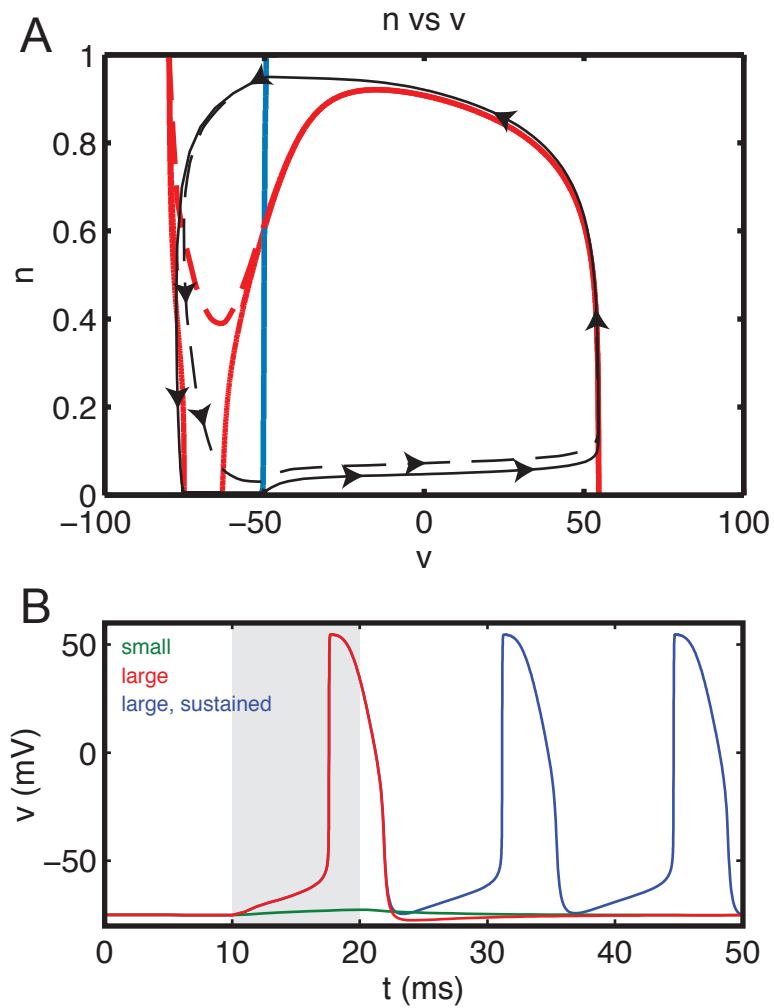


Figure 5.2: The effect of raising I_{app} on the phase plane. (A) Raising I_{app} to 0 raises the v -nullcline from the solid red line to the dashed red line. This triggers an action potential (black trajectory). If the applied current remains elevated, firing becomes periodic (dotted black line). (B) Comparison of effects of brief small increase in I_{app} , brief large increase (to 0 as in A), and sustained large increase to I_{app} . For the brief pulses, the increase was sustained during the shaded time period.

up as well. However, potassium gating occurs on a far slower time scale than changes to the electrical state, so v increases faster than n does. If v changes infinitely faster than n , then the trajectory would move perfectly horizontal to the right until it hits the v -nullcline. Thus if the local minimum is elevated above the old fixed point, there will be a large change in v , while if it is not, then the change will be relatively small. Thus there is a threshold value of I_{app} where the behavior abruptly changes. In the context of a neuron, this is the distinction between firing an action potential and not firing an action potential. If the applied current is restored to its original value, the v -nullcline returns to its original position, and the system approaches the fixed point.

5.2. If, on the other hand, applied current is sufficiently elevated and stays elevated, then the fixed points can lose their stability and become centers, resulting in periodic firing, as shown in Figure 5.3.

5.1.2 Sag Current

A sag current, by definition, is a current that activates in response to membrane hyperpolarization; that is, it activates when the membrane potential is lowered. For this section, consider the excitatory cell model from Section 3.2 and Appendix A.3.

For now, neglect the dynamics of the sag gating variable m_h , and treat it as a parameter. The synaptic gating variable s has no role in the single cell case, and calcium concentration c only affects the dynamics via m_h , so once again the only state variables left are v and n , so phase plane analysis applies.

At rest, the cell is not hyperpolarized so m_h should be low. If $m_h = 0$, then the initial dynamics are the same as for the simplified single cell model, discussed above. Inhibition shifts the v -nullcline lower, causing a trajectory that started from the fixed point to move left and down in the diagram. Hyperpolarization activates the sag current, raising the value of m_h , and thereby admitting a depolarizing current,

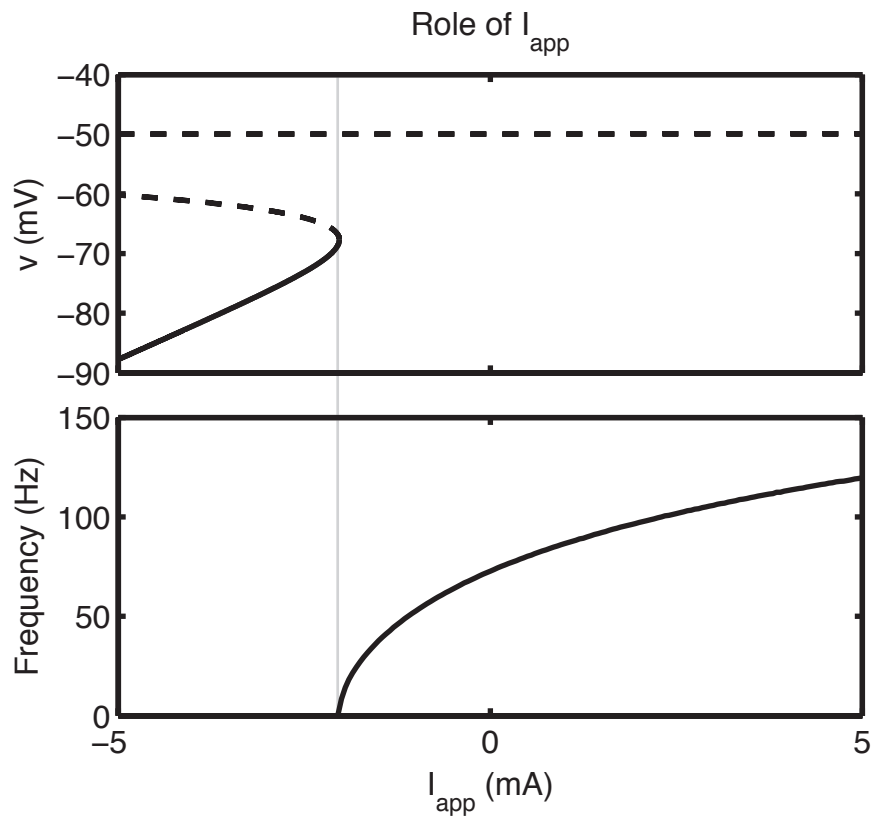


Figure 5.3: Elevated I_{app} leads to periodic firing. The bifurcation diagram is on top; the frequency-current relationship is plotted below. The gray line denotes the location of the SNIC bifurcation.

shifting the v -nullcline up. When m_h is sufficiently elevated, the two left-most fixed points of the system disappear via a saddle-node bifurcation. The state now lies below the v -nullcline, so v begins to increase, triggering an action potential. As the membrane potential rises, the sag current deactivates. This process is illustrated in Figure 5.4.

The sag current half-activation (i.e. $m_h = 0.5$) occurs when $v = \theta_h$, which depends on calcium as shown in Figure 5.5. If the maximum possible value of θ_h , here -84.5 mV, is too high, then the afterhyperpolarization will activate the sag current, leading to periodic firing, as shown in Figure 5.6.

5.2 Noisy Inputs

The working memory system constantly receives input from the rest of the brain, modeled, as described in Section 3.4 by having each excitatory cell receive input from 50 noise sources firing at 5 Hz. I suppose that the synaptic gating variable immediately rises to 1 on an event, stays elevated for 3.5 ms, then begins to decay with time constant 2 ms. This choice is comparable to the behavior of the synaptic gating variables for the excitatory cell, as shown in Figure 5.7.

It will occasionally be useful to compare noiseless and noisy simulations. This cannot simply be done by setting $g_{\text{noise}} = 0$, because the noise provides a depolarizing current, so I adjust I_{app} as well.

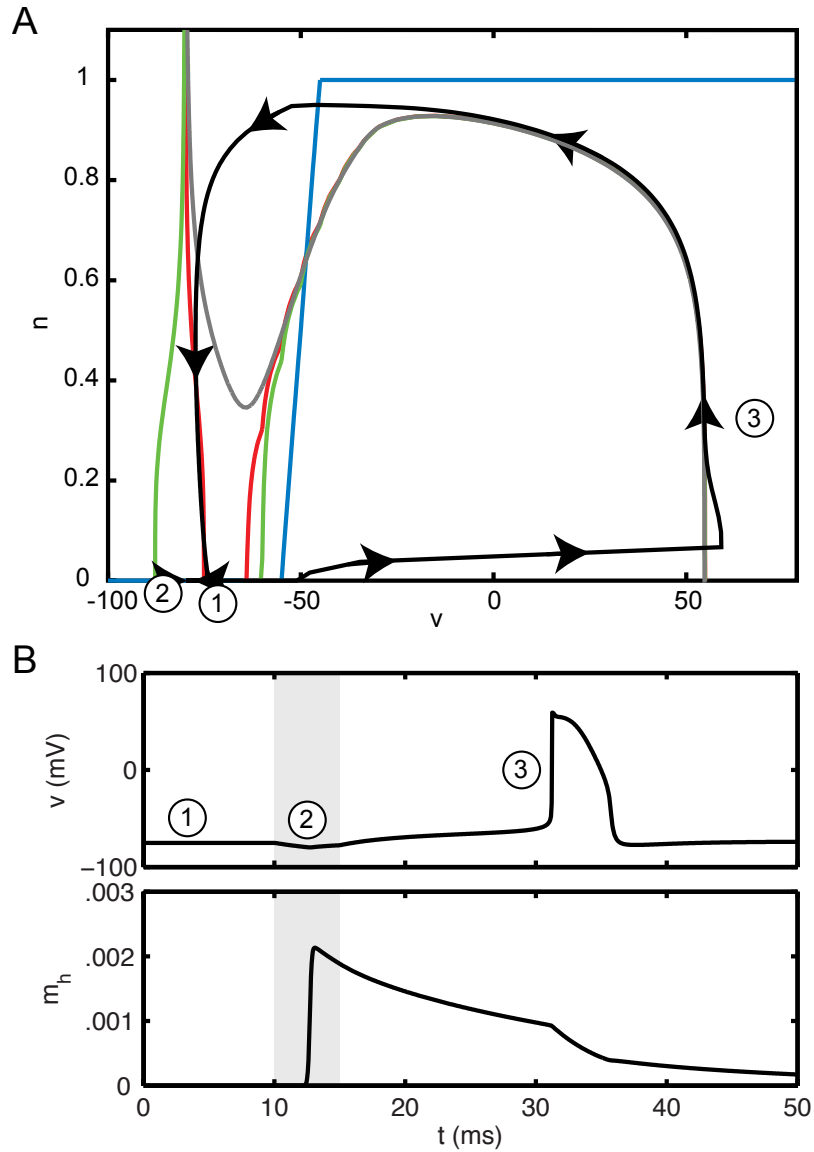


Figure 5.4: The role of the sag current. (A) Phase plane showing idealized dynamics (instantaneous changes in m_h), and a trajectory of the system (black) with a non-calcium modulated m_h , taking $\theta_h = -80$. The blue curve is the n -nullcline; the red, green, and gray curves are the v -nullcline at rest, with inhibition $I_{\text{app}} = -5$, and with $m_h = .004$ and inhibition, respectively. (B) Traces of the membrane potential and sag current gating variable over time in the trajectory shown in (A). Inhibition was applied during the shaded time period.

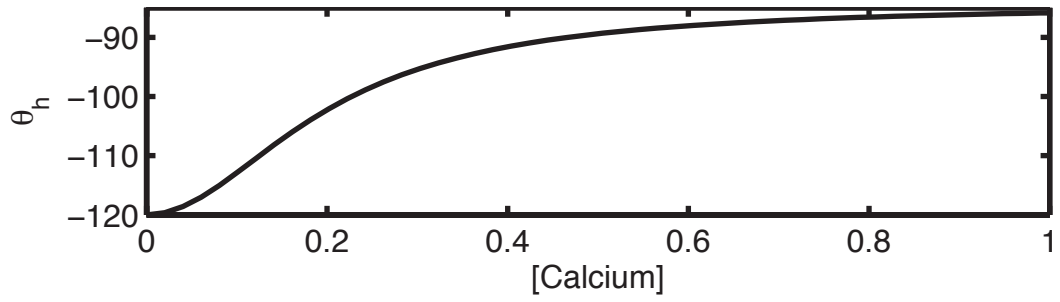


Figure 5.5: Calcium dependence of θ_h .

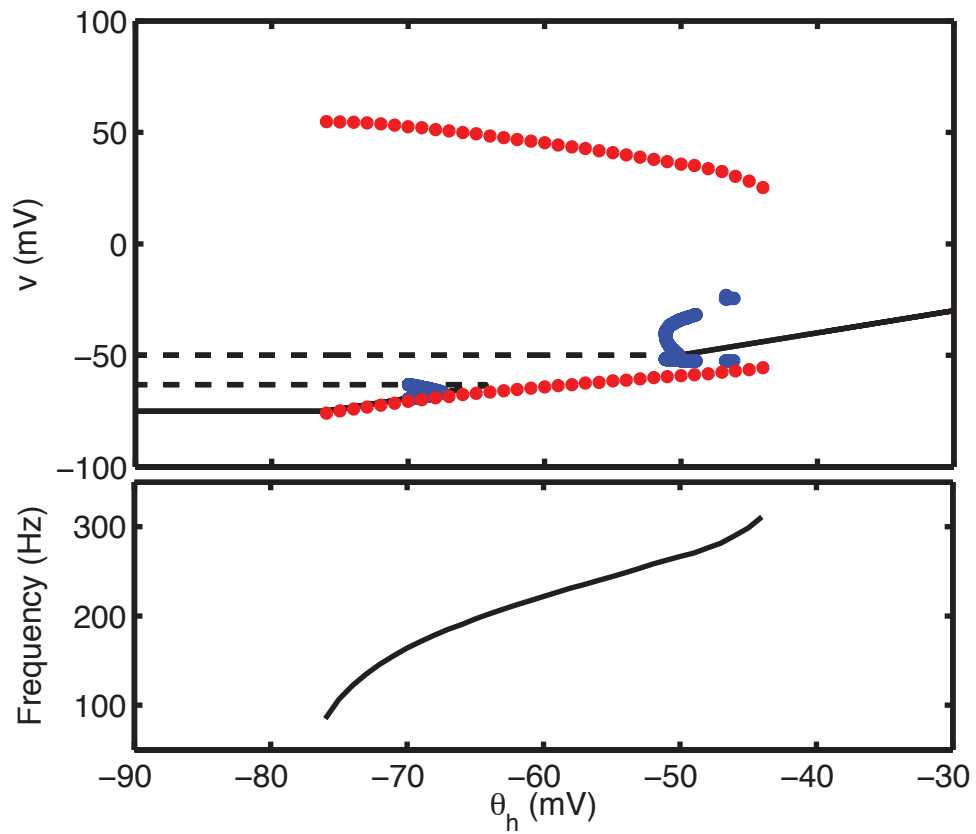


Figure 5.6: High values of θ_h lead to periodic firing. (A) Bifurcation diagram with stable limit cycle extrema in red, unstable limit cycle extrema in blue, stable fixed points as solid lines, and unstable fixed points as dashed lines. (B) Frequency of stable limit cycle as a function of θ_h .

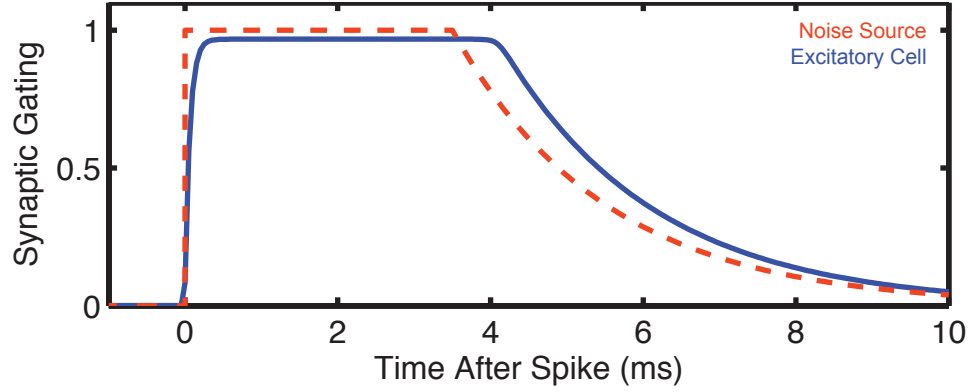


Figure 5.7: Comparison of noise synapse with modeled excitatory synapse. The solid and dashed lines correspond to the excitatory cell and noise source, respectively.

5.2.1 Calculation of Average Noise Input

Each excitatory cell is connected to 50 noise sources firing at 5 Hz with synaptic gating variables of the form

$$s(t) = \begin{cases} 1 & \text{if } t_{\text{spike}} \leq t < t_{\text{spike}} + 3.5 \\ \exp((t_{\text{spike}} - t)/2) & \text{if } t_{\text{spike}} + 3.5 \leq t \end{cases} \quad (5.2.1)$$

The average value of $\sum s$ where the sum is over all the noise sources to a given cell is thus

$$\bar{s} = \frac{5 \cdot 50}{1000} \left(\int_0^{3.5} dt + \int_0^{\infty} \exp(-t/2) dt \right) = 1.375 \quad (5.2.2)$$

The form of the noise current is $I_{\text{noise}} = g_{\text{noise}} \left(\sum s \right) (v - v_{\text{noise}})$ where $v_{\text{noise}} = 0$ mV and $g_{\text{noise}} = .005$. Assuming the average membrane potential is at about -75 mV, that gives an estimated equivalent increment in I_{app} of 0.515625 mA. (Note, due to the sign convention, I_{app} is increased by the opposite of the synaptic input.)

5.2.2 Numerical Comparison

To test the above calculation, I ran single cell simulations with $g_{\text{noise}} = 0$ for varying levels of I_{app} . Input from inhibitory cells was simulated by 15 noise sources each firing according to a Poisson process at 15 Hz. GABA_A synapses decay slower than the excitatory AMPA synapses, so I used the 5 ms decay rate time constant from the inhibitory cell model. At the beginning of each simulation, I presented a strong ($I_{\text{app}} = 2$ mA) cue for 300 ms; this causes the cell to fire, admitting calcium. Since the parameters were chosen (Appendix B.1) to allow the excitatory cells to not activate unless the network is silent or the input is very strong, I wait until after the cue to connect the inhibitory input. I then remove the cue, integrate for 2000 ms, then compute the average calcium concentration over the next 1000 ms. This concentration acts as a measure of the firing rate. I performed this procedure twenty times per data point to account for variations in the inhibitory signal, and averaged the results. In section 5.4, I show that a typical calcium concentration of an excitatory cell in the persistent state is 1.05, which occurs in the noiseless model when $I_{\text{app}} = 3.23$ mA, as shown in Figure 5.8A.

Two major factors contribute to the nearly twelve-fold difference between the analytic figure and the numerical estimate ($3.23 - (-2.8) = 6.03$): First, the noise source is non-constant. Due to the threshold nature of action potential firing, small fluctuations in membrane potential can make a large difference in firing rate. Second, the inhibitory cells do not fire independently; their activity is correlated. Two near-simultaneous applications of inhibition may be sufficient to activate the sag-current, while either one independently would not.

At this high level of applied current, the cell would fire on its own, if not for the inhibitory input. Since the inhibition occurs randomly, it is occasionally weak enough, that it fails to overcome this firing tendency, resulting in a low but nonzero

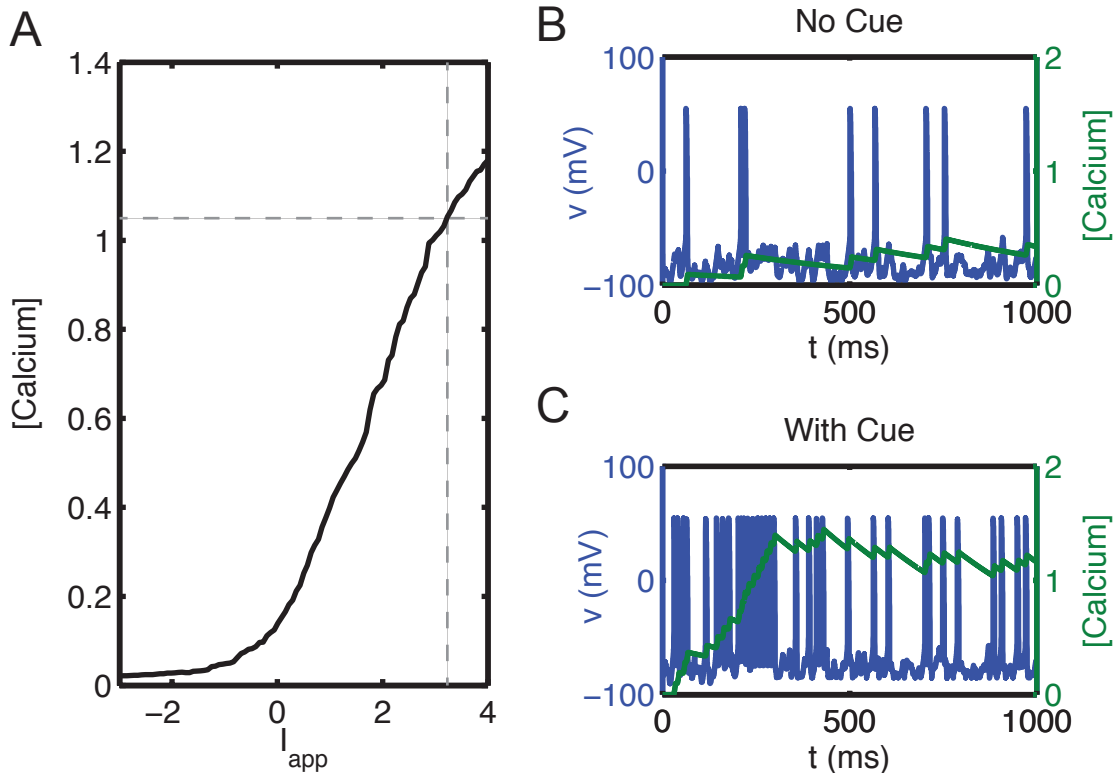


Figure 5.8: Behavior in the absence of external excitatory noise. (A) Average calcium concentration in noiseless cells as a function of I_{app} . The vertical dashed line indicates the applied current corresponding to typical calcium concentrations of network cells during the persistent state. (B) Membrane potential and calcium concentration traces for an excitatory cell with elevated I_{app} as in the dashed line in (A). Without a cue stimulus, the neuron has a low level of firing activity. (C) Same as (B) except a cue was presented for 300 ms, leading to a higher firing rate.

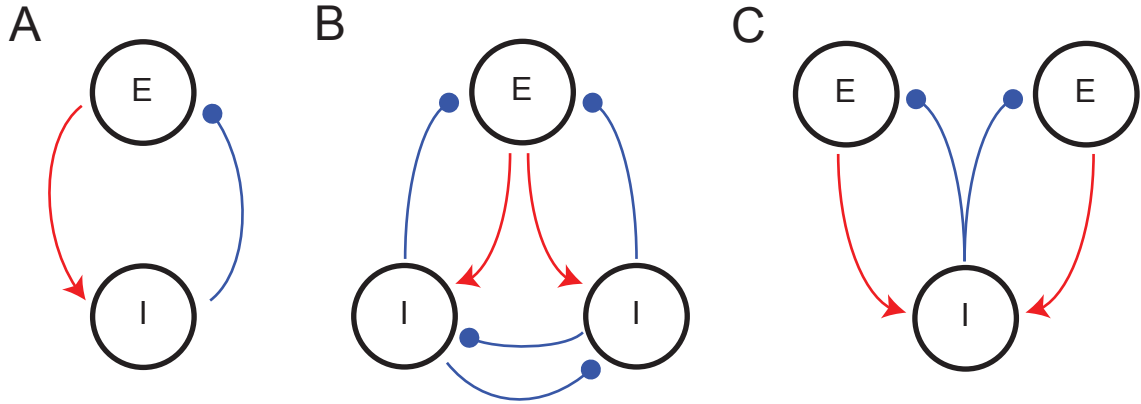


Figure 5.9: Example small network architectures. Arrows denote excitatory synapses; circles denote inhibitory synapses. (A) Two cell network. (B, C) Three cell networks.

firing rate in the absence of calcium. Higher calcium still leads to higher firing rates; see Figure 5.8B and C.

5.3 Small Networks

To get insight into the network behavior, I begin by considering small networks. The parameters for these simulations are adjusted to compensate for the different number of synaptic inputs. The smallest possible excitatory-inhibitory network consists of two cells: one excitatory and one inhibitory. See Figure 5.9.

5.3.1 Two Cell Network

The two cell network (Figure 5.9A) is the simplest possible example of an excitatory-inhibitory network. When a cue is presented to the excitatory cell, it begins to fire. If its calcium concentration rises sufficiently, it will be able to respond to future inhibition by firing action potentials.

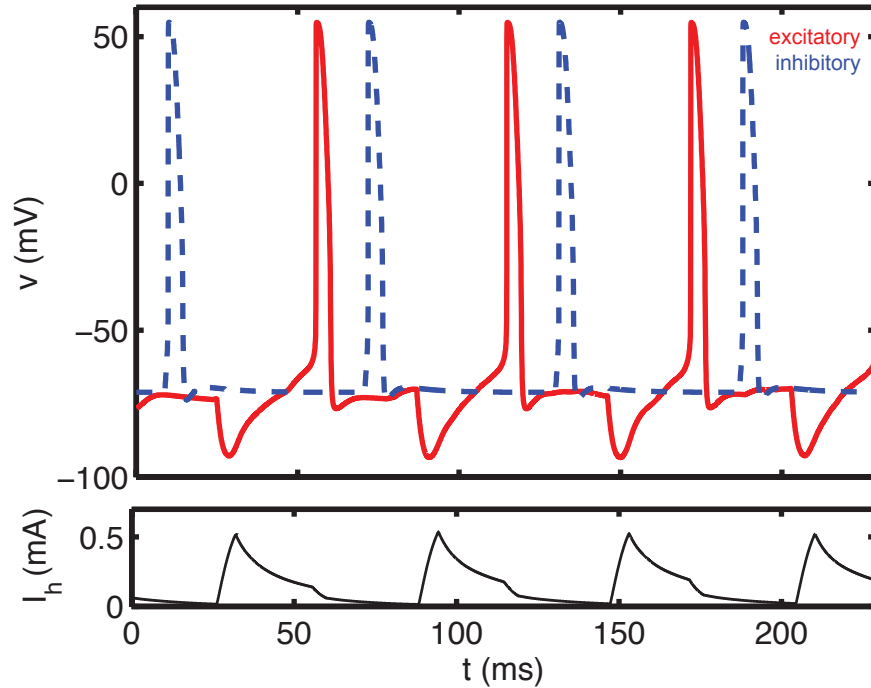


Figure 5.10: Two cell network performance during persistence. In the top figure, the solid and dashed lines are excitatory and inhibitory cell membrane potentials, respectively. The sag current is plotted below. Parameters were the same as for the full model, except $g_{\text{AHP}} = 0$, $g_{\text{syn}} = .4$, $g_{\text{syn},g} = .15$, $g_{\text{h}} = .11$, and delays of 15 ms were used with each synaptic transmission.

Once the stimulus is removed, there are two possibilities: either the last action potential from the excitatory cell triggered a response from the inhibitory cell, or it did not. In the $g_{\text{AHP}} = 0$ case, this is essentially a function of the synaptic conductance strength. (If g_{AHP} is large enough to suppress inhibitory cell activity, then persistent activity will be impossible, since there are no other sources of inhibition.) If the inhibitory cell does not produce a response, or if its response is not strong enough to activate the sag current, network activity immediately ends.

Neither cell is capable of firing spontaneously or of firing more than once in response to the other cell; thus, persistent activity can only be maintained if each cell

responds to every action potential of the other cell. This leads to a very regular high frequency firing pattern, although the firing rate can be slowed by introducing delays in synaptic transmission; these delays correspond to the time required for a signal to propagate along the pre-synaptic cell's axon and through the post-synaptic cell's dendrites. Figure 5.10 shows the cellular interaction during the persistent state.

5.3.2 Three Cell Networks

There are two possible three cell networks where all of the excitatory cells are connected to all of the inhibitory cells in both directions and all the inhibitory cells are bidirectionally connected to each other: networks with two inhibitory cells and networks with two excitatory cells, Figures 5.9B and C, respectively.

In networks with multiple inhibitory cells, each inhibitory cell need not fire on every cycle. In an inhibitory cell, recent activity activates the AHP current which delays subsequent firing activity. If this delay is long enough, other inhibitory cells will fire first, inhibiting the selected cell, blocking its response entirely. In the case of two nearly identical inhibitory cells, this process leads to the inhibitory cells firing on alternate cycles after an initial transient as illustrated in Figure 5.11A. In larger networks, I found that including AHP improves the ability to maintain persistent activity, which I suspect is because this turn-taking phenomenon increases the number of active synaptic connections.

The two excitatory, one inhibitory cell network illustrates the role of past activity in determining present response properties. Each excitatory cell necessarily receives identical inhibitory input, but if one was presented with a cue stimulus and the second was not, the first would have an elevated calcium concentration and therefore respond to inhibitory input with an action potential, while the second would not. This situation is shown in Figure 5.11B.

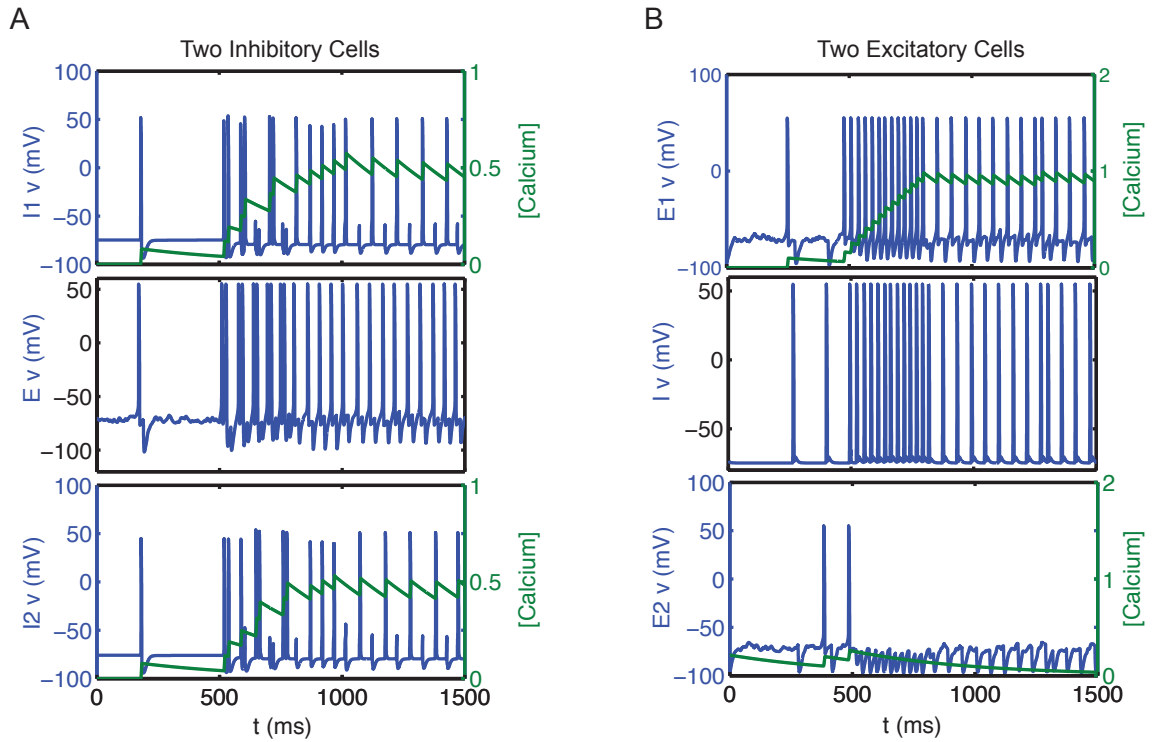


Figure 5.11: Three cell network traces. (A) With two inhibitory cells (top and bottom), the inhibitory cell that fired the most recently will have a stronger AHP current, making it take longer to fire, causing it to be inhibited by the other inhibitory cell. (B) Two excitatory cells (top and bottom) receive the same input from an inhibitory cell, but in the top case, the excitatory cell responds by firing an action potential due to the high calcium concentration, while in the lower case, the excitatory cell is suppressed.

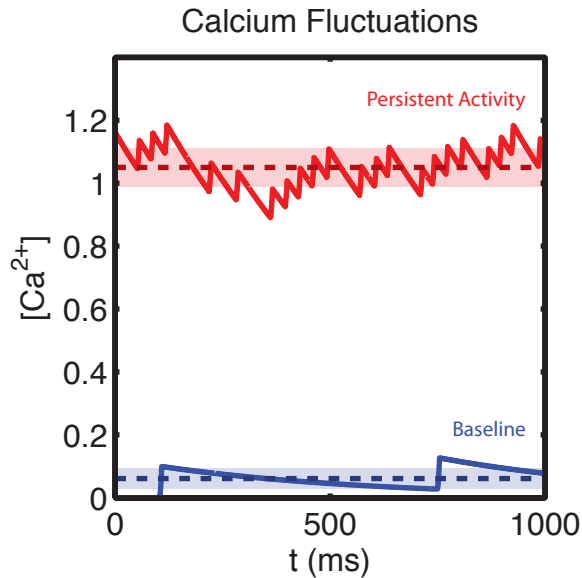


Figure 5.12: Example calcium time courses for cells in the baseline state (blue) and the persistent state (red). Dotted lines indicate the mean value, and the shaded areas are the region within one standard deviation of the mean.

5.4 Calcium and State Discrimination

The fundamental concept motivating this model is that cytosolic calcium accumulates in response to neural activity and that response to inhibitory input depends on calcium concentration. Since the cells fire irregularly, calcium concentration fluctuates significantly over time in both the baseline and persistent activity states, see Figure 5.12.

If this calcium hypothesis is true, then regardless of the mechanisms involved to respond to calcium, in order for both persistence and baseline behavior to be stable, there must be statistically significant differences between the calcium concentrations in the two states. Calcium concentration is primarily a function of the influx and efflux rates g_{Ca} and k_{Ca} as well as the firing rate. For now, I treat g_{Ca} as fixed.

To get excitatory cells to fire at a given frequency, I drive them with a square-wave

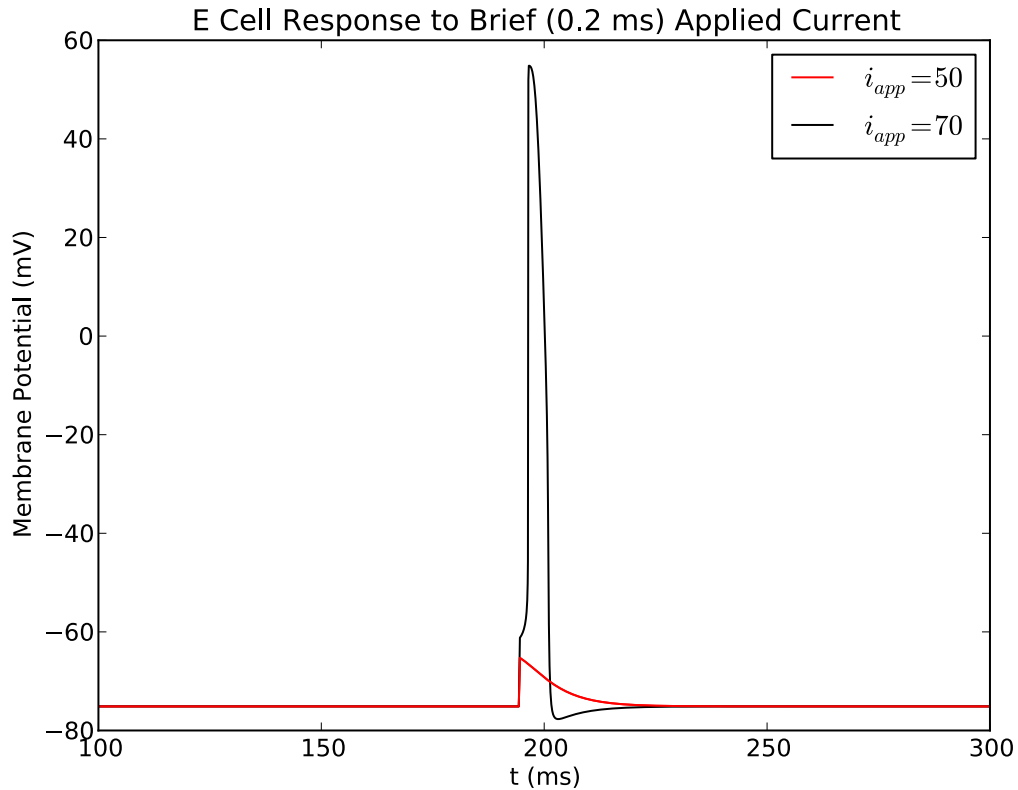


Figure 5.13: Excitatory cell response to 50 mA, 0.2 ms square-wave pulse (red) and 70 mA, 0.2 ms square-wave pulse (black). The weaker pulse fails to trigger an action potential; the stronger pulse succeeds. Note that the duration of the action potential far exceeds the duration of the stimulus.

pulse of 70 mA for 0.2 ms at the desired time points, chosen from a Poisson process. This stimulus was chosen because it is near the threshold for reliably triggering an action potential, see Figure 5.13.

To measure the reliability with which different firing rates can be distinguished from a given baseline rate, taken to be 3 Hz, for various choices of the calcium removal rate k_{Ca} , I take one excitatory cell and compute its corresponding calcium time course for 51,000 ms. The first thousand milliseconds are discarded as an initial transient;

the average and standard deviation are computed for the rest. This procedure was done for all points on a 40×40 grid, where k_{Ca} ranged between 0 and 10, and the firing rate ranged between 1 and 40 Hz.

The significance of variation between the calcium time course at a given firing rate and at 3 Hz was quantified as the ratio between the difference of the average concentrations and the sum of their standard deviations. Thus calcium concentrations that are very different or are very stable (and hence low standard deviation) have larger significance. The higher the significance, the easier it should be for a calcium-based mechanism to distinguish between the two cases.

The results of this investigation are shown in Figure 5.14. Colors denote average calcium concentration. White stripes denote a region where the significance of variation as defined above is less than 1; that is, in the white-striped region, the sum of the standard deviations is bigger than the difference between the averages. A calcium-based model would not be very effective for these $(k_{Ca}, \text{firing rate})$ pairs. In the black-striped domain, the significance lies between 1 and 2, while in the non-striped region, the significance is bigger than 2.

Another perspective on state discrimination as a function of calcium comes from considering the relationship between calcium concentration and activation probabilities. To quantify this, for each of 46 choices of initial calcium concentration, I ran 100 simulations of a single excitatory cell receiving input from a subset of a pool of 30 artificial inhibitory cells firing at 10 Hz, with each inhibitory cell connected with 50 percent probability. In particular, note that the number of inhibitory connections averages 15 but the exact number varies between simulations. To partially compensate for the lack of correlation in the inhibitory inputs, I raised $\theta_{h,\max}$, taking $\theta_{h,\max} = -82$, which makes it easier for the sag-current to activate. The probability that a given excitatory cell is active between 1000 and 2000 ms (defined as firing more

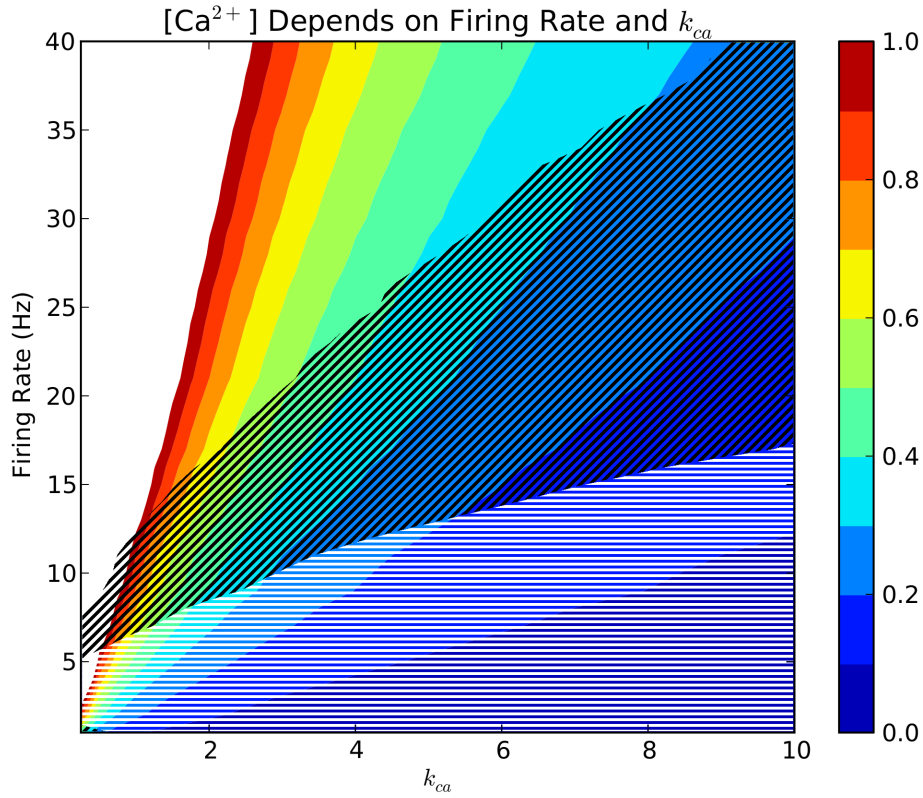


Figure 5.14: Average cytosolic calcium concentration in an excitatory cell in arbitrary units as a function of firing rate and calcium decay, k_{Ca} . Concentration in the white region exceeds 1. In the white striped region, 1 standard deviation about the mean calcium concentration overlaps with 1 standard deviation about the mean for the given k_{Ca} value at 3 Hz. In the black striped region, the overlap occurs between 1 and 2 standard deviations; the rest are more than two standard deviations apart.

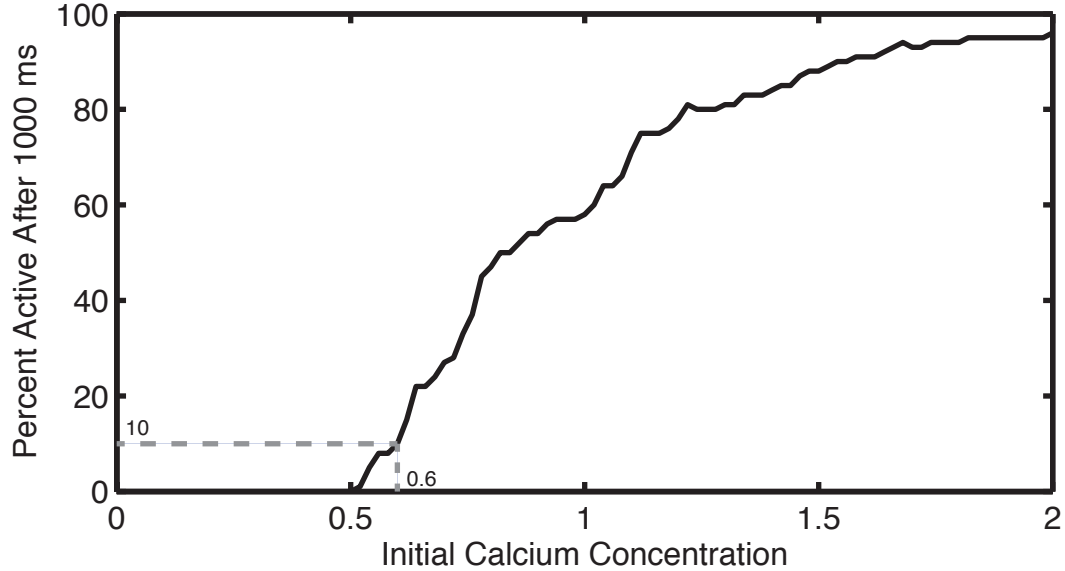


Figure 5.15: Probability of activation as a function of initial calcium concentration.

than 10 action potentials during that time interval) as a function of initial calcium concentration is shown in Figure 5.15.

In particular, note that 10 percent of cells are active 1000 ms after having a calcium concentration of 0.6. As shown in Figure 5.12, a typical calcium concentration for a cell maintaining persistent activity is 1.05. By equation (A.3.3), calcium is cleared with mass action dynamics with rate $\varepsilon k_{Ca} = 0.002$. Thus the time τ for calcium to drop from 1.05 to 0.6 assuming no additional calcium flux satisfies $1.05 \exp(-\varepsilon k_{Ca} \tau) = 0.6$. Solving, we find $\tau = 279.8079$ ms as an estimate for the time an active excitatory cell must be suppressed to be deactivated to allow pattern switching or network shutdown. For 95% probability of not being active, the calcium concentration would need to be lower than 0.54, which would correspond to 332.4882 ms suppression. Note that if a pattern consists of 30 cells, then even with 95% inactivation, on average 1.5 cells will remain active.

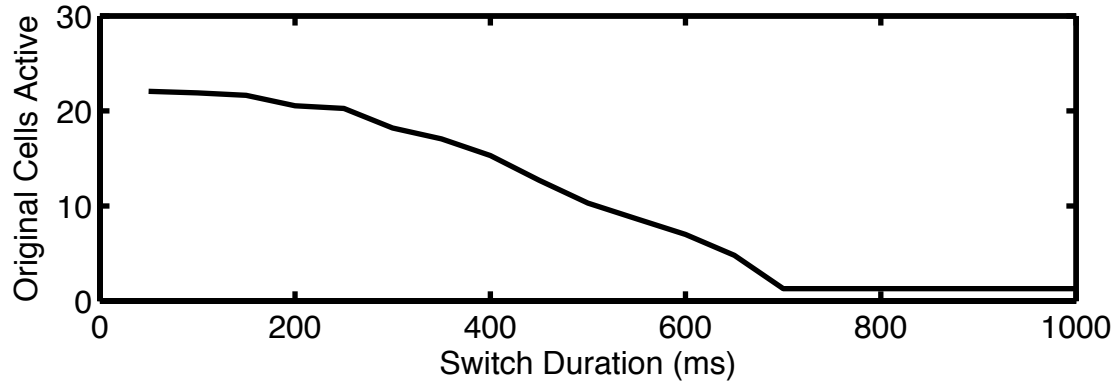


Figure 5.16: Switching effectiveness as a function of distract duration. The vertical axis shows the average number of cells out of 30 of the original pattern still active after the switching event.

In practice, pattern switching in the network model will take longer because the irregular inhibition will not be able to fully suppress the original pattern for a sustained period of time. To test the consequences of this irregular signal, I chose 20 random networks, presented a pattern of 30 cells to each for 300 ms, removed the cue, advanced for another 1000 ms, then applied a strong disjoint distracting pattern for various durations and advanced the entire simulation until 2500 ms after the removal of the cue stimulus. On average 18.2 cells from the original pattern remained on after a 300 ms distractor. With a 500 ms signal, an average of 10.3 remained active, and with a 700 ms distractor only 1.3 were active, on average. The results are summarized in Figure 5.16.

5.5 Excitatory-Inhibitory Interactions

I now consider the dependence on the nature of the excitatory-inhibitory interactions.

5.5.1 Firing Rate

As inhibition drives the excitatory cell activity, the amount of inhibition received by an excitatory cell controls its firing rate. Recall from Figure 5.14 that the firing rate is not merely a question of physiological relevance; if the firing rate during persistent activity is too low, it becomes statistically impossible to reliably identify persistence vs baseline states based on the calcium concentration. Not only does this mean a formerly active cell will eventually lose its elevated calcium and become quiescent, but it also implies that fluctuations due to noise-driven firing have the potential to activate non-pattern cells, further degrading the pattern.

Inhibitory input is a multi-dimensional value. For simplicity, I suppose that spike times are generated according to a Poisson process with each source cell firing at the same rate. Three independent parameters remain: the firing rate, the number of connected cells, and the strength of each of these connections. Two cells firing at 5 Hz are not equivalent to one cell firing at 10 Hz: with each spike, a cell applies a fixed current to the post-synaptic cell. Thus the peak theoretical current flow from two cells is double the effect of one cell. Since the sag current requires strong inhibition to activate, synchronized low frequency firing is more effective than unsynchronized higher frequency firing. Likewise, doubling the number of presynaptic cells is not equivalent to doubling the connection strength, because the latter is equivalent to the new cells being in perfect synchrony with the old.

To study the role of the number of synaptic connections and their strengths, I considered the firing rate of the inhibitory cells fixed at 15 Hz, and chose values for the remaining two parameters. I simulated an excitatory cell connected to the chosen number of artificially firing inhibitory neurons. I presented a strong cue (10 mA) for 500 ms to build up an elevated calcium level and then measured the average firing rate ($1000 / \text{average ISI}$) and duration of persistence. For each of the parameter choices,

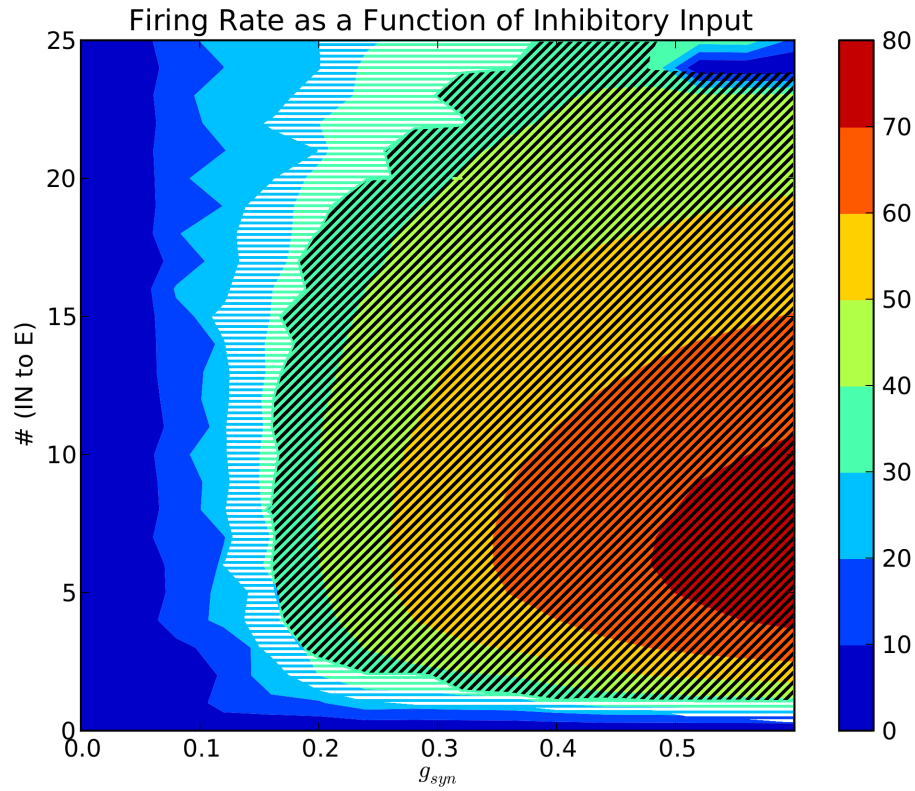


Figure 5.17: Firing rates and duration of persistent activity are functions of inhibitory input. Median firing rates are shown by color in Hz. White stripes indicate regions where persistent activity is maintained for a median duration between 1,000 and 10,000 ms; diagonal stripes indicate regions where persistent activity is maintained beyond 10,000 ms. Here the IN cells are assumed to be firing at 15 Hz.

I ran 25 such simulations and averaged the results. If the connection strength is too low, then no matter how many inhibitory cells are connected, the excitatory cell will not be able to maintain persistent activity. Persistence performance exhibits an inverted-U shaped relationship with both the firing rate and the number of inhibitory cells. If the parameters are too small, then the sag current fails to activate; if they are too high, then the inhibition suppressed the excitatory cell activity. The results are summarized in Figure 5.17.

5.5.2 Connection Probabilities in Networks

In the full network, as the percentage of inhibitory cells attached to each excitatory cell increases, the firing rate again increases. As the input becomes more consistent, the cells synchronize and fire faster and more rhythmically, resulting in a lower CV. Due to the synchrony, even with full connectivity, the inhibition is not consistent enough to suppress persistent activity. Robustness to distractors improves with an increase of inhibitory to excitatory connections because this increase causes a greater difference in baseline and persistent state inhibition. Switching performance, however, is degraded as the old patterns become more likely to reactivate following suppression due to the increase in inhibitory input. Increasing the probability of excitatory to inhibitory connections and decreasing the probability of inhibitory to inhibitory connections both serve to increase the inhibition received by excitatory cells, and therefore produce similar effects in all five metrics.

To quantify these effects, I ran 20 full network simulations for 11 choices of connection probability for each of the three types of conductances, computed their performance in each of the five metrics and averaged the results, as shown in Figure 5.18.

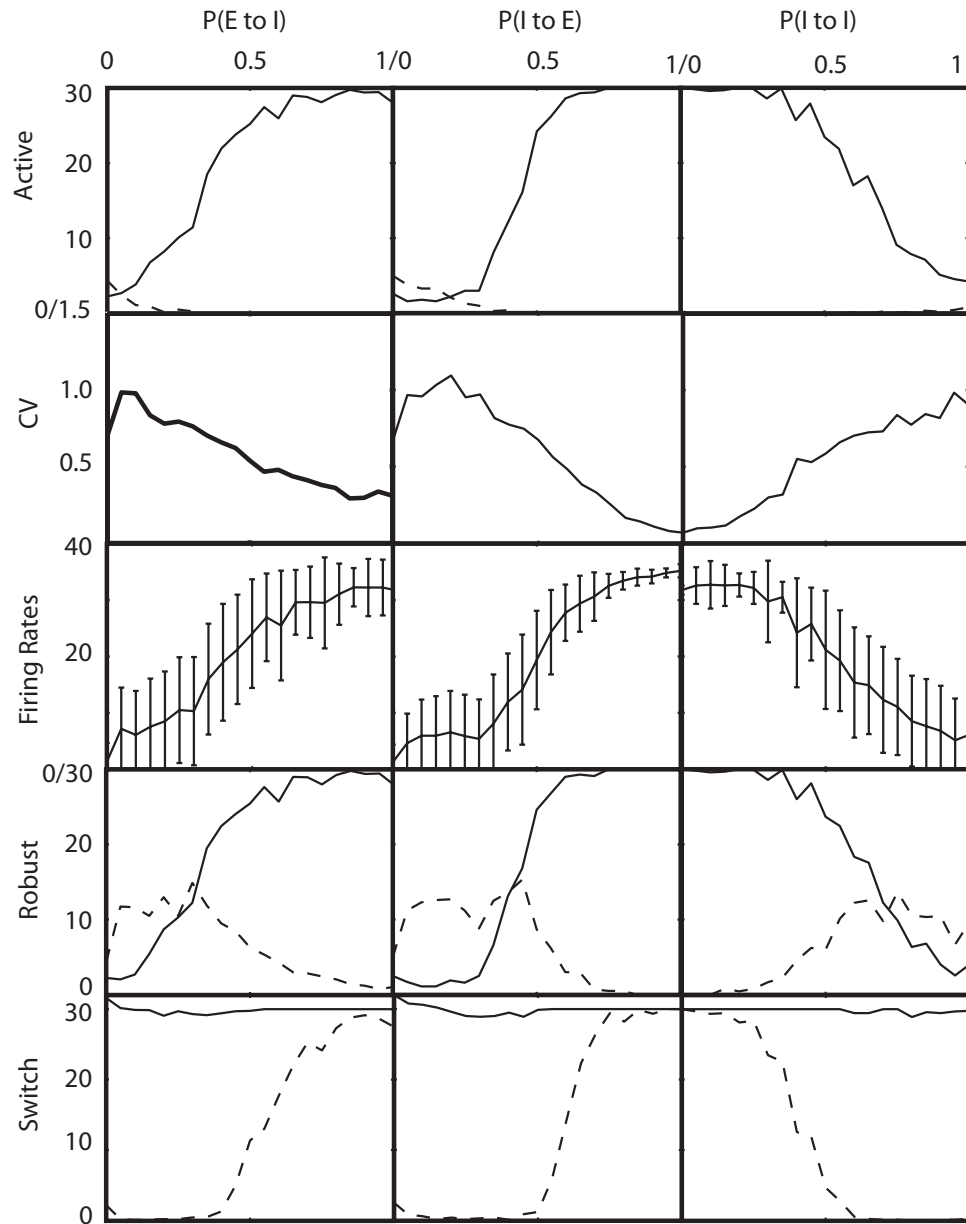


Figure 5.18: Network statistics as functions of connectivity. For the activity rows (active, robust, switch), solid lines indicate the number of active cells belonging to the pattern; dotted lines indicate the number of active cells not belonging to the pattern. Error bars on the firing rate figures denote one standard deviation.

5.5.3 Rebound

In the two cell network (Figure 5.10), only one cell provided inhibition, so the membrane potential traces are very smooth; it is clear that inhibition precedes the excitatory cell activity. In a large network, the inhibitory input is much less regular; the excitatory cells frequently receive subthreshold inhibition, including after the activation of the sag current.

To see the role of inhibition coincidence in large networks, I ran a network simulation and considered the spike-triggered-averages of membrane potential, sag current, and synaptic current for a particular neuron. That is, for all 53 times it fired an action potential, I averaged the traces for each of these variables over the preceding 30 ms. I found that the total inhibition peaked around 25 ms prior to a spike and that the sag current peaked about 13 ms before the action potential.

5.6 Rhythmicity and Irregularity

Some models of working memory [Brunel 01] achieve a coefficient of variation (CV) of their interspike intervals near 1 by careful balancing of excitation and inhibition combined with abundant near 1 CV external noise sources. In these models, the combination of network activity and irregular noise input are necessary to trigger action potentials, which are then themselves distributed very irregularly.

The current model, by contrast, generates its own irregular activity as a consequence of the excitatory and inhibitory cell interactions. In the absence of noise, additional applied current is necessary to compensate for lack of the net depolarizing effect from the noise, but in simulations beginning with a 300 ms cue, with the appropriate choice of I_{app} persistent activity is maintained for the following 1000 ms with a CV well over 0.5, on average. See Figure 5.20.

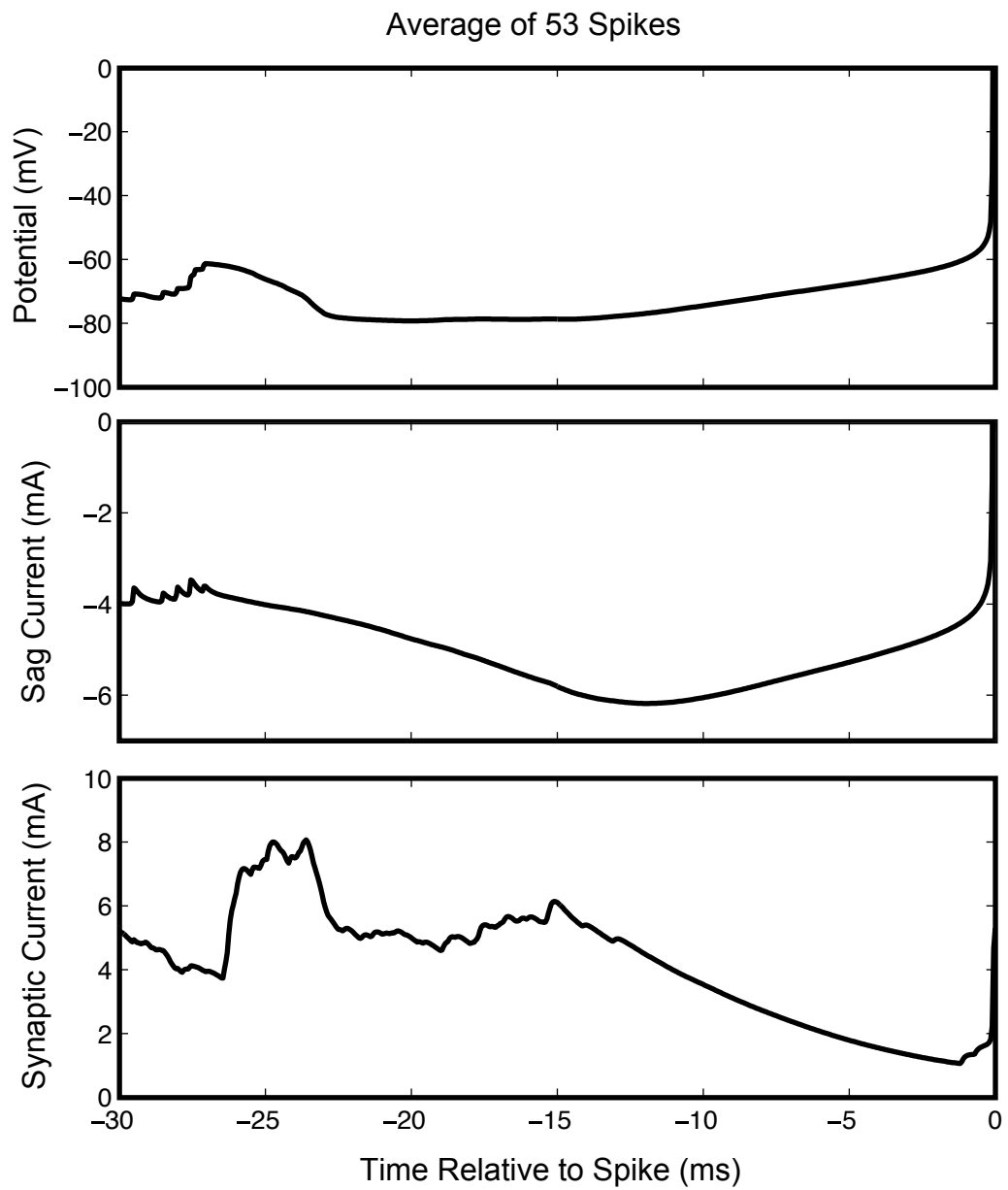


Figure 5.19: Spike-triggered averages reveal the role of inhibition coincidence in triggering activity. Recall that negative current causes an increase in membrane potential.

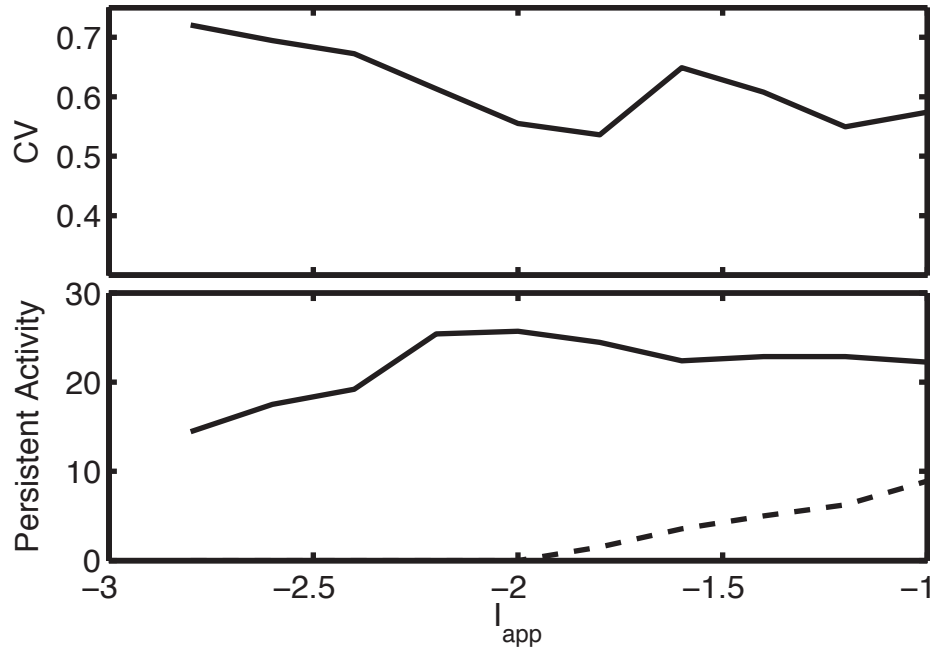


Figure 5.20: Network performance in a noiseless simulation, as a function of I_{app} . The solid line in the activity plot denotes the number of pattern cells active 1700 ms after the end of the cue (defined as having fired an action potential within the previous 200 ms); the dotted line denotes the non-pattern cells active at that time. Each data point is based on the average of 20 simulations.

The working memory system is not completely irregular, however. Experimental evidence shows that the field potential exhibits a gamma rhythm during the performance of working memory tasks [Pesaran 00, Tiesinga 09].

To measure the relationship between regularity, irregularity, and the maintenance of persistent activity, I ran 100 different networks with the standard parameter set. For these tests, I defined a cell maintaining persistent activity to be a cell that fires an action potential between 2300 and 2500 ms after the removal of a cue stimulus. More successful maintenance of persistent activity was correlated with lower CV ($r^2 \approx 0.403229$) and higher firing rate ($r^2 \approx 0.713721$) but uncorrelated with field potential frequency ($r^2 \approx 0.0701306$). High firing rates were correlated with low CVs ($r^2 \approx 0.662122$). The results are summarized in Figure 5.21. The CV measure used here is the CV of the combined interspike intervals of all of the trained cells; this measure is correlated with the mean of the CVs for the individual cells with $r^2 \approx 0.75298$.

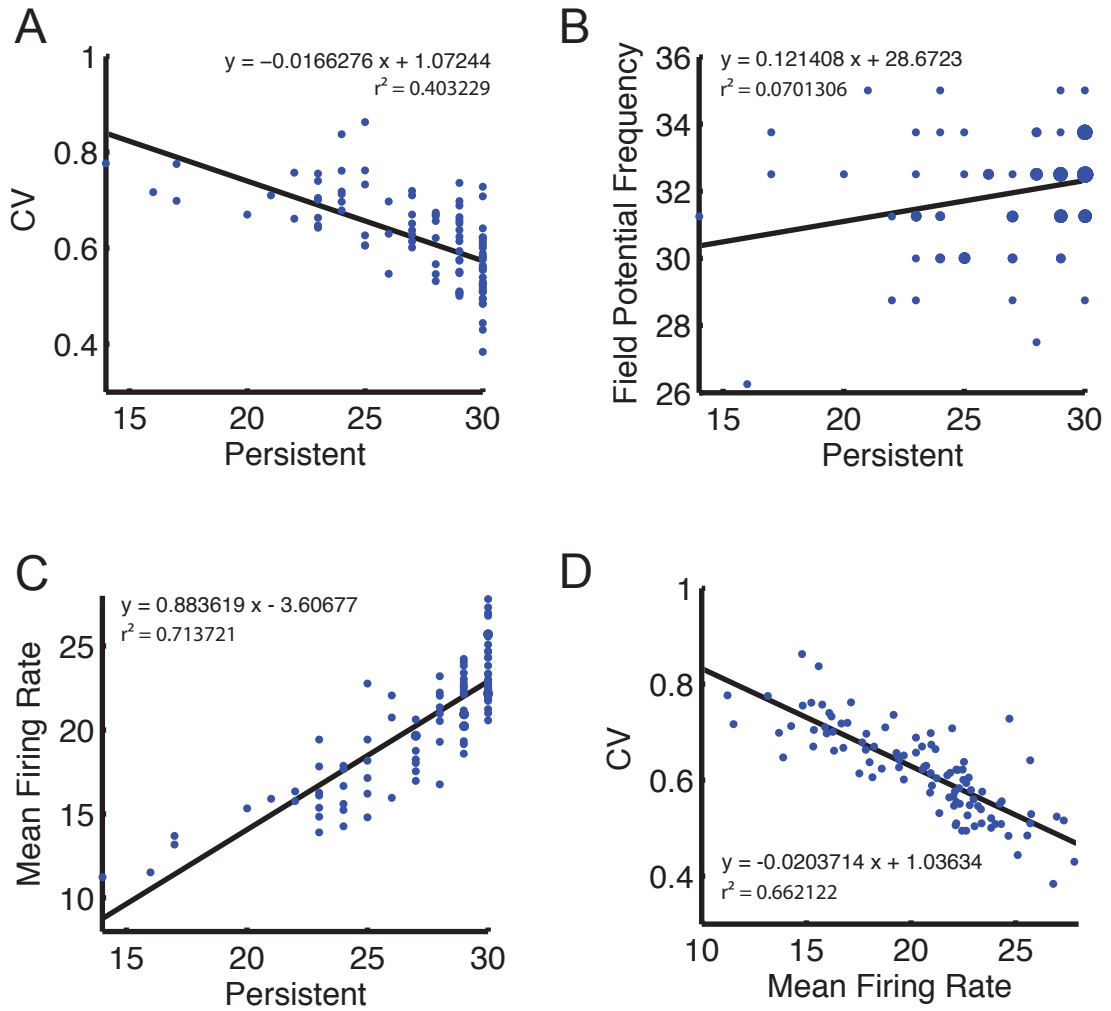


Figure 5.21: Scatter plots of performance metrics, showing least squares solution and r^2 values. Figures represent 100 simulations with the standard parameter set. Area of each point is proportional to multiplicity.

CHAPTER 6

CALCIUM WAVES

The model as presented in Chapter 3 treats cytosolic calcium, along with all the other state variables, as being uniform throughout the cell. It assumes calcium increases with each action potential and is cleared exponentially. The reality is more complicated: calcium distribution is non-uniform. Calcium is an important second messenger molecule [Kretsinger 80] and is heavily regulated by the cellular machinery.

The endoplasmic reticulum permeates the dendrites and acts as a calcium store. Its SERCA pumps constantly extract calcium from the cytosol. When triggered by InsP_3 , it releases some of this calcium back into the cytosol. Regions of elevated calcium then spread throughout portions of the dendritic tree, as observed in [Ross 05]. A model of this behavior was introduced in Section 2.2.6, and the full equations are listed in Appendix A.5.

The working memory model considered here uses a very simple model of calcium dynamics to make the individual excitatory cells bistable. The ER allows the calcium to be bistable as well.

6.1 Active Dendrites and Calcium Wave Initiation

The key question then is what is necessary to setup the system to create the bistability. Does an individual metabotropic glutamate receptor produce enough InsP_3 to trigger

and sustain a calcium wave, or does the InsP_3 need to be amplified and spread in a wave itself? What is the role of the back-propagating action potentials?

The theory that a wave of InsP_3 may accompany a calcium wave was first proposed in [Fall 04, Wagner 04] in the context of the calcium wave accompanying the fertilization of *Xenopus* oocytes.

Experimental evidence suggests that back-propagating action potentials temporarily elevate dendritic calcium levels [Berridge 98, Hong 07]. This change is very brief; the calcium is quickly cleared by either being pumped back into the extracellular space or by being absorbed in internal organelles like the mitochondria. Since glutamate stimulation typically does not trigger a calcium wave unless the neuron was recently active [Moore 09, Sidiropoulou 09], it is theorized [Berridge 98] that the calcium admitted by back-propagating action potentials serves to prime the ER, increasing its sensitivity to InsP_3 .

The working memory model of [Fall 06] uses a combination of ER calcium dynamics and calcium influx as a response to action potentials to maintain elevated calcium levels and thereby persistent activity. Their model was a firing rate model with no explicit ion channels and no concept of space.

In 2003, Poirazi et al [Poirazi 03] published a very detailed spatial model of a CA1 pyramidal neuron, complete with a non-uniform distribution of many types of ion channels.

I started with their model, then deleted all of the neuron except for a continuous portion of the apical trunk; see Figure 6.1. I inserted ER calcium dynamics as defined in Appendix A.5. InsP_3 was permitted to diffuse freely, but no degradation or production was modeled.

Periodic back-propagating action potentials were initiated by periodically instantaneously depolarizing the dendrite near the somatic end.

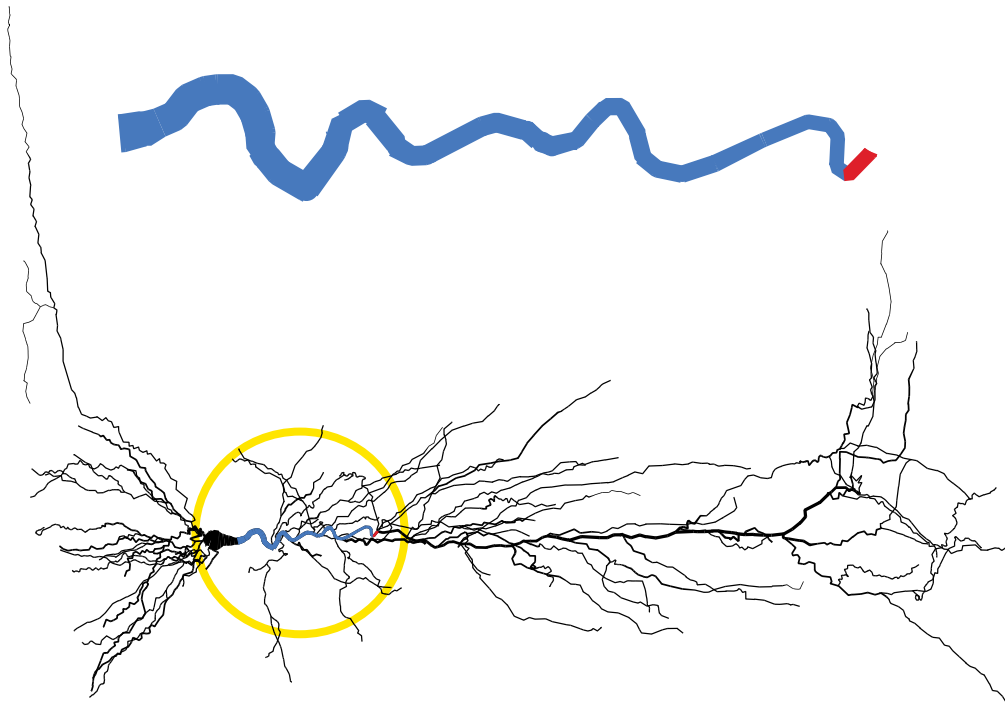


Figure 6.1: Dendrite cutting, showing its location on the CA1 pyramidal neuron of Poirazi et al [Poirazi 03]. The red region denotes the location where InsP_3 will be administered to trigger a calcium wave in some of the experiments.

Effects of BPAPs on Calcium Concentrations

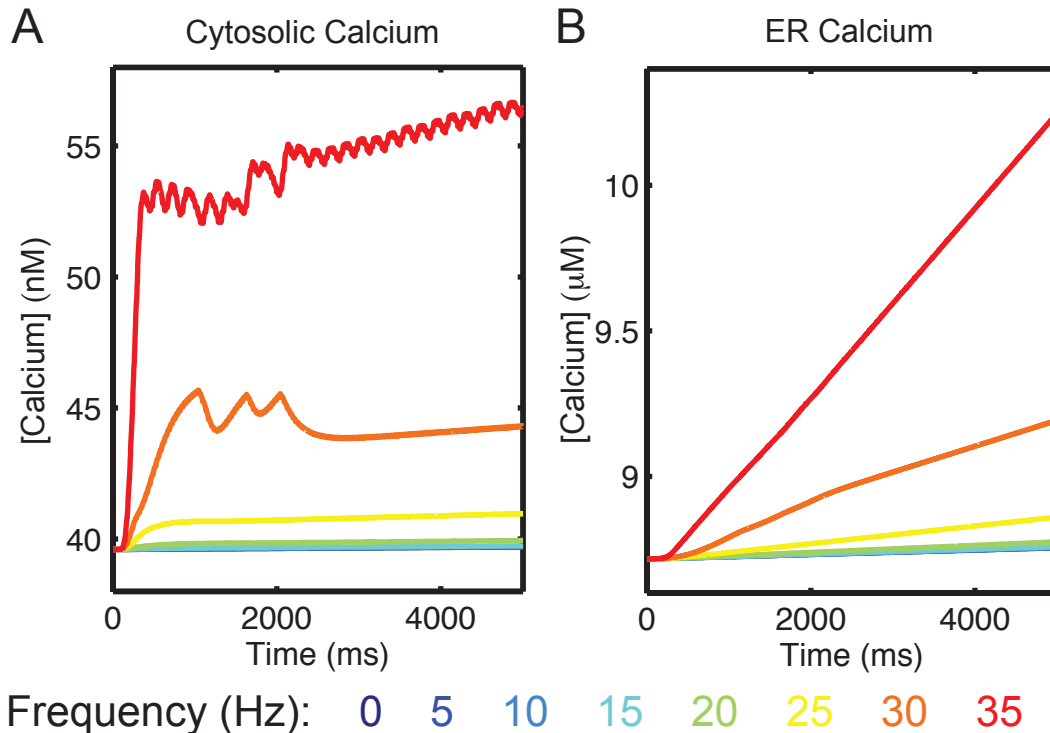


Figure 6.2: High firing rates lead to elevated internal calcium concentrations. Note the scale on the vertical axis for cytosolic calcium (A) is in nM while the corresponding axis for ER calcium (B) is in μM . The curves for many of the lower frequencies overlap.

Regardless of the driving frequency, the calcium will always enter no faster than the rate it would enter if the channels were fixed open. As long as this maximum is low enough, the cell will be able to pump out the calcium and prevent back-propagating action potentials from triggering a calcium wave on their own. Indeed, in the parameter regime tested, back-propagating action potentials were never sufficient to initiate a calcium wave. The effects of firing rate on calcium concentrations is

shown in Figure 6.2. Concentration was measured at the point farthest from the soma.

I then applied various concentrations of InsP_3 on the non-somatic side and used the method of bisection to locate the minimum amount of InsP_3 necessary to trigger a calcium wave for each firing rate. The threshold InsP_3 level is initially almost constant for low firing rates, but beyond a certain rate, it drops dramatically. The results of this experiment are summarized in Figure 6.3.

6.2 Role of Geometry

The reaction diffusion equations governing calcium dynamics apply only within the dendrite, with Neumann boundary conditions along the plasma membrane when neglecting ion channel contributions. The dendrites of an actual neuron twist and turn, as in the reconstruction of the CA1 pyramidal neuron from [Poirazi 03] in Figure 2.1. The three-dimensional structure is complex with many branches and turns; in a rat, the dendrites of the corresponding cell type have a combined length of $11,900 \pm 1,000 \mu\text{m}$ [Bannister 95]. To study how this geometry influences the propagation of calcium waves, I consider five two-dimensional analogs for dendritic-like geometry, illustrated in Figure 6.4: a straight dendrite, a curved dendrite, an abrupt opening, a gradual widening, and a branch point.

To avoid issues unique to the specific choice of calcium model, I consider simpler dynamics with only one variable:

$$u_t = \Delta u - u(1-u)(\alpha - u), \tag{6.2.1}$$

with $0 < \alpha < 1$.

By inspection, this equation has three constant solutions: $u = 0$, $u = \alpha$, and $u = 1$. The $u = 0$ and $u = 1$ solutions are stable; the $u = \alpha$ solution is unstable. The

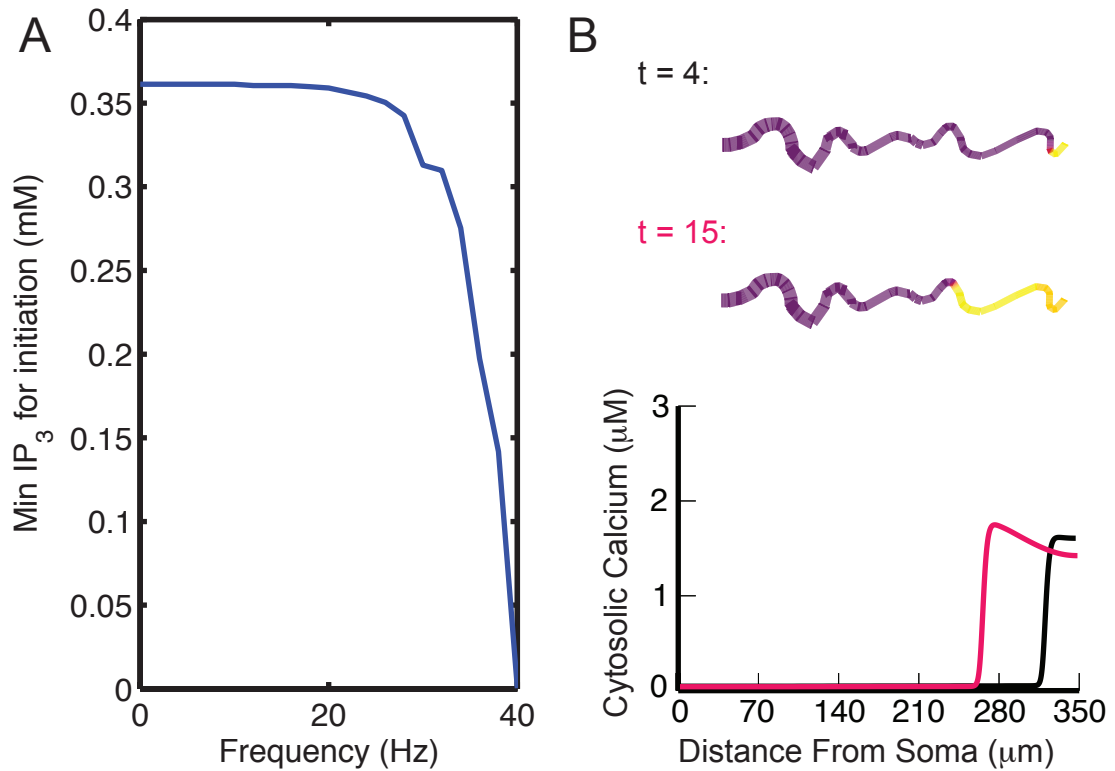


Figure 6.3: Electrical activity facilitates calcium wave initiation. (A) Relationship between firing rate and amount of IP_3 necessary to trigger a wave. (B) Example wave at two time points, as seen on the dendrite's geometry (top) and as a function of distance from the soma (bottom). In the top part of (B), yellow indicates regions of elevated calcium concentration. Time is in arbitrary units; biologically these waves travel at $26 \pm 2 \mu m/sec$ [Power 02].

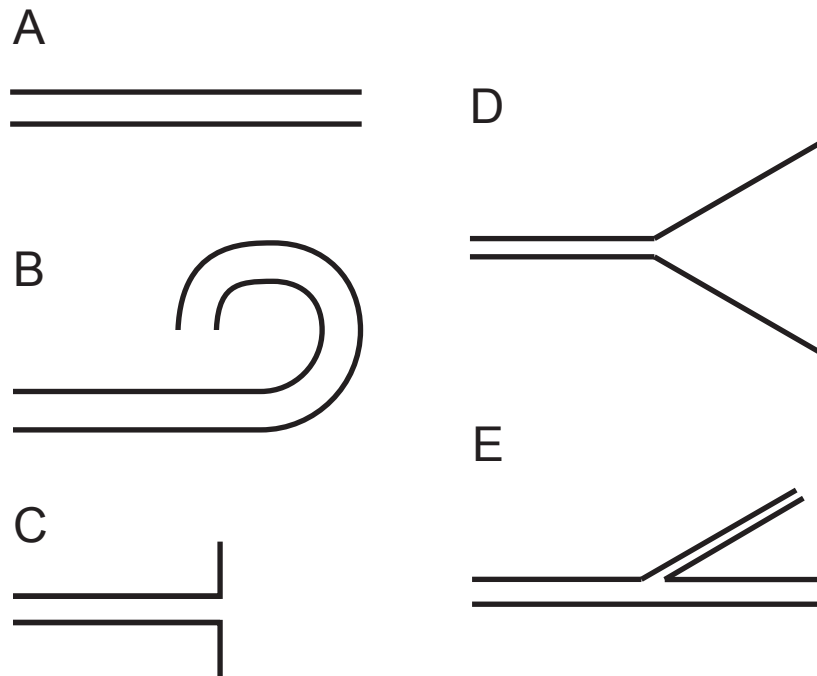


Figure 6.4: Two dimensional dendritic-like geometries. (A) Straight dendrite. (B) Curved dendrite. (C) Abrupt opening (e.g. soma). (D) Gradual widening. (E) Branch point.

simulations in this section were performed using Virtual Cell [Loew 01] or MATLAB's PDE Toolkit.

6.2.1 Straight and Curved Dendrites

The equation (6.2.1) admits a non-constant traveling front solution, that is, a solution of the form $u(x, t) = U(x - ct)$ with velocity $c = \sqrt{2} \left(\frac{1}{2} - \alpha \right)$ such that $\lim_{\xi \rightarrow -\infty} U(\xi) = 1$ and $\lim_{\xi \rightarrow \infty} U(\xi) = 0$. This result is well known in the literature, see for example [Fife 79], but the proof is brief and follows.

Consider for a moment instead the separable equation

$$\phi' = -b\phi(1 - \phi), \tag{6.2.2}$$

Notice that

$$\begin{aligned} \phi'' &= -b\phi(-\phi') + (1 - \phi)(-b\phi') \\ &= b\phi\phi' - b\phi' + b\phi\phi' \\ &= 2b\phi\phi' - b\phi' \\ &= 2b\phi'(\phi - 1/2) \\ &= 2b\phi'(\phi - \alpha - (1/2 - \alpha)) \\ &= 2b\phi'(\phi - \alpha) - 2(1/2 - \alpha)b\phi' \\ &= -2b^2\phi(1 - \phi)(\phi - \alpha) - 2(1/2 - \alpha)b\phi'. \end{aligned}$$

Thus if we let $A = 2b^2$ and $p = 2b(1/2 - \alpha)$, we find ϕ satisfies

$$\phi'' + p\phi' + A\phi(1 - \phi)(\phi - \alpha) = 0. \tag{6.2.3}$$

Note that U satisfies $U'' + cU' - U(1 - U)(\alpha - U) = 0$. Thus, working backwards, it follows that the wave-speed of (6.2.1) in the one-dimensional case is $c = (1 - 2\alpha)/\sqrt{2}$. (Since (6.2.2) is separable, one can also find an explicit formula for U , but it is not needed here.)

If a wave is uniform in all but one spatial dimension, then the wave dynamics are identical to the one-dimensional solution. In a straight dendrite with reflecting (Neumann) boundary conditions, the cross-sections are small compared to the length, so they equilibrate quickly and the wave is essentially one-dimensional.

Furthermore, my numerical investigations using Virtual Cell revealed only minor slowing in wave speed when propagating around a curve.

6.2.2 Abrupt Opening

Abrupt openings, by contrast, have been analytically proven to have drastic consequences for wave propagation [Chapuisat 05]: if the original source is too small and the wider area too large, then wave propagation will stall. This is of biological interest as the soma is far bigger than the dendrites. Calcium waves that enter the soma have the potential to regulate gene transcription.

An example of a stalled bistable wave at an abrupt opening is given in Figure 6.5. The contours are not quite circular due to the width of the source region. We show both horizontal and vertical profile views of the concentration along the coordinate axes. The right half-plane by itself supports an unstable radially symmetric stationary solution, shown for comparison purposes in the lower-right graph. The x -axis denotes the distance from the origin. Negative values are included to illustrate the symmetry. For each simulation that I tried, stalling waves have a value at the origin (the location of the maximum value in the right half plane) less than that of the radially symmetric stationary solution. As the source radius increases, the maximum value in the right half plane increases. It appears that this value gets arbitrarily close to that of the radially symmetric case as the source radius approaches the critical size for wave propagation.

The eikonal equation implies that for an infinitely sharp wavefront, $v = c - D \kappa$

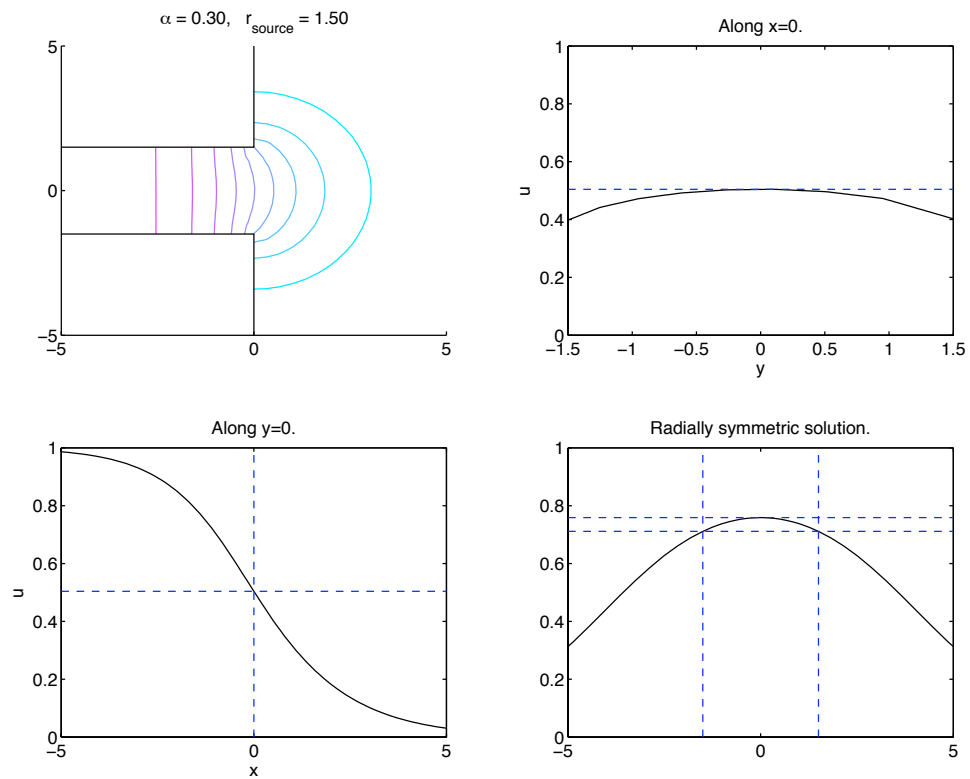


Figure 6.5: A close inspection of a stalled bistable wave reveals the nature of the stationary solution. Here we take threshold value $\alpha = 0.30$ and source radius $r = 1.50$. Contour lines for u -concentration are shown, from the left as $u = 0.9, u = 0.8, \dots, u = 0.1$.

where v is the local velocity of the front, c is the velocity of a plane wave, D is the diffusion constant, and κ the local curvature of the front. This formula provides one strategy for experimentally estimating the diffusion constant [Lechleiter 91].

Strictly speaking, this curvature-velocity formula does not apply since the wave front is not infinitely steep, but I use it to provide an estimate for the blocking source radius. Wave blocking implies the existence of a stationary solution, that is, one where $v = 0$. In equation (6.2.1), $D = 1$, so that implies $c = \kappa$ at all points along the front. That is, the front would be an arc of a circle of radius $1/\kappa = 1/c$. In particular, if the source has width greater than $1/c$, then no such arc can be drawn to block the entire front. Thus, if the source has width greater than $1/c$, the wave will propagate into the half-plane.

The group that proved the existence of waving blocking later published a numerical study to locate the threshold between wave propagation and wave blocking [Dronne 09]. Their equation was scaled differently, but otherwise I performed the same numerical study.

I then compared my results to the eikonal prediction. As expected, all of the threshold widths were less than $1/c$. I wanted to see how these widths compared with $1/c$, so I plotted the ratio as a function of α , and found the relationship was very nearly linear. Taking the line of best fit, the threshold radius $r_{\text{threshold}}$ satisfies

$$r_{\text{threshold}} \approx \frac{2.0016\alpha - .0265}{c} \tag{6.2.4}$$

or simply $r_{\text{threshold}} \approx \frac{2\alpha}{c}$. The results are summarized in Figure 6.6.

Additional Threshold Evidence

As an alternative to the continuous bistable equation, consider the piecewise linear PDE

$$u_t = \Delta u - u + H(u - \alpha), \tag{6.2.5}$$

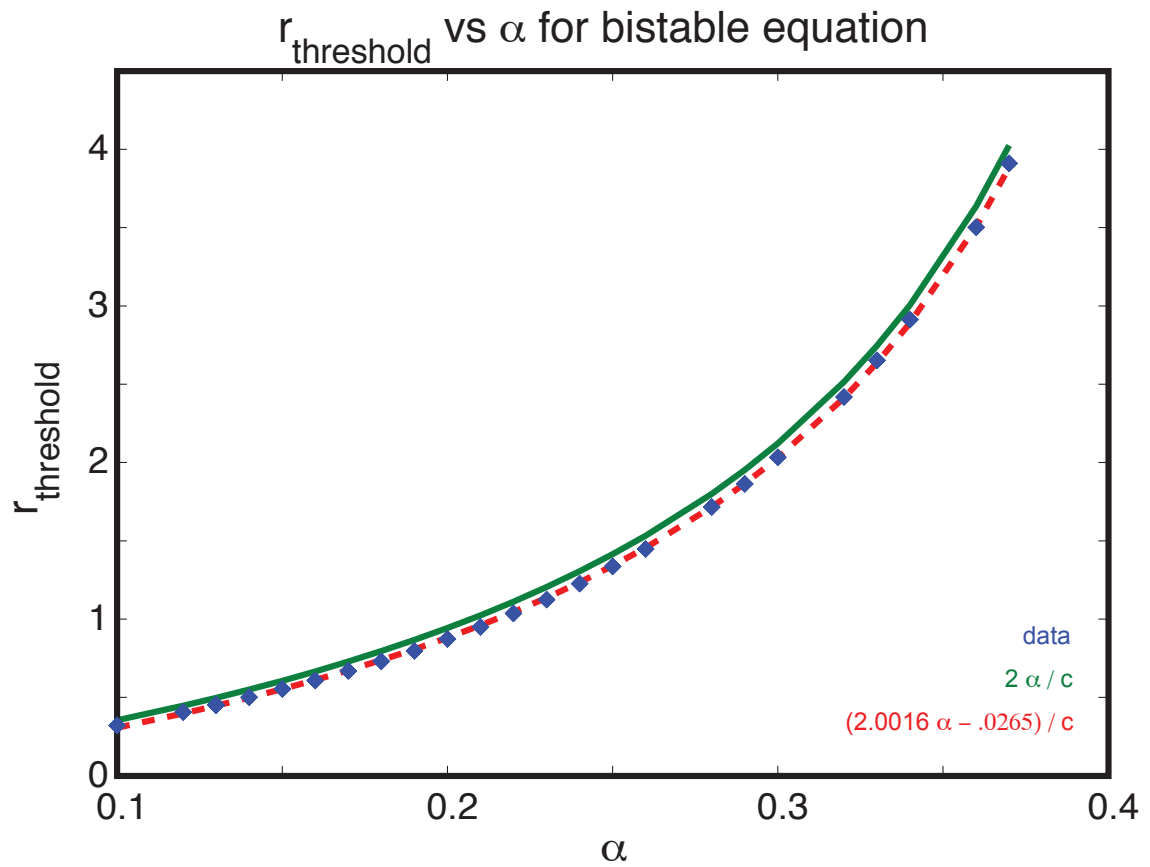


Figure 6.6: Minimum source width to propagate into half-plane. The threshold radius very closely follows the $2\alpha/c$ curve.

for some $\alpha \in (0, 1/2)$, where H is the Heaviside step function. That is, $H(u - \alpha) = 1$ for $u > \alpha$ and is 0 for $u < \alpha$.

Unlike the reactions in (6.2.1), the reactions here are not continuous. In the other model if u was near α , there would be next to no reaction. With this piecewise linear model, $f(u)$ has its most positive and most negative values near the threshold α .

Start by determining the speed of a 1-dimension traveling wave, $u = U(\xi)$, where $\xi = x - ct$, where $U(-\infty) = 1$ and $U(\infty) = 0$. Choose coordinate axes such that $U(0) = \alpha$. Let U_L represent the solution for $\xi < 0$ and U_R the solution for $\xi > 0$. We must have $U_L(0) = U_R(0) = U(0) = \alpha$ and $U'_L(0) = U'_R(0)$.

Then for $\xi < 0$, $U > \alpha$, so U_L is a solution to

$$\phi_{\xi\xi} + c\phi_{\xi} - \phi + 1 = 0, \quad (6.2.6)$$

which has general solution

$$\phi(\xi) = C_1 e^{r_+\xi} + C_2 e^{r_-\xi} + 1, \quad (6.2.7)$$

where

$$r_{\pm} = \frac{-c \pm \sqrt{c^2 + 4}}{2}. \quad (6.2.8)$$

Imposing the conditions $U_L(-\infty) = 1$ and $U_L(0) = \alpha$ we find $C_2 = 0$, and $C_1 = \alpha - 1$.

Thus

$$U_L(\xi) = 1 - (1 - \alpha)e^{r_+\xi} \quad (6.2.9)$$

and hence $U'_L(0) = (\alpha - 1)r_+$.

Similarly, for $\xi > 0$, $U < \alpha$, so U_R is a solution to

$$\psi_{\xi\xi} + c\psi_{\xi} - \psi = 0, \quad (6.2.10)$$

which has general solution

$$\psi(\xi) = C_3 e^{r_+\xi} + C_4 e^{r_-\xi}, \quad (6.2.11)$$

where r_{\pm} are as above. Imposing the boundary conditions $U_R(\infty) = 0$ and $U_R(0) = \alpha$, we find $C_3 = 0$ and $C_4 = \alpha$, thus

$$U_R(\xi) = \alpha e^{r-\xi}, \tag{6.2.12}$$

and hence $U'_R(0) = \alpha r_-$.

Since $U'_L(0) = U'_R(0)$, it follows that $(r_+ - r_-)\alpha = r_+$, so after plugging in the definitions of r_{\pm} and solving for c , one finds

$$c = \frac{1 - 2\alpha}{\sqrt{\alpha - \alpha^2}}. \tag{6.2.13}$$

The discontinuity makes numerical simulations more challenging, but using the same procedure as before, I found

$$r_{\text{threshold}} \approx \frac{2.2613\alpha - .0760}{c}. \tag{6.2.14}$$

6.2.3 Gradual Widening

I then considered the gradually widening geometry. At this point, the opening angle matters: if the angle is 0 degrees, then the dendrite is perfectly straight, and the wave propagates according to the one-dimensional solution; the thickness of the dendrite has no effect, and 0 is the infimum of the set of all possible source radii with propagation. On the other hand, if each side opens up at 90 degrees, then the geometry is a rectangle propagating into the half-plane as described in the previous section, which has a threshold radius of about $2\alpha/c$, where $c = \frac{1 - 2\alpha}{\sqrt{2}}$ is the planar wave velocity. Any formula for the effects of the angle should satisfy these two points.

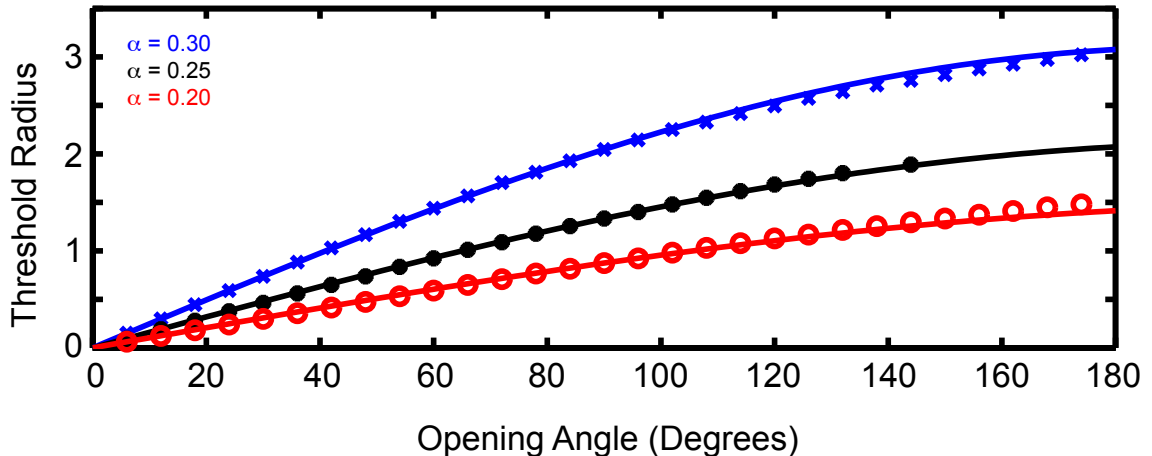


Figure 6.7: Threshold source radii in the gradually widening geometry. The opening angle is the deviation of each edge from straight, and so it necessarily lies between 0 and 180 degrees. Tic marks indicated computed values; solid lines are computed via equation (6.2.15).

I originally considered $\frac{2\alpha}{c} \sin(\theta/2)$, but found that this formula consistently underestimated the threshold radius, although the error decreased as α increased, suggesting that the angle dependence also had an α dependence. Ultimately, I arrived at the following conjecture:

$$r_{\text{threshold}} = \frac{2\alpha}{c} \frac{\sin\left(\theta \sqrt{\alpha(1-\alpha)}\right)}{\sin\left(\frac{\pi}{2} \sqrt{\alpha(1-\alpha)}\right)} \quad (6.2.15)$$

The planar wave velocity c for waves with threshold α and $1 - \alpha$ are opposites, so it is reasonable to expect both terms to appear symmetrically in the threshold formula. The denominator of the second factor scales the result to be consistent with the conjecture for the half-plane.

Like the half-plane formula, equation (6.2.15) is just a conjecture, but it gives good agreement with numerical experiments, as shown in Figure 6.7. This formula

also gives good agreement for the piecewise-continuous bistable equation (6.2.5) where c is as in (6.2.13).

6.2.4 Branch Points

To define a branch point geometry, one must know all three radii and the angles between one branch and the other two. The propagation of calcium waves towards and away from the soma both have important, though distinct, biological ramifications. Waves extending into the dendritic tree alter the neuron's excitability, by modulating sag currents [Egorov 02] or calcium-gated potassium channels [Poolos 99, Sah 02]. Waves entering the soma have the potential to alter gene transcription.

For simplicity, I restrict my attention to waves entering a straight branch from an angle, as in Figure 6.4E. This choice is reasonable because waves are generally able to pass from a large geometry into a smaller one, and because this is approximately the structure of the apical trunk; the branches are much smaller than the trunk, as illustrated in Figure 6.1.

As a first case, consider a wave propagating from a branch entering the trunk at a right angle. If the far side of the dendrite is infinitely far away, then this is the abruptly expanding geometry of Section 6.2.2. As the destination trunk gets thinner, the reflective nature of the far wall's boundary conditions concentrates the diffusing substance, facilitating wave propagation. A numerical study of this behavior is given in Figure 6.8.

If instead the destination radius is fixed, then for a given source radius, the angle of the branch controls whether or not the wave will block. The steeper the angle or the smaller the radius, the harder it is for the wave to propagate. The threshold curves are illustrated in Figure 6.9.

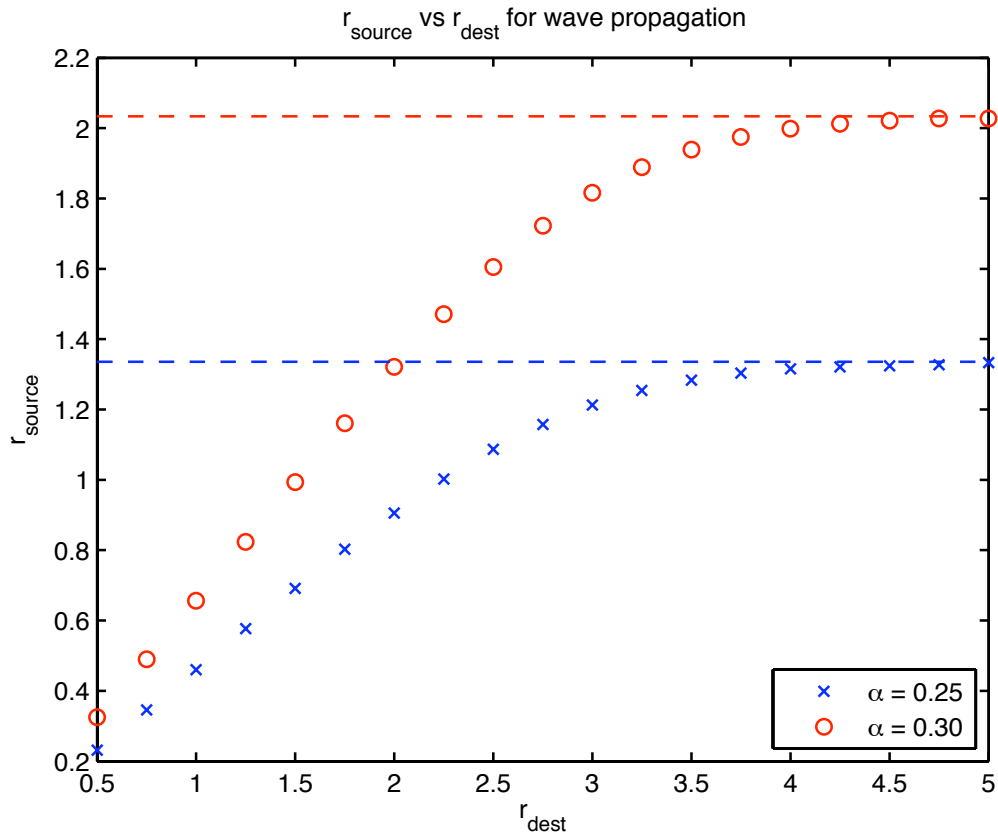


Figure 6.8: Propagation across orthogonal branches. Wave propagation in a dendritic tree is more closely modeled by having one narrow channel with radius r_{source} feeding into a new region with radius r_{dest} . Here we assume that the two regions intersect orthogonally. Narrow destinations help confine the substrate to the region near the opening, making it easier for waves to propagate. The horizontal dashed lines indicate numerically estimated values for propagation into the half-plane. This graph is for the scalar bistable equation (6.2.1).

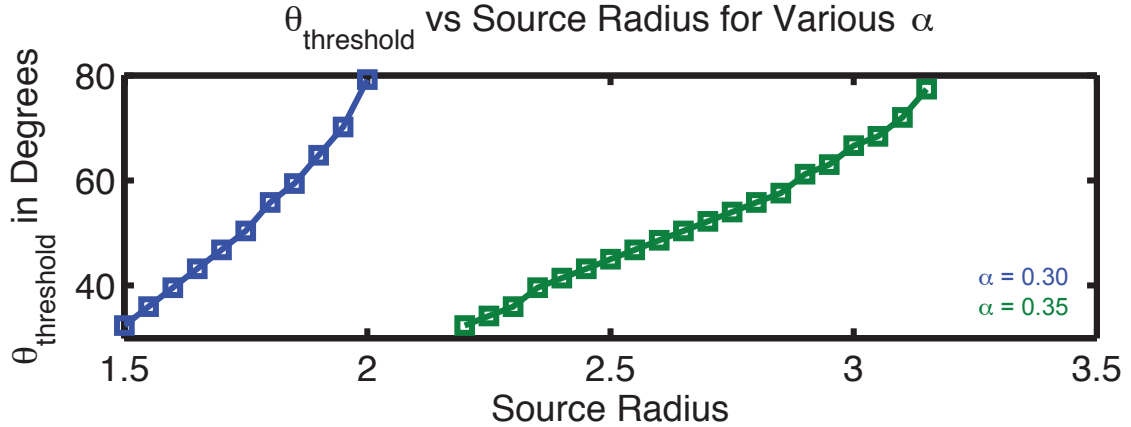


Figure 6.9: Branch angle affects wave propagation. Dynamics are as in (6.2.1). The destination radius is fixed at 5. Waves are blocked in regions lying above the curves; waves propagate below.

6.3 Future Directions

This calcium investigation can be extended in several ways. The working memory model can be combined with the model for ER-based calcium dynamics. Metabotropic glutamate receptor activation then allows input from the rest of the brain to help maintain elevated calcium. Due to the ER priming effect of back-propagating action potentials (Figure 6.2), only cells with high activity will respond with a calcium wave. A spatial model of the excitatory cells would allow them to have locally elevated calcium levels, allowing them to selectively increase their response. Conjectures can be developed and proved to describe propagation through a branch, including other types of branches not considered in Section 6.2.4. Using an approach as in [Sneyd 93], it may be possible to make a conjecture about the curvature-velocity relationship for the scalar bistable equation.

CHAPTER 7

INTERACTION WITH OTHER BRAIN SYSTEMS

The working memory system does not exist in isolation; it constantly interacts with other brain systems. Dopamine concentration is elevated during working memory tasks [Watanabe 97]. Other systems [Gabrieli 95, Gruber 04] provide feedback regulating and potentially correcting the memory.

7.1 Dopamine

Dopamine modulates GABA_A conductances; as dopamine increases, the connection strength increases. There is both a slow global dopamine tone [Romanides 99] and faster local fluctuations triggered by the performance of working memory tasks [Watanabe 97].

Figure 4.8 introduced the effects of dopamine tone by studying the effects of altering the inhibitory to excitatory conductance strength g_{syn} . In short, if dopamine (and thus the conductance) is too low, the excitatory cells do not receive a strong signal, so the sag-current barely activates, and the network fails to maintain persistent activity. If dopamine concentration is high, then the signal is too strong, and the excitatory cells become too active and switching performance is impaired. Thus either

extreme concentration impairs working memory performance, leading to an inverted-U-shaped performance vs dopamine curve, consistent with experimental observation [Zahrt 97].

On a more local perspective, the dopamine dependence improves working memory performance, in particular, the ability of the network to be robust to distractors. I define a distractor as a pattern presented to the excitatory cells after a cue stimulus of the same magnitude in applied current, number of cells, and duration. If the cue stimulus had not been applied, the distracting pattern would activate. This is the same definition used in [Brunel 01].

The base model is somewhat robust (Figure 5.18, third row), but dopamine improves its performance. The fundamental difficulty with robustness is that there is a trade off between robustness and persistence. The stronger the initial cue, the higher the probability of successful activation, but then robustness demands an equally strong cue, which increases the probability of activation of the distracting pattern.

When the network is inactive, dopamine is low and GABA_A synapses are weak, so the excitatory cells receive little inhibition. In an active network, dopamine is high, and the excitatory cells receive more inhibition and are therefore harder to activate. The primary benefit then is that with dopamine modulated synapses, the network may activate with a weaker cue.

Average persistence and robustness for dopamine modulated networks and networks not modulated by dopamine for various cue strengths are compared in Figure 7.1. Activity is measured 1000 ms after the end of the relevant stimulus. The maximum robustness performance – defined here as the geometric mean of active original cells and inactive distracting cells – is higher for the dopamine-modulated case. In

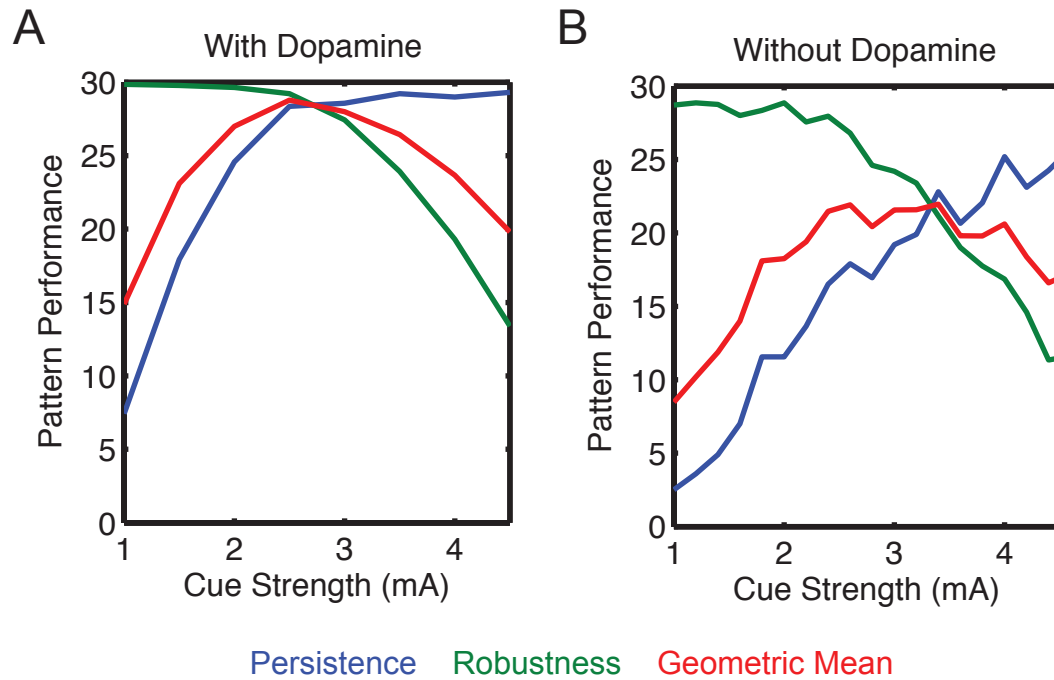


Figure 7.1: Dopamine modulation of synaptic transmission improves working memory performance. Persistence (blue) measures the active cells in the original pattern, robustness (green) the number of inactive cells from the distracting pattern, and red is their geometric mean. (A) Dopamine-modulated networks. (B) Networks without dopamine dynamics.

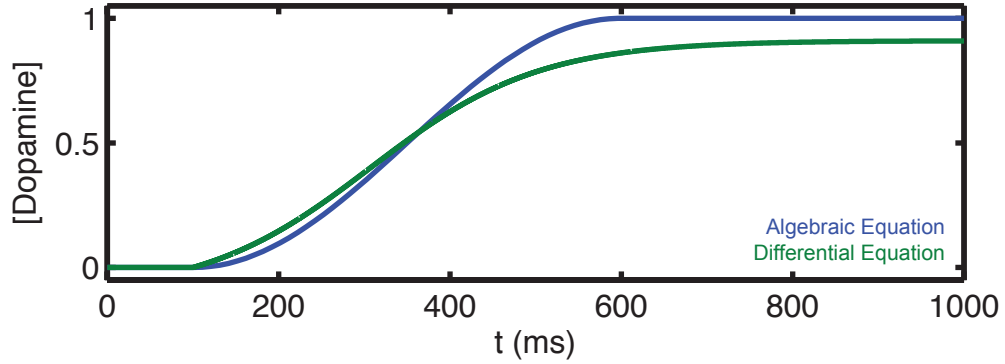


Figure 7.2: Comparison of dopamine models. The algebraic model is equation (7.1.1). Parameters for the differential equation model (7.1.2) are $\varepsilon = .1$, $\beta = .2$, and $\tau = 100$. I took A to be 0 until $t = 100$, then I set $A = 1$.

these simulations, I took $g_{\text{syn}} = D g_{\text{syn},1}$ where D is the dopamine concentration in normalized units, which I took to be governed by

$$D = \frac{1}{2} \text{H}(t - 100) \left(1 - \cos \left(\frac{t - 100}{1000/(2\pi)} \right) \right) \text{H}(600 - t) + \text{H}(t - 600), \quad (7.1.1)$$

whose graph is the blue curve in Figure 7.2. A more sophisticated model for dopamine regulation would respond directly to the network's activity A . One such approach is to average the output synaptic gating variables of the excitatory cells (possibly with a delay), then pass that value through a sigmoidal function to estimate A . A differential equation that gives similar dynamics to (7.1.1) is

$$\frac{dD}{dt} = \frac{D(1 - D)A + \varepsilon A - \beta D}{\tau}, \quad (7.1.2)$$

the green curve in Figure 7.2.

7.2 Electrical Modulation

Dopamine modulation is an example of chemical feedback to the working memory system; other brain systems, like the basal ganglia [Gabrieli 95], provide feedback

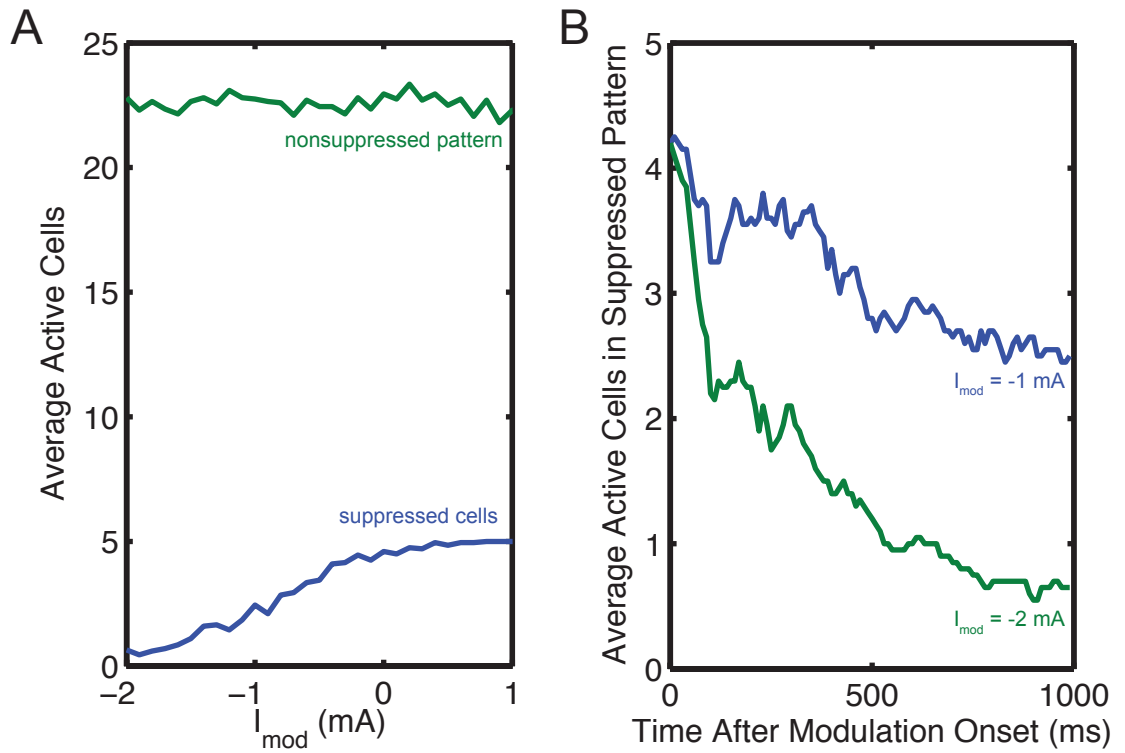


Figure 7.3: External modulation can selectively deactivate excitatory cells. (A) Modulatory current is applied to five pattern cells. If the current is sufficiently hyperpolarizing, the cells will be removed from the pattern (blue); the rest of the cells are unaffected (green). Activity is measured after 1000 ms of modulation. (B) Activity of suppressed cells over time, for $I_{\text{mod}} = -2$ mA (green) and $I_{\text{mod}} = -1$ mA (blue).

by other mechanisms. To test the ability of electrical feedback to selectively refine a working memory retained pattern without disrupting persistent activity in the remaining portions of the network, I chose 20 random networks, presented a cue pattern to 30 cells for 300 ms, waited an additional 200 ms, then applied varying amounts of applied current to a subset of 5 of the pattern cells for 1000 ms.

I found that moderate values of applied current had minimal impact on the rest of the pattern's persistent activity, but hyperpolarizing currents were able to suppress the activity of the selected subset. Examples are shown in Figure 7.3.

Mongillo et al has shown that strong excitatory pulses may play a role in reinstating persistent activity in a calcium based model of working memory and argues that this approach may make working memory performance less energy intensive [Mongillo 08].

CHAPTER 8

SIMULATING THE MODEL

Simple differential equations may be solved analytically, and simple systems of differential equations may be analyzed geometrically [Strogatz 94], but in general the complex differential equation based models found in mathematical neuroscience are not easily studied with traditional analytic techniques. The most practical solution is often to numerically integrate the models. Many simulation tools have been developed over the years, some of which are introduced in Section 8.1.

Most of these simulators for running one particular simulation with one particular network. While this approach would work, it clashes with one of the objectives of this project; namely to develop a general model of working memory that works with a variety of network architectures of heterogeneous cells across a large region of the parameter space. This work focuses on the performance statistics of the general model, not the results of an individual simulation.

To efficiently perform this study, I needed a simulator optimized for abstraction: Cell parameters should be describable as probability distributions, not just numbers. Networks consist of connections between groups of cells. Time can be measured relative to events (e.g. the removal of the cue stimulus) not just as fixed numbers. Simulations may fork and follow different paths with different parameter choices. Analyzing the results requires comparing groups of simulations.

Since none of the standard simulators work on this level of abstraction, I built my

own: `snnnet` is a python library designed to facilitate the abstract specification and study of neural networks. It is an extensible intermediary that can in principle be used with any numerical integration package. As part of its abstraction layer, `snnnet` optionally performs repeated runs, parameter sweeps, and analysis – even with user supplied analysis functions – in parallel to take advantage of the modern trend for multi-core computers.

8.1 Overview of Standard Tools

XPPAUT [Ermentrout 02] is a general-purpose integration tool, supporting a wide variety of integration algorithms. Equations are specified using standard mathematical notation. Neural network simulations can be done in XPPAUT by using an array-like notation to define a group of neurons at once and tables to define network connectivity and heterogeneities, but single cell models are a more typical use case. After simulation, all data must be exported to another tool for analysis.

Simulators designed specifically for working with neurons include NEURON [Hines 97], MOOSE [HarshaRani 11], NEST [Gewaltig 07], and Brian [Goodman 09]. The different simulators support different features: NEURON and MOOSE allow spatially extended neurons, while Brian works only with point models. NEST works well with large heterogeneous networks of simple cells. NEURON offers a graphical tool for defining the network architecture. Brian lets the model be defined directly from the equations with a minimum of syntactic overhead. It also has experimental support for algebraic preprocessing to simplify the model equations.

All four of the simulators mentioned above offer a Python interface or – in the case of Brian – are written in Python. Python is an interpreted programming language often described as a “glue” for combining other programs, and the abundance of Python-compatible libraries available is part of what makes Python so compelling.

There is a large collection of scientific software available for Python, much of it freely available, including numpy for numerical calculations, sympy for symbolic math, and matplotlib for graphics. Code written for NEURON (or MOOSE, etc. . .) using its Python interface is free to access these or any other installed Python library, vastly increasing the capabilities of the simulator.

The PyNN project [Davison 08] is developing a high-level front end in Python for these and other simulators that would allow a single model description to work with any of the supported simulators. Models are currently not easily portable between the simulators.

8.2 Snnet

Just as a biological experiment consists of two distinct parts: the cells, organisms, etc. . . that are being experimented with, and the protocol that is being used, there are two phases to defining a snnet simulation: specifying the dynamics, and specifying the protocol (parameter changes, etc. . .). The dynamics are specified using a simplified XPPAUT-like syntax [Ermentrout 02], extended to support probability distributions. The protocol is specified in Python using a series of calls to snnet, although minimal to no Python knowledge is required: in principle the only pure Python line required is a line ordering it to load the snnet library. Using one additional line, a `def` statement to identify the simulation protocol, allows parameter sweeps and repeated runs.

The remainder of this section focuses on highlighting a few design decisions. The snnet library, examples, and a user's guide are available online at: <http://ramcdougal.com/snnnet/>

8.2.1 Dynamics Specification

Each cell type is described once; the control code instantiates multiple copies as needed. The primary objective was to keep the specification language as simple and math-like as possible; this naturally led to an XPPAUT-like syntax although `snet` accepts more liberal use of white space and does not use special tags to denote parameters and initial conditions. As an example, the differential equation $x' = x - 1$ is written in the `snet` specification as `x' = x - 1`. Likewise, $f(x, y) = x + \frac{y}{2}$ becomes `f(x, y) = x + y / 2`.

Heterogeneities

In other simulators, the control code is responsible for explicitly setting any heterogeneous parameters, but this is more logically a property of the cell type, not of the simulation. To solve this problem, I introduce a notation for select probability distributions: “[$a : b$]” is a uniform random variable between a and b , “ $a [b]$ ” is a normal random variable with mean a and standard deviation b , and “ $a [b\%]$ ” is a normal random variable with mean a and standard deviation b percent of the mean.

Probability distributions are treated as numbers during parsing and may be used in any formula that takes numbers. Specific values are chosen from the parameter distribution for each cell in a simulation at the moment of instantiation.

Algebraic Expressions

With the exception of special cases, `snet` classifies every line of a model description as either a differential equation or an algebraic expression. There are no subtypes of algebraic expressions; constants, functions, and other expressions are treated as macros to be expanded only when needed. This approach has several advantages: unused values are never calculated, line order is no longer relevant, and it allows parameters

to be replaced by functions at run-time. For example, in most of the working memory simulations, the strength of the inhibitory to excitatory synapses, g_{syn} , was a fixed probability distribution. For those simulations that considered dopamine modulation of this conductance, I kept the same model description and replaced the conductance rule as part of my simulation protocol.

8.2.2 Protocol Specification

One of `snet`'s great strengths is that it is designed around simulation protocols rather than simulations. Programmatically, a simulation protocol looks like a description of a simulation, except it is declared as a Python function. When `snet` calls this function to run a simulation, it passes state information that overrides parameter declarations in the model description, etc. . . . This communication occurs via thread local variables so it is invisible to the user but still supports parallelization. At the end of the protocol, `snet` optionally extracts the simulation history by the same method and saves it to disk. Once the protocol has been declared, it only takes the user one line to run repeated parameter sweeps in parallel and save the results.

`Snet` simulations are written in Python with calls to `snet`, so the full power of Python is available for declaring protocol simulations, although they typically consist only of configuring the model, changing parameters, integrating, and repeating the last two.

Cell Groups

To configure the model or change parameters, the fundamental unit in `snet` is not a neuron; it is a collection of neurons. Collections of neurons are created at one time from the same dynamics. New collections are formed by set operations. Random networks are formed by rules for connections between groups of neurons. Parameter

changes typically occur to groups of neurons simultaneously. The details of an individual neuron are less important. This concept is not unique to snet; Brian supports working with collections of neurons as well.

Each collection is an object in Python. Every time a snet function is called, it updates an internal list of names for neuron collections by comparing with Python's list. This way the collections can be referred to by name during analysis.

Naming is important because the same collection may refer to a different group of cells in different experiments. For example, in the working memory experiments, different patterns may be presented to the same network; the persistent activity of the cue pattern groups is the relevant behavior, not the activity of a given excitatory cell. Likewise, snet supports naming time points, so that the same conceptual time points are identified not just those points with the same numeric time value.

Simulation Forks

Easy simulation forking is a feature that is, to the best of my knowledge, unique to snet. Forking is the process of exploring multiple options from the same simulation state. For example, after a period of persistent activity, a working memory experiment may involve the presentation of a weak distractor or of a strong distractor. Forking allows the exploration of both without recomputing the persistent state. The user simply declares a `fork()` and `end_fork()` at the beginning and ending of the simulation fork. At the beginning, snet copies the simulation state and stores it on a stack; it pops the value from the stack at the end. The simulation state is more than just the value of the state variables; it includes connectivity information, the status of the pseudo-random noise sources, and more.

8.2.3 Integrator Independence

When `snet` parses a model description file, it stores the data in a custom internal format, based on Reverse Polish Notation [Burks 54]. `Snet` integration methods are Python objects whose class implements a standard interface that can read this format and communicate with a program that does the actual integration. In this way, new methods can be added without modifying a single line of existing code.

8.2.4 Data Storage

Long simulations for large networks generate a large quantity of data, and it is not always practical to save all the data for every simulation, so `snet` supports saving with multiple data types which are each free to store any subset of the data.

A data type is a class inheriting from the empty data type. The constructor takes one argument, the state of the simulation and stores the relevant data in its member fields. The empty data type defines a `save` method that serializes the class via Python's `pickle` function, compresses the result using `zlib` compression, and outputs the result to disk. Data is loaded by reversing the process.

The class structure provides a standard interface for reading the data. Thus, analysis routines work without regard to the underlying data type; all that is necessary is that the data type supports the underlying functions.

8.2.5 Data Analysis

To simplify the writing of data analysis tools, `snet` provides `run_f_on_dir`, a function whose task is to load all the data files from a directory one-by-one and perform a function on them; it returns a list of the function return values. Furthermore, it optionally runs these function calls concurrently, using either separate processes or

threads, depending on the machine architecture. The analysis tools developed for this project are included in the standard snnet distribution.

BIBLIOGRAPHY

- [Abbott 90] L. Abbott & T. Kepler. *Model neurons: From Hodgkin-Huxley to Hopfield*. Statistical mechanics of neural networks, pages 5–18, 1990.
- [Abel 04] H.J. Abel, J.C.F. Lee, J.C. Callaway & R.C. Foehring. *Relationships between intracellular calcium and afterhyperpolarizations in neocortical pyramidal neurons*. Journal of neurophysiology, vol. 91, no. 1, page 324, 2004.
- [Amit 94] D.J. Amit, N. Brunel & M.V. Tsodyks. *Correlations of cortical Hebbian reverberations: theory versus experiment*. The Journal of neuroscience, vol. 14, no. 11, page 6435, 1994.
- [Amit 97] D.J. Amit & N. Brunel. *Model of global spontaneous activity and local structured activity during delay periods in the cerebral cortex*. Cerebral Cortex, vol. 7, no. 3, page 237, 1997.
- [Aoki 00] T. Aoki & S.C. Baraban. *Properties of a calcium-activated K^+ current on interneurons in the developing rat hippocampus*. Journal of neurophysiology, vol. 83, no. 6, page 3453, 2000.
- [Araque 99] A. Araque, V. Parpura, R.P. Sanzgiri & P.G. Haydon. *Tripartite synapses: glia, the unacknowledged partner*. Trends in Neurosciences, vol. 22, no. 5, pages 208–215, 1999.
- [Azevedo 09] FA Azevedo, L.R. Carvalho, L.T. Grinberg, J.M. Farfel, R.E. Ferretti, R.E. Leite, F.W. Jacob, R. Lent & S. Herculano-Houzel. *Equal numbers of neuronal and nonneuronal cells make the human brain an isometrically scaled-up primate brain*. The Journal of comparative neurology, vol. 513, no. 5, page 532, 2009.
- [Baddeley 91] AD Baddeley, S. Bressi, S. Della, R. Logie & H. Spinnler. *The decline of working memory in Alzheimer’s disease*. Brain, vol. 114, no. 6, page 2521, 1991.

- [Baddeley 94] A.D. Baddeley & G.J. Hitch. *Developments in the concept of working memory*. *Neuropsychology*, vol. 8, no. 4, page 485, 1994.
- [Baker 02] H.L. Baker, R.J. Errington, S.C. Davies & A.K. Campbell. *A mathematical model predicts that calreticulin interacts with the endoplasmic reticulum Ca^{2+} -ATPase*. *Biophysical journal*, vol. 82, no. 2, pages 582–590, 2002.
- [Bannister 95] N.J. Bannister & A.U. Larkman. *Dendritic morphology of CA1 pyramidal neurones from the rat hippocampus: I. Branching patterns*. *The Journal of comparative neurology*, vol. 360, no. 1, pages 150–160, 1995.
- [Barbieri 08] F. Barbieri & N. Brunel. *Can attractor network models account for the statistics of firing during persistent activity in prefrontal cortex?* *Frontiers in Neuroscience*, vol. 2, no. 1, page 114, 2008.
- [Berridge 98] M.J. Berridge. *Neuronal Calcium Signaling Review*. *Neuron*, vol. 21, pages 13–26, 1998.
- [Borg-Graham 87] L.J. Borg-Graham. *Modelling the somatic electrical response of hippocampal pyramidal neurons*. Master’s thesis, Massachusetts Institute of Technology, 1987.
- [Borg-Graham 91] L. Borg-Graham. *Modelling the non-linear conductances of excitable membranes*. *Cellular Neurobiology: A Practical Approach*, vol. 13, pages 247–275, 1991.
- [Box 79] G.E.P. Box. *Some problems of statistics and everyday life*. *Journal of the American Statistical Association*, pages 1–4, 1979.
- [Boyce 92] W.E. Boyce, R.C. DiPrima & D. Mitrea. *Elementary differential equations and boundary value problems*. Wiley New York:, 1992.
- [Britton 86] N.F. Britton. *Reaction-diffusion equations and their applications to biology*. Academic Press, 1986.
- [Brunel 01] N. Brunel & X.J. Wang. *Effects of neuromodulation in a cortical network model of object working memory dominated by recurrent inhibition*. *Journal of Computational Neuroscience*, vol. 11, no. 1, pages 63–85, 2001.

- [Burks 54] A.W. Burks, D.W. Warren & J.B. Wright. *An analysis of a logical machine using parenthesis-free notation*. Mathematical tables and other aids to computation, vol. 8, no. 46, pages 53–57, 1954.
- [Busa 85] W.B. Busa & R. Nuccitelli. *An elevated free cytosolic Ca^{2+} wave follows fertilization in eggs of the frog, *Xenopus laevis**. The Journal of cell biology, vol. 100, no. 4, page 1325, 1985.
- [Buzsák 98] G.Ö. Buzsák. *Memory consolidation during sleep: a neurophysiological perspective*. Journal of Sleep Research, vol. 7, no. S1, pages 17–23, 1998.
- [Camperi 98] M. Camperi & X.J. Wang. *A model of visuospatial working memory in prefrontal cortex: recurrent network and cellular bistability*. Journal of Computational Neuroscience, vol. 5, no. 4, pages 383–405, 1998.
- [Cantrell 97] A.R. Cantrell, R.D. Smith, A.L. Goldin, T. Scheuer & W.A. Catterall. *Dopaminergic modulation of sodium current in hippocampal neurons via cAMP-dependent phosphorylation of specific sites in the sodium channel α subunit*. The Journal of neuroscience, vol. 17, no. 19, page 7330, 1997.
- [Chapuisat 05] G. Chapuisat & E. Grenier. *Existence and nonexistence of traveling wave solutions for a bistable reaction-diffusion equation in an infinite cylinder whose diameter is suddenly increased*. Communications in Partial Differential Equations, vol. 30, no. 12, pages 1805–1816, 2005.
- [Compte 03] A. Compte, C. Constantinidis, J. Tegnér, S. Raghavachari, M.V. Chafee, P.S. Goldman-Rakic & X.J. Wang. *Temporally irregular mnemonic persistent activity in prefrontal neurons of monkeys during a delayed response task*. Journal of neurophysiology, vol. 90, no. 5, page 3441, 2003.
- [Connor 71] J.A. Connor & C.F. Stevens. *Prediction of repetitive firing behaviour from voltage clamp data on an isolated neurone soma*. The Journal of Physiology, vol. 213, no. 1, page 31, 1971.
- [Constantinidis 96] C. Constantinidis & M.A. Steinmetz. *Neuronal activity in posterior parietal area γa during the delay periods of a spatial memory task*. Journal of Neurophysiology, vol. 76, no. 2, page 1352, 1996.

- [Crank 47] J. Crank & P. Nicolson. *A practical method for numerical evaluation of solutions of partial differential equations of the heat-conduction type*. In *Mathematical Proceedings of the Cambridge Philosophical Society*, volume 43, pages 50–67. Cambridge Univ Press, 1947.
- [Curtis 03] C.E. Curtis & M. D’Esposito. *Persistent activity in the prefrontal cortex during working memory*. *Trends in Cognitive Sciences*, vol. 7, no. 9, pages 415–423, 2003.
- [Dahl 74] JL Dahl & L.E. Hokin. *The sodium-potassium adenosinetriphosphatase*. *Annual review of biochemistry*, vol. 43, no. 1, pages 327–356, 1974.
- [Davison 08] A.P. Davison, D. Brüderle, J. Eppler, J. Kremkow, E. Müller, D. Pecevski, L. Perrinet & P. Yger. *PyNN: a common interface for neuronal network simulators*. *Frontiers in neuroinformatics*, vol. 2, 2008.
- [De Young 92] G.W. De Young & J. Keizer. *A single-pool inositol 1, 4, 5-trisphosphate-receptor-based model for agonist-stimulated oscillations in Ca^{2+} concentration*. *Proceedings of the National Academy of Sciences of the United States of America*, vol. 89, no. 20, page 9895, 1992.
- [Delaney 01] A.J. Delaney & P. Sah. *Pathway-specific targeting of GABAA receptor subtypes to somatic and dendritic synapses in the central amygdala*. *Journal of neurophysiology*, vol. 86, no. 2, page 717, 2001.
- [D’Esposito 95] M. D’Esposito, J.A. Detre, D.C. Alsop, R.K. Shin, S. Atlas & M. Grossman. *The neural basis of the central executive system of working memory*. *Nature*, vol. 378, no. 6554, pages 279–281, 1995.
- [D’Esposito 96] M. D’Esposito, K. Onishi, H. Thompson, K. Robinson, C. Armstrong & M. Grossman. *Working memory impairments in multiple sclerosis: Evidence from a dual-task paradigm*. *Neuropsychology*, vol. 10, no. 1, page 51, 1996.
- [Destexhe 94a] A. Destexhe, D. Contreras, T.J. Sejnowski & M. Steriade. *A model of spindle rhythmicity in the isolated thalamic reticular nucleus*. *Journal of neurophysiology*, vol. 72, no. 2, page 803, 1994.

- [Destexhe 94b] A. Destexhe, Z.F. Mainen & T.J. Sejnowski. *Synthesis of models for excitable membranes, synaptic transmission and neuromodulation using a common kinetic formalism*. Journal of Computational Neuroscience, vol. 1, no. 3, pages 195–230, 1994.
- [Driesen 08] N.R. Driesen, H.C. Leung, V.D. Calhoun, R.T. Constable, R. Gueorguieva, R. Hoffman, P. Skudlarski, P.S. Goldman-Rakic & J.H. Krystal. *Impairment of working memory maintenance and response in schizophrenia: functional magnetic resonance imaging evidence*. Biological psychiatry, vol. 64, no. 12, pages 1026–1034, 2008.
- [Dronne 09] M.A. Dronne, S. Descombes, E. Grenier & H. Gilquin. *Examples of the influence of the geometry on the propagation of progressive waves*. Mathematical and Computer Modelling, vol. 49, no. 11-12, pages 2138–2144, 2009.
- [Durstewitz 00] D. Durstewitz, J.K. Seamans & T.J. Sejnowski. *Dopamine-mediated stabilization of delay-period activity in a network model of prefrontal cortex*. Journal of Neurophysiology, vol. 83, no. 3, page 1733, 2000.
- [Edwards 96] D.A. Edwards. *Non-Fickian diffusion in thin polymer films*. Journal of Polymer Science-B-Polymer Physics Edition, vol. 34, no. 5, page 981, 1996.
- [Egorov 02] A.V. Egorov, B.N. Hamam, E. Fransén, M.E. Hasselmo & A.A. Alonso. *Graded persistent activity in entorhinal cortex neurons*. Nature, vol. 420, no. 6912, pages 173–178, 2002.
- [Ermentrout 93] G.B. Ermentrout & L. Edelstein-Keshet. *Cellular automata approaches to biological modeling*. Journal of Theoretical Biology, vol. 160, pages 97–97, 1993.
- [Ermentrout 02] B. Ermentrout. *Simulating, analyzing, and animating dynamical systems: a guide to xppaut for researchers and students*. Society for Industrial Mathematics, 2002.
- [Ermentrout 10] G.B. Ermentrout & D. Terman. *Mathematical foundations of neuroscience*, volume 35. Springer Verlag, 2010.
- [Fall 04] C.P. Fall, J.M. Wagner, L.M. Loew & R. Nuccitelli. *Cortically restricted production of IP₃ leads to propagation of the fertilization Ca²⁺ wave along the cell surface in a model of the Xenopus egg*. Journal of theoretical biology, vol. 231, no. 4, pages 487–496, 2004.

- [Fall 05] C.P. Fall, T.J. Lewis & J. Rinzel. *Background-activity-dependent properties of a network model for working memory that incorporates cellular bistability*. Biological cybernetics, vol. 93, no. 2, pages 109–118, 2005.
- [Fall 06] C.P. Fall & J. Rinzel. *An intracellular Ca^{2+} subsystem as a biologically plausible source of intrinsic conditional bistability in a network model of working memory*. Journal of Computational Neuroscience, vol. 20, no. 1, pages 97–107, 2006.
- [Fife 79] P.C. Fife. *Mathematical aspects of reacting and diffusing systems*. Springer Verlag., 1979.
- [Fontanilla 98] R.A. Fontanilla & R. Nuccitelli. *Characterization of the sperm-induced calcium wave in Xenopus eggs using confocal microscopy*. Biophysical journal, vol. 75, no. 4, pages 2079–2087, 1998.
- [Fransén 06] E. Fransén, B. Tahvildari, A.V. Egorov, M.E. Hasselmo & A.A. Alonso. *Mechanism of graded persistent cellular activity of entorhinal cortex layer v neurons*. Neuron, vol. 49, no. 5, pages 735–746, 2006.
- [Funahashi 89] S. Funahashi, C.J. Bruce & P.S. Goldman-Rakic. *Mnemonic coding of visual space in the monkey's dorsolateral prefrontal cortex*. Journal of Neurophysiology, vol. 61, no. 2, page 331, 1989.
- [Funahashi 94] S. Funahashi & K. Kubota. *Working memory and prefrontal cortex*. Neuroscience research, vol. 21, no. 1, pages 1–11, 1994.
- [Fuster 73] J.M. Fuster. *Unit activity in prefrontal cortex during delayed-response performance: neuronal correlates of transient memory*. Journal of Neurophysiology, vol. 36, no. 1, page 61, 1973.
- [Fuster 08] J.M. Fuster. *The prefrontal cortex*. Academic Press, 2008.
- [Gabbott 05] P.L.A. Gabbott, T.A. Warner, P.R.L. Jays, P. Salway & S.J. Busby. *Prefrontal cortex in the rat: projections to subcortical autonomic, motor, and limbic centers*. The Journal of comparative neurology, vol. 492, no. 2, pages 145–177, 2005.
- [Gabrieli 95] J. Gabrieli. *Contribution of the basal ganglia to skill learning and working memory in humans*. 1995.

- [Gabrieli 96] J.D.E. Gabrieli, J. Singh, G.T. Stebbins & C.G. Goetz. *Reduced working memory span in Parkinson's disease: Evidence for the role of frontostriatal system in working and strategic memory*. *Neuropsychology*, vol. 10, no. 3, page 322, 1996.
- [Gewaltig 07] Marc-Oliver Gewaltig & Markus Diesmann. *NEST (NEural Simulation Tool)*. *Scholarpedia*, vol. 2, no. 4, page 1430, 2007.
- [Goldberg 02] J.A. Goldberg, T. Boraud, S. Maraton, S.N. Haber, E. Vaadia & H. Bergman. *Enhanced synchrony among primary motor cortex neurons in the 1-methyl-4-phenyl-1, 2, 3, 6 - tetrahydropyridine primate model of Parkinson's disease*. *The Journal of neuroscience*, vol. 22, no. 11, page 4639, 2002.
- [Goldman-Rakic 95] P.S. Goldman-Rakic. *Cellular basis of working memory*. *Neuron*, vol. 14, no. 3, page 477, 1995.
- [Golomb 07] D. Golomb, K. Donner, L. Shacham, D. Shlosberg, Y. Amitai & D. Hansel. *Mechanisms of firing patterns in fast-spiking cortical interneurons*. *PLoS Comput Biol*, vol. 3, no. 8, page e156, 2007.
- [Gonzalez-Burgos 08] G. Gonzalez-Burgos & D.A. Lewis. *GABA neurons and the mechanisms of network oscillations: implications for understanding cortical dysfunction in schizophrenia*. *Schizophrenia bulletin*, vol. 34, no. 5, page 944, 2008.
- [Goodman 09] D.F.M. Goodman & R. Brette. *The Brian simulator*. *Frontiers in neuroscience*, vol. 3, no. 2, page 192, 2009.
- [Grigsby 94] J. Grigsby, S.D. Ayarbe, N. Kravcisin & D. Busenbark. *Working memory impairment among persons with chronic progressive multiple sclerosis*. *Journal of neurology*, vol. 241, no. 3, pages 125–131, 1994.
- [Gruber 04] O. Gruber & T. Goschke. *Executive control emerging from dynamic interactions between brain systems mediating language, working memory and attentional processes*. *Acta Psychologica*, vol. 115, no. 2-3, pages 105–121, 2004.
- [Guigon 95] E. Guigon, B. Dorizzi, Y. Burnod & W. Schultz. *Neural correlates of learning in the prefrontal cortex of the monkey: A predictive model*. *Cerebral Cortex*, vol. 5, no. 2, page 135, 1995.

- [Gunter 04] T.E. Gunter, D.I. Yule, K.K. Gunter, R.A. Eliseev & J.D. Salter. *Calcium and mitochondria*. FEBS letters, vol. 567, no. 1, pages 96–102, 2004.
- [Häfner 91] H. Häfner, S. Behrens, J. De Vry & W.F. Gattaz. *An animal model for the effects of estradiol on dopamine-mediated behavior: implications for sex differences in schizophrenia*. Psychiatry research, vol. 38, no. 2, pages 125–134, 1991.
- [Hagiwara 89] N. Hagiwara & H. Irisawa. *Modulation by intracellular Ca^{2+} of the hyper-polarization-activated inward current in rabbit single sino-atrial node cells*. The Journal of Physiology, vol. 409, no. 1, page 121, 1989.
- [Harris 94] K.M. Harris. *Dendritic spines*. 1994.
- [HarshaRani 11] G.V. HarshaRani. *Multiscale Object-Oriented Simulation Environment*. <http://moose.ncbs.res.in/>, 2011. [Online; accessed 6-July-2011].
- [Hartsfield 05] J.W. Hartsfield. *A quantitative study of neuronal calcium signaling*. PhD thesis, Baylor College of Medicine, 2005.
- [Hasenstaub 05] A. Hasenstaub, Y. Shu, B. Haider, U. Kraushaar, A. Duque & D.A. McCormick. *Inhibitory postsynaptic potentials carry synchronized frequency information in active cortical networks*. Neuron, vol. 47, no. 3, pages 423–435, 2005.
- [Hebb 49] D.O. Hebb. *The organisation of behaviour*, 1949.
- [Higgins 06] E.R. Higgins, M.B. Cannell & J. Sneyd. *A buffering SERCA pump in models of calcium dynamics*. Biophysical journal, vol. 91, no. 1, pages 151–163, 2006.
- [Hines 97] M.L. Hines & N.T. Carnevale. *The NEURON simulation environment*. Neural computation, vol. 9, no. 6, pages 1179–1209, 1997.
- [Hodgkin 52] A.L. Hodgkin & A.F. Huxley. *A quantitative description of membrane current and its application to conduction and excitation in nerve*. The Journal of physiology, vol. 117, no. 4, page 500, 1952.
- [Hong 07] M. Hong & W.N. Ross. *Priming of intracellular calcium stores in rat CA1 pyramidal neurons*. The Journal of Physiology, vol. 584, no. 1, page 75, 2007.

- [Hopfield 82] J.J. Hopfield. *Neural networks and physical systems with emergent collective computational abilities*. Proceedings of the National Academy of Sciences of the United States of America, vol. 79, no. 8, page 2554, 1982.
- [Hurtado 99] J.M. Hurtado, C.M. Gray, L.B. Tamas & K.A. Sigvardt. *Dynamics of tremor-related oscillations in the human globus pallidus: a single case study*. Proceedings of the National Academy of Sciences, vol. 96, no. 4, page 1674, 1999.
- [Jaffe 94] D.B. Jaffe & T.H. Brown. *Metabotropic glutamate receptor activation induces calcium waves within hippocampal dendrites*. Journal of neurophysiology, vol. 72, no. 1, page 471, 1994.
- [Johnston 96] D. Johnston, J.C. Magee, C.M. Colbert & B.R. Christie. *Active properties of neuronal dendrites*. Annual Review of Neuroscience, vol. 19, no. 1, pages 165–186, 1996.
- [Jonides 93] J. Jonides, E.E. Smith, R.A. Koeppe, E. Awh, S. Minoshima & M.A. Mintun. *Spatial working-memory in humans as revealed by PET*. Nature, vol. 363, no. 6430, pages 623–625, 1993.
- [Kandel 00] E.R. Kandel, J.H. Schwartz & T.M. Jessell. Principles of neural science. McGraw-Hill Medical, fourth edition, 2000.
- [Kensinger 03] E.A. Kensinger, D.K. Shearer, J.J. Locascio, J.H. Growdon & S. Corkin. *Working memory in mild Alzheimer's disease and early Parkinson's disease*. Neuropsychology, vol. 17, no. 2, page 230, 2003.
- [Keysers 04] C. Keysers & D.I. Perrett. *Demystifying social cognition: a Hebbian perspective*. Trends in Cognitive Sciences, vol. 8, no. 11, pages 501–507, 2004.
- [Kole 08] M.H.P. Kole, S.U. Ilshner, B.M. Kampa, S.R. Williams, P.C. Ruben & G.J. Stuart. *Action potential generation requires a high sodium channel density in the axon initial segment*. Nature Neuroscience, vol. 11, no. 2, pages 178–186, 2008.
- [Kretsinger 80] R.H. Kretsinger. *Structure and evolution of calcium-modulated proteins*. CRC critical reviews in biochemistry, vol. 8, no. 2, page 119, 1980.
- [Kritzer 95] M.F. Kritzer & P.S. Goldman-Rakic. *Intrinsic circuit organization of the major layers and sublayers of the dorsolateral prefrontal cortex in the rhesus monkey*. The Journal of Comparative Neurology, vol. 359, no. 1, pages 131–143, 1995.

- [Lakoff 08] G. Lakoff. *The neural theory of metaphor*. The Cambridge handbook of metaphor and thought, 2008.
- [Lancaster 86] B. Lancaster & P.R. Adams. *Calcium-dependent current generating the afterhyperpolarization of hippocampal neurons*. Journal of Neurophysiology, vol. 55, no. 6, page 1268, 1986.
- [Laubenbacher 04] R. Laubenbacher & B. Stigler. *A computational algebra approach to the reverse engineering of gene regulatory networks*. Journal of Theoretical Biology, vol. 229, no. 4, pages 523–537, 2004.
- [Lechleiter 91] J. Lechleiter, S. Girard, E. Peralta & D. Clapham. *Spiral calcium wave propagation and annihilation in Xenopus laevis oocytes*. Science, vol. 252, no. 5002, page 123, 1991.
- [Levy 00] R. Levy, W.D. Hutchison, A.M. Lozano & J.O. Dostrovsky. *High-frequency synchronization of neuronal activity in the subthalamic nucleus of parkinsonian patients with limb tremor*. The Journal of Neuroscience, vol. 20, no. 20, page 7766, 2000.
- [Lewinsohn 72] P.M. Lewinsohn *et al.* *Short-term memory: A comparison between frontal and nonfrontal right-and left-hemisphere brain-damaged patients*. Journal of Comparative and Physiological Psychology, vol. 81, no. 2, page 248, 1972.
- [Li 94] Y.X. Li & J. Rinzel. *Equations for InsP3 receptor-mediated $[Ca^{2+}]_i$ oscillations derived from a detailed kinetic model: a Hodgkin-Huxley like formalism*. Journal of theoretical biology, vol. 166, no. 4, pages 461–473, 1994.
- [Lirk 08] P. Lirk, M. Poroli, M. Rigaud, A. Fuchs, P. Phillip, C.Y. Huang, M. Ljubkovic, D. Sapunar & Q. Hogan. *Modulators of calcium influx regulate membrane excitability in rat dorsal root ganglion neurons*. Anesthesia & Analgesia, vol. 107, no. 2, page 673, 2008.
- [Lodish 00] H. Lodish, A. Berk, L.S. Zipursky, P. Matsudaira, D. Baltimore & J.E. Darnell. *Molecular cell biology*. WH Freeman, 2000.
- [Loew 01] L.M. Loew & J.C. Schaff. *The Virtual Cell: a software environment for computational cell biology*. TRENDS in Biotechnology, vol. 19, no. 10, pages 401–406, 2001.
- [Loewenstein 03] Y. Loewenstein & H. Sompolinsky. *Temporal integration by calcium dynamics in a model neuron*. Nature neuroscience, vol. 6, no. 9, pages 961–967, 2003.

- [Magee 98] J.C. Magee. *Dendritic hyperpolarization-activated currents modify the integrative properties of hippocampal CA1 pyramidal neurons*. The Journal of neuroscience, vol. 18, no. 19, page 7613, 1998.
- [Melchitzky 98] D.S. Melchitzky, S.R. Sesack, M.L. Pucak & D.A. Lewis. *Synaptic targets of pyramidal neurons providing intrinsic horizontal connections in monkey prefrontal cortex*. The Journal of comparative neurology, vol. 390, no. 2, pages 211–224, 1998.
- [Miller 96] E.K. Miller, C.A. Erickson & R. Desimone. *Neural mechanisms of visual working memory in prefrontal cortex of the macaque*. The Journal of Neuroscience, vol. 16, no. 16, page 5154, 1996.
- [Miller 01] E.K. Miller & J.D. Cohen. *An integrative theory of prefrontal cortex function*. Annual review of neuroscience, vol. 24, no. 1, pages 167–202, 2001.
- [Milner 82] B. Milner. *Some cognitive effects of frontal-lobe lesions in man*. Philosophical Transactions of the Royal Society of London. B, Biological Sciences, vol. 298, no. 1089, page 211, 1982.
- [Miyakawa 92] H. Miyakawa, W.N. Ross, D. Jaffe, J.C. Callaway, N. Lasser-Ross, J.E. Lisman & D. Johnston. *Synaptically activated increases in Ca^{2+} concentration in hippocampal CA1 pyramidal cells are primarily due to voltage-gated Ca^{2+} channels*. Neuron, vol. 9, no. 6, pages 1163–1173, 1992.
- [Mongillo 08] G. Mongillo, O. Barak & M. Tsodyks. *Synaptic theory of working memory*. Science, vol. 319, no. 5869, page 1543, 2008.
- [Moore 09] S.J. Moore, D.C. Cooper & N. Spruston. *Plasticity of burst firing induced by synergistic activation of metabotropic glutamate and acetylcholine receptors*. Neuron, vol. 61, no. 2, pages 287–300, 2009.
- [Mountcastle 69] V.B. Mountcastle, W.H. Talbot, H. Sakata & J. Hyvarinen. *Cortical neuronal mechanisms in flutter-vibration studied in unanesthetized monkeys. Neuronal periodicity and frequency discrimination*. Journal of neurophysiology, vol. 32, no. 3, page 452, 1969.
- [Nagle 00] S. Nagle, E. Saff & D. Snider. *Fundamentals of differential equations and boundary value problems*. Addison-Wesley, 2000.

- [Orrenius 03] S. Orrenius, B. Zhivotovsky & P. Nicotera. *Regulation of cell death: the calcium–apoptosis link*. Nature Reviews Molecular Cell Biology, vol. 4, no. 7, pages 552–565, 2003.
- [Oster 06] A.M. Oster & P.C. Bressloff. *A developmental model of ocular dominance column formation on a growing cortex*. Bulletin of mathematical biology, vol. 68, no. 1, pages 73–98, 2006.
- [Owen 97] A.M. Owen, J.L. Iddon, J.R. Hodges, B.A. Summers & T.W. Robbins. *Spatial and non-spatial working memory at different stages of Parkinson’s disease*. Neuropsychologia, vol. 35, no. 4, pages 519–532, 1997.
- [Pan 03] Z.Z. Pan. *κ -Opioid receptor-mediated enhancement of the hyperpolarization-activated current (I_h) through mobilization of intracellular calcium in rat nucleus raphe magnus*. The Journal of Physiology, vol. 548, no. 3, pages 765–775, 2003.
- [Percy 08] B.E. Percy. *Initiation and propagation of a neuronal intracellular calcium wave*. Journal of Computational Neuroscience, vol. 25, no. 2, pages 334–348, 2008.
- [Pelosi 97] L. Pelosi, J.M. Geesken, M. Holly, M. Hayward & L.D. Blumhardt. *Working memory impairment in early multiple sclerosis. Evidence from an event-related potential study of patients with clinically isolated myelopathy*. Brain, vol. 120, no. 11, page 2039, 1997.
- [Pesaran 00] B. Pesaran, J.S. Pezaris, M. Sahani, P.P. Mitra & R.A. Andersen. *Temporal structure in neuronal activity during working memory in macaque parietal cortex*. Arxiv preprint q-bio/0309034, 2000.
- [Petrides 93] M. Petrides, B. Alivisatos, A.C. Evans & E. Meyer. *Dissociation of human mid-dorsolateral from posterior dorsolateral frontal cortex in memory processing*. Proceedings of the National Academy of Sciences, vol. 90, no. 3, page 873, 1993.
- [Petrides 95] M. Petrides. *Impairments on nonspatial self-ordered and externally ordered working memory tasks after lesions of the mid-dorsal part of the lateral frontal cortex in the monkey*. The Journal of neuroscience, vol. 15, no. 1, page 359, 1995.
- [Poirazi 03] P. Poirazi, T. Brannon & B.W. Mel. *Arithmetic of subthreshold synaptic summation in a model CA1 pyramidal cell*. Neuron, vol. 37, no. 6, pages 977–987, 2003.

- [Poolos 99] N.P. Poolos & D. Johnston. *Calcium-activated potassium conductances contribute to action potential repolarization at the soma but not the dendrites of hippocampal CA1 pyramidal neurons*. The Journal of neuroscience, vol. 19, no. 13, page 5205, 1999.
- [Power 02] J.M. Power & P. Sah. *Nuclear calcium signaling evoked by cholinergic stimulation in hippocampal CA1 pyramidal neurons*. The Journal of neuroscience, vol. 22, no. 9, page 3454, 2002.
- [Pozzo-Miller 97] L.D. Pozzo-Miller, N.B. Pivovarova, R.D. Leapman, R.A. Buchanan, T.S. Reese & S.B. Andrews. *Activity-dependent calcium sequestration in dendrites of hippocampal neurons in brain slices*. The Journal of neuroscience, vol. 17, no. 22, page 8729, 1997.
- [Quintana 99] J. Quintana & J.M. Fuster. *From perception to action: temporal integrative functions of prefrontal and parietal neurons*. Cerebral Cortex, vol. 9, no. 3, page 213, 1999.
- [Raz 96] A. Raz, A. Feingold, V. Zelanskaya, E. Vaadia & H. Bergman. *Neuronal synchronization of tonically active neurons in the striatum of normal and parkinsonian primates*. Journal of neurophysiology, vol. 76, no. 3, page 2083, 1996.
- [Rieke 99] F. Rieke. *Spikes: exploring the neural code*. The MIT Press, 1999.
- [Rinzel 85] J. Rinzel. *Excitation dynamics: insights from simplified membrane models*. In Fed. Proc. 44, volume 2944, 1985.
- [Romanides 99] A.J. Romanides, P. Duffy & P.W. Kalivas. *Glutamatergic and dopaminergic afferents to the prefrontal cortex regulate spatial working memory in rats*. Neuroscience, vol. 92, no. 1, pages 97–106, 1999.
- [Ross 05] W. N. Ross, T. Nakamura, S. Watanabe, M. Larkum & N. Lasser-Ross. *Synaptically activated Ca^{2+} release from internal stores in CNS neurons*. Cell Mol Neurobiol, vol. 25, no. 2, pages 283–95, 2005.
- [Rozsa 04] B. Rozsa, T. Zelles, E.S. Vizi & B. Lendvai. *Distance-dependent scaling of calcium transients evoked by backpropagating spikes and synaptic activity in dendrites of hippocampal interneurons*. The Journal of neuroscience, vol. 24, no. 3, page 661, 2004.

- [Rudolph 07] M. Rudolph, M. Pospischil, I. Timofeev & A. Destexhe. *Inhibition determines membrane potential dynamics and controls action potential generation in awake and sleeping cat cortex*. The Journal of neuroscience, vol. 27, no. 20, page 5280, 2007.
- [Sah 02] P. Sah & E.S. Louise Faber. *Channels underlying neuronal calcium-activated potassium currents*. Progress in neurobiology, vol. 66, no. 5, pages 345–353, 2002.
- [Sams-Dodd 96] F. Sams-Dodd. *Phencyclidine-induced stereotyped behaviour and social isolation in rats: A possible animal model of schizophrenia*. Behavioural Pharmacology, 1996.
- [Schwindt 92] P.C. Schwindt, W.J. Spain & W.E. Crill. *Effects of intracellular calcium chelation on voltage-dependent and calcium-dependent currents in cat neocortical neurons*. Neuroscience, vol. 47, no. 3, pages 571–578, 1992.
- [Seamans 01] J.K. Seamans, N. Gorelova, D. Durstewitz & C.R. Yang. *Bidirectional dopamine modulation of GABAergic inhibition in prefrontal cortical pyramidal neurons*. The Journal of Neuroscience, vol. 21, no. 10, page 3628, 2001.
- [Shannon 48] C.E. Shannon. *A mathematical theory of communication*. Bell Systems Tech. J, vol. 27, no. 379, page 623, 1948.
- [Sidiropoulou 09] K. Sidiropoulou, F.M. Lu, M.A. Fowler, R. Xiao, C. Phillips, E.D. Ozkan, M.X. Zhu, F.J. White & D.C. Cooper. *Dopamine modulates an intrinsic mGluR5-mediated depolarization underlying prefrontal persistent activity*. Nature neuroscience, vol. 12, no. 2, page 190, 2009.
- [Silver 03] H. Silver, P. Feldman, W. Bilker & R.C. Gur. *Working memory deficit as a core neuropsychological dysfunction in schizophrenia*. American Journal of Psychiatry, vol. 160, no. 10, page 1809, 2003.
- [Skou 65] J.C. Skou. *Enzymatic basis for active transport of Na^+ and K^+ across cell membrane*. Physiological reviews, vol. 45, page 596, 1965.
- [Sneyd 93] J. Sneyd & A. Atri. *Curvature dependence of a model for calcium wave propagation*. Physica D: Nonlinear Phenomena, vol. 65, no. 4, pages 365–372, 1993.

- [Somers 95] D.C. Somers, S.B. Nelson & M. Sur. *An emergent model of orientation selectivity in cat visual cortical simple cells*. The Journal of neuroscience, vol. 15, no. 8, page 5448, 1995.
- [Spacek 97] J. Spacek & K.M. Harris. *Three-dimensional organization of smooth endoplasmic reticulum in hippocampal CA1 dendrites and dendritic spines of the immature and mature rat*. The Journal of neuroscience, vol. 17, no. 1, page 190, 1997.
- [Spencer 03] K.M. Spencer, P.G. Nestor, M.A. Niznikiewicz, D.F. Salisbury, M.E. Shenton & R.W. McCarley. *Abnormal neural synchrony in schizophrenia*. The Journal of neuroscience, vol. 23, no. 19, page 7407, 2003.
- [Stern 92] M.D. Stern. *Buffering of calcium in the vicinity of a channel pore*. Cell Calcium, vol. 13, no. 3, pages 183–192, 1992.
- [Stevens 98] C.F. Stevens & A.M. Zador. *Input synchrony and the irregular firing of cortical neurons*. Nature Neuroscience, vol. 1, no. 3, pages 210–217, 1998.
- [Storm 88] J.F. Storm. *Temporal integration by a slowly inactivating K^+ current in hippocampal neurons*. Nature, vol. 336, no. 6197, pages 379–381, 1988.
- [Strogatz 94] S.H. Strogatz. *Nonlinear dynamics and chaos: With applications to physics, biology, chemistry, and engineering*. Westview Pr, 1994.
- [Swerdlow 87] N.R. Swerdlow & G.F. Koob. *Dopamine, schizophrenia, mania, and depression: toward a unified hypothesis of cortico-striatopallido-thalamic function*. Behavioral and Brain Sciences, vol. 10, no. 02, pages 197–208, 1987.
- [Takahashi 89] K. Takahashi, M. Wakamori & N. Akaike. *Hippocampal CA1 pyramidal cells of rats have four voltage-dependent calcium conductances*. Neuroscience letters, vol. 104, no. 1-2, pages 229–234, 1989.
- [Tallon-Baudry 98] C. Tallon-Baudry, O. Bertrand, F. Peronnet & J. Pernier. *Induced γ -band activity during the delay of a visual short-term memory task in humans*. The Journal of neuroscience, vol. 18, no. 11, page 4244, 1998.
- [Tanaka 06] S. Tanaka. *Dopaminergic control of working memory and its relevance to schizophrenia: a circuit dynamics perspective*. Neuroscience, vol. 139, no. 1, pages 153–171, 2006.

- [Tiesinga 09] P. Tiesinga & T.J. Sejnowski. *Cortical Enlightenment: Are Attentional Gamma Oscillations Driven by ING or PING?* *Neuron*, vol. 63, no. 6, pages 727–732, 2009.
- [Verduzco-Flores 09] S. Verduzco-Flores, M. Bodner, B. Ermentrout, J.M. Fuster & Y. Zhou. *Working Memory Cells' Behavior May Be Explained by Cross-Regional Networks with Synaptic Facilitation*. *PLoS one*, vol. 4, no. 8, page e6399, 2009.
- [Verin 93] M. Verin, A. Partiot, B. Pillon, C. Malapani, Y. Agid & B. Dubois. *Delayed response tasks and prefrontal lesions in man—evidence for self generated patterns of behaviour with poor environmental modulation*. *Neuropsychologia*, vol. 31, no. 12, pages 1379–1396, 1993.
- [Vijayraghavan 07] S. Vijayraghavan, M. Wang, S.G. Birnbaum, G.V. Williams & A.F.T. Arnsten. *Inverted-U dopamine D1 receptor actions on prefrontal neurons engaged in working memory*. *Nature Neuroscience*, vol. 10, no. 3, pages 376–384, 2007.
- [Wagner 04] J. Wagner, C.P. Fall, F. Hong, C.E. Sims, N.L. Allbritton, R.A. Fontanilla, I.I. Moraru, L.M. Loew & R. Nuccitelli. *A wave of IP₃ production accompanies the fertilization Ca²⁺ wave in the egg of the frog, *Xenopus laevis*: theoretical and experimental support*. *Cell calcium*, vol. 35, no. 5, pages 433–447, 2004.
- [Wang 06] Y. Wang, H. Markram, P.H. Goodman, T.K. Berger, J. Ma & P.S. Goldman-Rakic. *Heterogeneity in the pyramidal network of the medial prefrontal cortex*. *Nature neuroscience*, vol. 9, no. 4, pages 534–542, 2006.
- [Watanabe 97] M. Watanabe, T. Kodama & K. Hikosaka. *Increase of extracellular dopamine in primate prefrontal cortex during a working memory task*. *Journal of Neurophysiology*, vol. 78, no. 5, page 2795, 1997.
- [West 01] A.E. West, W.G. Chen, M.B. Dalva, R.E. Dolmetsch, J.M. Kornhauser, A.J. Shaywitz, M.A. Takasu, X. Tao & M.E. Greenberg. *Calcium regulation of neuronal gene expression*. *Proceedings of the National Academy of Sciences of the United States of America*, vol. 98, no. 20, page 11024, 2001.
- [Wilson 94] F.A. Wilson, S.P. O'Scalaidhe & P.S. Goldman-Rakic. *Functional synergism between putative gamma-aminobutyrate-containing neurons and pyramidal neurons in prefrontal cortex*.

Proceedings of the National Academy of Sciences of the United States of America, vol. 91, no. 9, page 4009, 1994.

- [Wilson 06] C.J. Wilson & J.A. Goldberg. *Origin of the slow afterhyperpolarization and slow rhythmic bursting in striatal cholinergic interneurons*. Journal of neurophysiology, vol. 95, no. 1, page 196, 2006.
- [Winograd 08] M. Winograd, A. Destexhe & M.V. Sanchez-Vives. *Hyperpolarization - activated graded persistent activity in the prefrontal cortex*. Proceedings of the National Academy of Sciences, vol. 105, no. 20, page 7298, 2008.
- [Zahrt 97] J. Zahrt, J.R. Taylor, R.G. Mathew & A.F.T. Arnsten. *Supranormal stimulation of D1 dopamine receptors in the rodent prefrontal cortex impairs spatial working memory performance*. The Journal of neuroscience, vol. 17, no. 21, page 8528, 1997.
- [Zucker 02] R.S. Zucker & W.G. Regehr. *Short-term synaptic plasticity*. Annual review of physiology, vol. 64, no. 1, pages 355–405, 2002.

Appendix A

MODEL EQUATIONS

The previous chapters contained only subsets of the model equations. The full equations for each of the nonspatial models are listed below.

For notational convenience, we define

$$\Gamma(v; \theta, \sigma) = \frac{1}{1 + \exp(-(v - \theta)/\sigma)},$$

a sigmoidal function. This function will be used to control gating variable switching.

A.1 Hodgkin-Huxley Cells

The full set of equations used for the Hodgkin-Huxley model [Hodgkin 52] follows. Parameters are as in Table A.1.

A.1.1 State Variables

Membrane potential, sodium activation, sodium inactivation, and potassium activation are denoted by v , m , h , and n , respectively.

$$C_m \frac{dv}{dt} = -I_{\text{Na}} - I_{\text{K}} - I_{\ell} + I_{\text{app}} \tag{A.1.1}$$

$$\frac{dm}{dt} = \frac{m_{\infty} - m}{\tau_m} = \alpha_m (1 - m) - \beta_m m \tag{A.1.2}$$

$$\frac{dh}{dt} = \frac{h_{\infty} - h}{\tau_h} = \alpha_h (1 - h) - \beta_h h \tag{A.1.3}$$

$$\begin{array}{cccc}
g_{\text{Na}} = 120 & g_{\text{K}} = 36 & g_{\ell} = .3 & C_m = 1 \\
v_{\text{Na}} = 50 & v_{\text{K}} = -77 & v_{\ell} = -54.4 &
\end{array}$$

Table A.1: Parameters for the Hodgkin-Huxley model. Reversal potentials are shifted from the original values.

$$\frac{dn}{dt} = \frac{n_{\infty} - n}{\tau_n} = \alpha_n (1 - n) - \beta_n n \quad (\text{A.1.4})$$

A.1.2 Currents

Sodium, potassium, and leak currents are denoted by I_{Na} , I_{K} , and I_{ℓ} , respectively.

$$I_{\text{Na}} = g_{\text{Na}} m^3 h (v - v_{\text{Na}}) \quad (\text{A.1.5})$$

$$I_{\text{K}} = g_{\text{K}} n^4 (v - v_{\text{K}}) \quad (\text{A.1.6})$$

$$I_{\ell} = g_{\ell} (v - v_{\ell}) \quad (\text{A.1.7})$$

A.1.3 Miscellaneous Equations

$$\alpha_m = \frac{0.1 (v + 25)}{1 - \exp(-(v + 40)/10)} \quad (\text{A.1.8})$$

$$\beta_m = 4 \exp(-(v + 65)/18) \quad (\text{A.1.9})$$

$$\alpha_h = .07 \exp(-(v + 65)/20) \quad (\text{A.1.10})$$

$$\beta_h = \Gamma(v; -35, 10) \quad (\text{A.1.11})$$

$$\alpha_n = \frac{.01 (v + 55)}{1 - \exp(-(v + 55)/10)} \quad (\text{A.1.12})$$

$$\beta_n = .125 \exp(-(v + 65)/80) \quad (\text{A.1.13})$$

$g_{\text{Na}} = 60$	$g_{\text{K}} = 5$	$g_{\ell} = .18$	$C_m = 1$	$I_{\text{app}} = -2.8$
$v_{\text{Na}} = 50$	$v_{\text{K}} = -77$	$v_{\ell} = -54.4$	$\theta_m = -37$	$\sigma_m = 10$
$\theta_n = -50$	$\sigma_n = .1$	$\tau_{n,0} = 1.5$	$\tau_{n,1} = 1.35$	$\theta_{\tau,n} = -40$
$\sigma_{\tau,n} = -12$				

Table A.2: Parameters for the simplified model, unless otherwise indicated.

A.2 Simplified Model

The full set of equations used for the simplified model, introduced in Section 2.2.4 follows. Parameters are as in Table A.2. This is a modification of the Hodgkin-Huxley model where the equations for m and h have been replaced with algebraic functions as in [Rinzel 85] and the limiting proportions and time functions for the remaining gating variable are defined in terms of Γ , as in [Borg-Graham 91, Borg-Graham 87].

A.2.1 State Variables

The membrane potential and potassium activation are represented by v and n , respectively.

$$C_m \frac{dv}{dt} = -(I_{\text{Na}} + I_{\text{K}} + I_{\ell}) + I_{\text{app}} \quad (\text{A.2.1})$$

$$\frac{dn}{dt} = \frac{n_{\infty} - n}{\tau_n} \quad (\text{A.2.2})$$

$$(\text{A.2.3})$$

A.2.2 Currents

Sodium, potassium, and leak currents are denoted by I_{Na} , I_{K} , and I_{ℓ} , respectively.

$$I_{\text{Na}} = g_{\text{Na}} m_{\infty}^3 (1 - n)(v - v_{\text{Na}}) \quad (\text{A.2.4})$$

$$I_K = g_K n^4 (v - v_K) \quad (\text{A.2.5})$$

$$I_\ell = g_\ell (v - v_\ell) \quad (\text{A.2.6})$$

A.2.3 Miscellaneous Equations

$$m_\infty = \Gamma(m; \theta_m, \sigma_m) \quad (\text{A.2.7})$$

$$n_\infty = \Gamma(n; \theta_n, \sigma_n) \quad (\text{A.2.8})$$

$$\tau_n = \tau_{n,0} + \tau_{n,1} \Gamma(v; \theta_{\tau,n}, \sigma_{\tau,n}) \quad (\text{A.2.9})$$

$$(\text{A.2.10})$$

A.3 Excitatory Cells

The full set of equations used for the excitatory cells, introduced in Section 3.2 follows.

Parameters are as in Table A.3.

A.3.1 State Variables

The membrane potential, potassium activation, cytosolic calcium concentration, sag (or h) current activation probability, and synaptic output are denoted by v , n , c , m_h , and s , respectively.

$$C_m \frac{dv}{dt} = -(I_{Na} + I_K + I_{Ca} + I_h + I_\ell + I_{syn} + I_{noise}) + I_{app} \quad (\text{A.3.1})$$

$$\frac{dn}{dt} = \frac{n_\infty - n}{\tau_n} \quad (\text{A.3.2})$$

$$\frac{dc}{dt} = \varepsilon (-I_{Ca} - k_{Ca} c) + c_{internal} + c_{NMDA} \quad (\text{A.3.3})$$

$$\frac{dm_h}{dt} = \frac{m_{h,\infty} - m_h}{\tau_h} \quad (\text{A.3.4})$$

$$\frac{ds}{dt} = \alpha (1 - s) s_\infty - \beta s \quad (\text{A.3.5})$$

$g_{\text{Na}} = 60$	$g_{\text{K}} = 5$	$g_{\ell} = .18$	$C_m = 1$	$I_{\text{app}} = -2.8$
$v_{\text{Na}} = 55$	$v_{\text{K}} = -80$	$v_{\ell} = -60$	$\theta_m = -37$	$\sigma_m = 10$
$\theta_n = -50$	$\sigma_n = .1$	$\tau_{n,0} = 1.5$	$\tau_{n,1} = 1.35$	$\theta_{\tau,n} = -40$
$\sigma_{\tau,n} = -12$	$g_{\text{Ca}} = .25$	$v_{\text{Ca}} = 120$	$\varepsilon = .001$	$k_{\text{Ca}} = 2$
$\theta_y = -35$	$\sigma_y = 2$	$k_h = .2$	$v_h = 0$	$g_h = 16.42$
$\tau_{h,0} = 5$	$\tau_{h,1} = 20$	$\sigma_h = -.1$	$\theta_{h,\text{min}} = -120$	$\theta_{h,\text{max}} = -84.5$
$\theta_s = -10$	$\sigma_s = 2$	$\alpha = 15$	$\beta = .5$	$g_{\text{syn}} = .2$
$g_{\text{noise}} = .005$	$v_{\text{noise}} = 0$	$v_{\text{syn}} = -110$		

Table A.3: Standard parameters for the excitatory cell model.

A.3.2 Currents

Sodium, potassium, calcium, sag, and leak currents are denoted by I_{Na} , I_{K} , I_{Ca} , I_h , and I_{ℓ} , respectively.

$$I_{\text{Na}} = g_{\text{Na}} m_{\infty}^3 (1 - n)(v - v_{\text{Na}}) \quad (\text{A.3.6})$$

$$I_{\text{K}} = g_{\text{K}} n^4 (v - v_{\text{K}}) \quad (\text{A.3.7})$$

$$I_{\text{Ca}} = g_{\text{Ca}} y_{\infty}^2 (v - v_{\text{Ca}}) \quad (\text{A.3.8})$$

$$I_h = g_h m_h (v - v_h) \quad (\text{A.3.9})$$

$$I_{\ell} = g_{\ell} (v - v_{\ell}) \quad (\text{A.3.10})$$

A.3.3 Miscellaneous Equations

$$m_{\infty} = \Gamma(m; \theta_m, \sigma_m) \quad (\text{A.3.11})$$

$$n_{\infty} = \Gamma(n; \theta_n, \sigma_n) \quad (\text{A.3.12})$$

$$\tau_n = \tau_{n,0} + \tau_{n,1} \Gamma(v; \theta_{\tau,n}, \sigma_{\tau,n}) \quad (\text{A.3.13})$$

$$m_{h,\infty} = \Gamma(v; \theta_h, \sigma_h) \quad (\text{A.3.14})$$

$$\tau_h = \tau_{h,0} + \frac{\tau_{h,1}}{\exp((v + 54.5)/14.2) + \exp(-(v + 72)/10)} \quad (\text{A.3.15})$$

$$\theta_h = \theta_{h,\min} + (\theta_{h,\max} - \theta_{h,\min}) \frac{c^2}{k_h^2 + c^2} \quad (\text{A.3.16})$$

$$y_\infty = \Gamma(v, \theta_y, \sigma_y) \quad (\text{A.3.17})$$

$$s_\infty = \Gamma(v; \theta_s, \sigma_s) \quad (\text{A.3.18})$$

A.4 Inhibitory Cells

The full equations for the inhibitory cells, as introduced in Section 3.3 follows. Parameters are as in Table A.4.

A.4.1 State Variables

The membrane potential, sodium activation, A current activation, A current inactivation, calcium concentration, and synaptic output variables are denoted v , n , a , b , c , and s , respectively.

$$C_m \frac{dv}{dt} = -(I_{Na} + I_K + I_{Ca} + I_{AHP} + I_A + I_\ell + I_{syn}) + I_{app} \quad (\text{A.4.1})$$

$$\frac{dn}{dt} = \frac{n_\infty - n}{\tau_n} \quad (\text{A.4.2})$$

$$\frac{da}{dt} = \frac{a_\infty - a}{\tau_a} \quad (\text{A.4.3})$$

$$\frac{db}{dt} = \frac{b_\infty - b}{\tau_b} \quad (\text{A.4.4})$$

$$\frac{dc}{dt} = \varepsilon (-I_{Ca} - k_{Ca} c) \quad (\text{A.4.5})$$

$$\frac{ds}{dt} = \alpha (1 - s) s_\infty - \beta s \quad (\text{A.4.6})$$

A.4.2 Currents

Sodium, potassium, calcium, A, AHP, and leak currents are denoted I_{Na} , I_{K} , I_{Ca} , I_{A} , I_{AHP} , and I_{ℓ} , respectively.

$$I_{\text{Na}} = g_{\text{Na}} m_{\infty}^3 (1 - n)(v - v_{\text{Na}}) \quad (\text{A.4.7})$$

$$I_{\text{K}} = g_{\text{K}} n^4 (v - v_{\text{K}}) \quad (\text{A.4.8})$$

$$I_{\text{Ca}} = g_{\text{Ca}} y_{\infty}^2 (v - v_{\text{Ca}}) \quad (\text{A.4.9})$$

$$I_{\text{A}} = g_{\text{A}} a^3 b (v - v_{\text{K}}) \quad (\text{A.4.10})$$

$$I_{\text{AHP}} = g_{\text{AHP}} \left(\frac{c^2}{c^2 + k_1^2} \right)^2 (v - v_{\text{K}}) \quad (\text{A.4.11})$$

$$I_{\ell} = g_{\ell} (v - v_{\ell}) \quad (\text{A.4.12})$$

A.4.3 Miscellaneous Equations

$$m_{\infty} = \Gamma(m; \theta_m, \sigma_m) \quad (\text{A.4.13})$$

$$n_{\infty} = \Gamma(n; \theta_n, \sigma_n) \quad (\text{A.4.14})$$

$$\tau_n = \tau_{n,0} + \tau_{n,1} \Gamma(v; \theta_{\tau,n}, \sigma_{\tau,n}) \quad (\text{A.4.15})$$

$$y_{\infty} = \Gamma(y; \theta_y, \sigma_y) \quad (\text{A.4.16})$$

$$a_{\infty} = \Gamma(a; \theta_a, \sigma_a) \quad (\text{A.4.17})$$

$$b_{\infty} = \Gamma(b; \theta_b, \sigma_b) \quad (\text{A.4.18})$$

$$s_{\infty} = \Gamma(s; \theta_s, \sigma_s) \quad (\text{A.4.19})$$

A.5 Calcium Waves

The full equations for the calcium wave model are from [Wagner 04], a spatial variant of [Li 94]. Parameters are as in Table A.5.

$g_{\text{Na}} = 60$	$g_{\text{K}} = 5$	$g_{\ell} = .18$	$C_m = 1$
$\sigma_m = 10$	$v_{\text{Na}} = 55$	$v_{\text{K}} = -80$	$v_{\ell} = -60$
$\theta_m = -37$	$v_{\text{syn,g}} = 60$	$\theta_n = -50$	$\sigma_n = .1$
$\tau_{n,0} = 1.5$	$\tau_{n,1} = 1.35$	$\theta_{\tau,n} = -40$	$\sigma_{\tau,n} = -12$
$g_{\text{Ca}} = .25$	$v_{\text{Ca}} = 120$	$k_{\text{Ca}} = 1.23$	$\sigma_s = 2$
$\theta_y = -35$	$\sigma_y = 2$	$g_{\text{A}} = .198$	$\theta_a = -50$
$\sigma_a = 20$	$\theta_b = -70$	$\sigma_b = -6$	$\tau_a = 2$
$\tau_b = 150$	$g_{\text{AHP}} = .9$	$k_1 = .208$	$\theta_s = 10$
$v_{\text{syn,gg}} = -100$	$\alpha = 68$	$\beta = .2$	$\varepsilon = .001$
$g_{\text{syn,g}} = .10 \pm .01$	$I_{\text{app}} = -2.8 \pm .28$	$g_{\text{syn,gg}} = .750 \pm .075$	

Table A.4: Standard parameters for the inhibitory cell model. $a \pm b$ means the value is chosen on a per-cell basis from a normal distribution with mean a and standard deviation b .

$v_{ip3r} = 20$	$k_{ip3} = .15$	$k_{act} = .4$	$v_{leak} = .01$	$v_{serca} = .65$
$k_{serca} = .1$	$k_{inh} = 1.9$	$\tau = 20$	$d_c = 1$	$d_e = 1$
$d_i = 16$	$f_c = .83$	$f_e = .17$		

Table A.5: Parameters for the calcium model, unless otherwise indicated.

A.5.1 State Variables

Cytosolic calcium concentration, ER calcium concentration, InsP₃ concentration, and InsP₃ receptor gating are denoted by C_c , C_e , I , and h , respectively.

$$\frac{\partial C_c}{\partial t} = d_c \Delta C_c + \frac{J_{IP3} - J_{SERCA} + J_{leak}}{f_c} + c_{ionic} \quad (\text{A.5.1})$$

$$\frac{\partial C_e}{\partial t} = d_e \Delta C_e - \frac{J_{IP3} - J_{SERCA} + J_{leak}}{f_e} \quad (\text{A.5.2})$$

$$\frac{\partial I}{\partial t} = d_i \Delta I \quad (\text{A.5.3})$$

$$\frac{\partial h}{\partial t} = \frac{h_\infty - h}{\tau}. \quad (\text{A.5.4})$$

A.5.2 Fluxes

Flux from the InsP₃ receptor, SERCA pump, and leak channels are denoted by J_{IP3} , J_{SERCA} , and J_{leak} , respectively.

$$J_{leak} = v_{leak} (C_e - C_c) \quad (\text{A.5.5})$$

$$J_{SERCA} = -\frac{v_{serca} C_c^2}{k_{serca}^2 + C_c^2} \quad (\text{A.5.6})$$

$$J_{IP3} = v_{ip3r} m^3 n^3 h^3 (C_e - C_c) \quad (\text{A.5.7})$$

A.5.3 Miscellaneous Equations

$$m = \frac{I}{I + k_{ip3}} \quad (\text{A.5.8})$$

$$n = \frac{C_c}{C_c + k_{act}} \quad (\text{A.5.9})$$

$$h_\infty = \frac{k_{inh}}{k_{inh} + C_c} \quad (\text{A.5.10})$$

$$\tau_{\text{delay}} = 3.5 \quad \tau_{\text{decay}} = 2 \quad g_{\text{noise}} = .01 \quad v_{\text{noise}} = 0$$

Table A.6: Parameters for noise, except where otherwise noted.

A.6 Noise

Each noise source fires according to a Poisson process. If t_i and t_{i+1} are consecutive spike times, then the synaptic output of a noise source in between those two times is governed by

$$s(t) = \begin{cases} 1 & \text{if } t_i \leq t < t_i + \tau_{\text{delay}} \\ \exp((t_i + \tau_{\text{delay}} - t)/\tau_{\text{decay}}) & \text{if } t_i + \tau_{\text{delay}} \leq t < t_{i+1} \end{cases} \quad (\text{A.6.1})$$

where the parameters are as in Table A.6, except where otherwise noted.

Appendix B

PARAMETER SELECTION

Selecting reasonable parameter values is a hard problem for three main reasons: first, many of the parameters have not been experimentally measured. Second, and even more fundamentally, modeling inherently involves simplifications. In particular, this model neglects neuron geometry (see Section 6.2 and the work by [Loewenstein 03]) and the effects of other ion channels. Measured parameter values in the full system need not necessarily correspond to the best fitting values for the model. Finally, the system contains a large number of parameters, most of which combine in a very nonlinear way. That is, if a change is made to one parameter to alter a particular behavior, then other behaviors are likely to be altered as well, requiring further changes in additional parameters.

My strategy: use typical values when known, locate reasonable parameter regime for model-specific parameters by a manual exploration, then do a Monte-Carlo search.

B.1 Excitatory Cells

As in Section 3.4, I assume that each excitatory cell receives excitatory input with strength g_{noise} and reversal potential 0 mV from 50 external sources firing at 5 Hz. I further assume that each excitatory cell is connected with some probability to some of a group of 30 inhibitory cells with strength g_{syn} and reversal potential -110 mV.

Inhibitory synapses are via GABA_A, which has a time constant τ_{decay} of about 5 ms [Ermentrout 10].

The inhibitory cells are supposed to be in one of two states: baseline or persistent. In the combined model, the activity of inhibitory cells is driven directly by the activity of the excitatory cells, but for now I consider specific fixed firing rates. During the baseline state, inhibitory cells fire according to a Poisson process at 5 Hz. During the persistent state, they fire at 15 Hz. With each spike, they maintain the maximum neurotransmitter output for 3.5 ms before decaying exponentially with a time constant of 5 ms. These times were chosen to be approximately consistent with the dynamics of the inhibitory cell model.

One hundred thousand parameter sets were chosen uniformly at random with $g_{\text{noise}} \in [.005, .03]$, $g_{\text{syn}} \in [.3, 1]$, $P(\text{IN} \rightarrow \text{E}) \in [.2, .6]$, $k_{\text{Ca}} \in [0, 10]$, $I_{\text{cue}} \in [2, 4]$, $k_{\text{h}} \in [0, .2]$, $g_{\text{h}} \in [10, 40]$, and $\theta_{\text{h,max}} \in [-85, -78]$. Here $P(\text{IN} \rightarrow \text{E})$ denotes the probability a given inhibitory cell is connected to a given excitatory cell.

Each parameter set was tested as follows:

- A single cell was integrated under baseline conditions for 250, 750, and 2000 ms. At each of the first two time points, the parameters would be rejected and no further tests run if the firing rate exceeded 10 Hz. At the final time point, it would be rejected if the rate was bigger than 5 Hz or less than 1 Hz.
- A new simulation with a single cell was run for 300 ms at baseline conditions with an additional applied current of I_{cue} . This simulates presentation of a pattern to be retained by working memory. The additional applied current was removed and the simulation integrated for an additional 2000 ms under the persistent case for inhibitory input. If the firing rate after the removal of I_{cue} was more than 30 Hz or less than 10 Hz, the parameter set was rejected.

- A new simulation with 100 excitatory cells, each connected to 50 external cells out of a pool of 300 and some subset of a pool of 30 inhibitory cells, run under baseline conditions for 500 and 2000 ms. At each time point, the parameter set would be rejected if any neuron was firing at more than 10 Hz. At the final time point, the parameter set would be rejected if the average firing rate was less than 1 Hz or more than 5 Hz.

The first and third tests check baseline behavior; the second test checks the ability of a cell to maintain persistent behavior. Simulating single cells and checking performance at multiple time points provides a quick way to discard unsatisfactory parameter sets.

Out of 100,000 parameter sets, only 14 passed all three tests. A low success rate is to be expected when exploring an 8 dimensional parameter space.

For each of the 14 candidate parameter sets, I considered the results of the large baseline test (test 3), a persistence test (like the second test above but with 100 excitatory cells), and a distractor test (same as the persistence test, except the inhibitory cells were firing at the persistent rate when I_{cue} was applied). Example results are shown in Figure B.1.

B.2 Inhibitory Cells

As with the excitatory cells, parameters relating to response rate for inhibitory cells were tuned via a Monte Carlo search after an initial manual exploration. This search is different, however, because in the basic model, excitatory cells do not interact. By contrast, in all the models, I assume that inhibitory cells do interact. In Section 5.6, I show that inhibitory-inhibitory interactions play a crucial role in maintaining irregular activity.

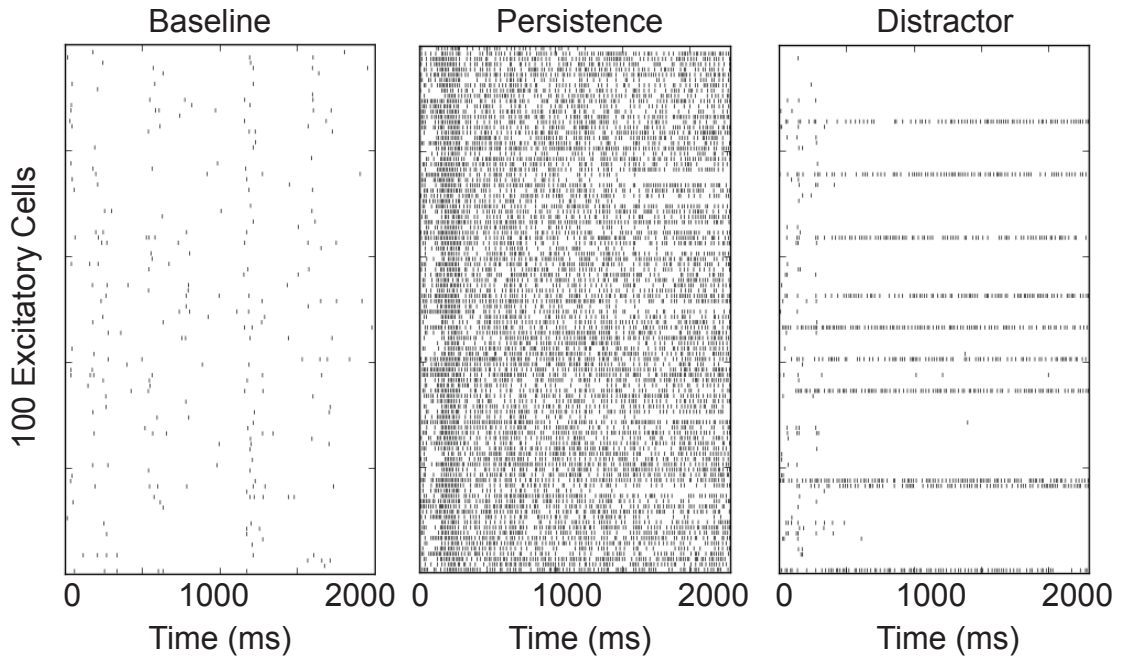


Figure B.1: Example excitatory cell parameter search results, showing baseline, persistence, and distractor. Each mark represents an action potential. Here $k_h = 0.1616$, $k_{Ca} = 3.8487$, $g_{syn} = 0.4161$, $g_{noise} = 0.01305$, $I_{cue} = 2.481$, $\theta_{h,max} = -81.99$, $P(IN \rightarrow E) = 0.3613$, and $g_h = 23.83$.

Thus instead of considering an individual inhibitory neuron, I work with a pool of 30 inhibitory neurons. Any two of these neurons are connected with probability $P(\text{IN} \rightarrow \text{IN})$ with conductance $g_{\text{syn,gg}}$ and reversal potential -100 mV. The inhibitory neurons receive excitatory input from a pool of excitatory neurons, with connection probability $P(\text{E} \rightarrow \text{IN})$, conductance $g_{\text{syn,g}}$ and reversal potential 60 mV.

Once again, I suppose that the network is in one of two states: baseline and persistent. During the baseline state, I suppose that the excitatory pool consists of 60 neurons firing according to a Poisson process at 3 Hz. During the persistent state, the excitatory pool consists of 30 neurons firing at 25 Hz.

One hundred thousand parameter sets were chosen uniformly at random from $g_{\text{syn,g}} \in [0, 0.1]$, $P(\text{E} \rightarrow \text{IN}) \in [.2, .6]$, $P(\text{IN} \rightarrow \text{IN}) \in [.2, .6]$, $g_{\text{syn,gg}} \in [0, 1]$, $g_{\text{AHP}} \in [0, 2]$, and $k_1 \in [0, 1]$. To partially account for the effects of random networks, parameter sets were required to pass each of the following two performance tests for three different networks. A single failure would cause the parameter set to be discarded.

- Baseline conditions were simulated for 1000 ms. A parameter set was considered successful if and only if the mean firing rate for inhibitory cells was between 4 and 6 Hz, inclusive, and no single cell fired at more than 15 Hz.
- Persistent conditions were simulated for 1000 ms. To be successful, the mean firing rate must lie between 13 and 17 Hz, inclusive, every cell must fire at least once, and no single cell may fire at more than 25 Hz.

Representative results for baseline and persistent conditions are shown in Figure B.2.

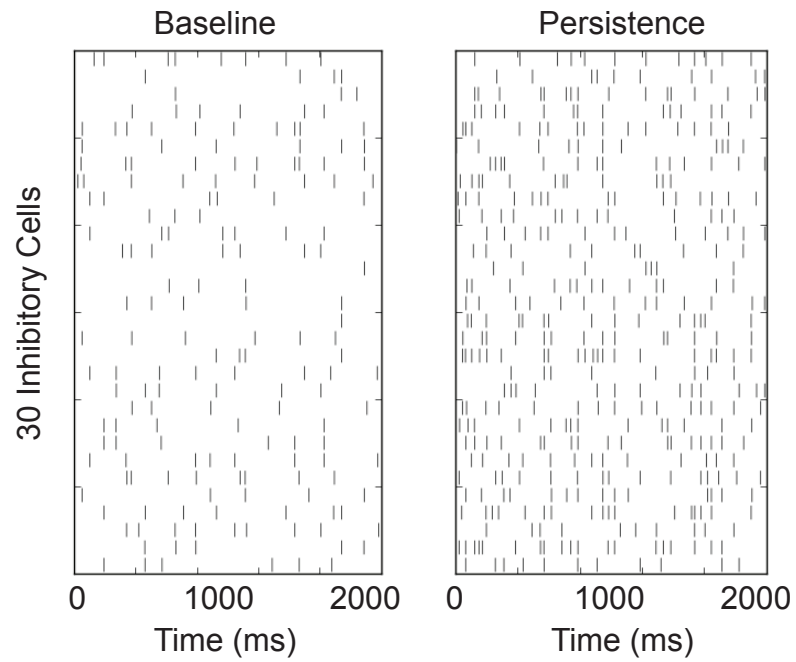


Figure B.2: Example inhibitory cell parameter search results, showing baseline and persistence. Here $g_{\text{AHP}} = 0.6278$, $P(\text{E} \rightarrow \text{IN}) = 0.5903$, $g_{\text{syn,g}} = 0.02790$, $P(\text{IN} \rightarrow \text{IN}) = 0.5436$, $k_1 = 0.2784$, and $g_{\text{syn,gg}} = 0.06425$.

Appendix C

ON INTERPRETING NEURON MORPHOLOGY

NeuroLucida, NEURON, and many other simulators treat neuron morphology as consisting of a collection of frustums. The difficulty with taking the frustum definition literally is that the frustums will intersect and/or leave gaps at branch points, see Figure C.1. Electrophysiology models treat dendrites as essentially one-dimensional, so they are not affected by these limitations. As observed in Section 6.2, wave propagation depends on the exact nature of the branch geometry, so these approximations are insufficient.

One strategy for defining a continuous membrane from a series of frustums is to cap the frustums with spheres lying tangent to their ends. A cross-section is shown

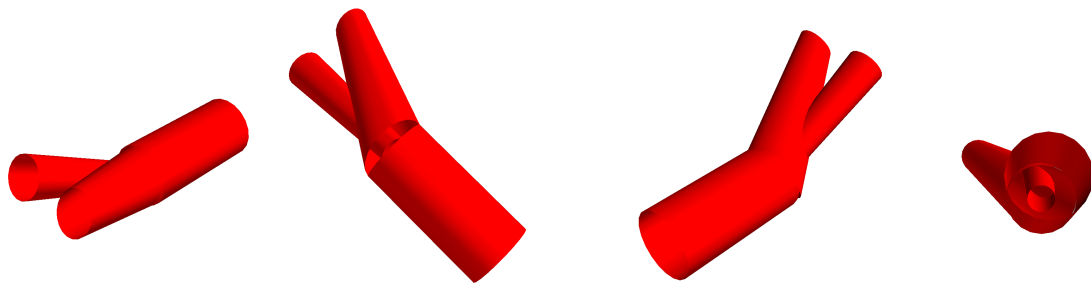


Figure C.1: Frustum description of dendrite geometry creates gaps and overlaps. Four different views of the same branch are shown.

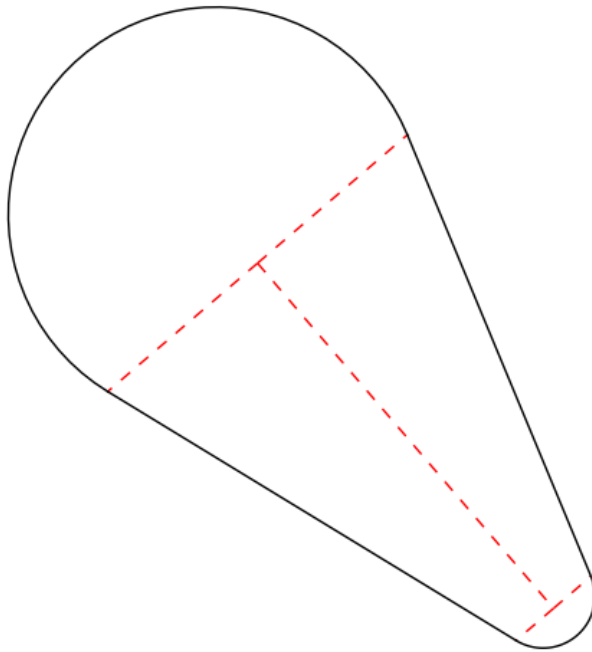


Figure C.2: Cross-section of a capped frustum, showing axis and original frustum edges.

in Figure C.2, while an example is shown in Figure C.3. This rule was used to render Figure 2.1.

The two-dimensional version may be calculated by locating the intersection of the perpendiculars to each edge, then drawing a circle with that center and radius the distance to the edges. The three-dimensional version is the solid of revolution of the two-dimensional version.

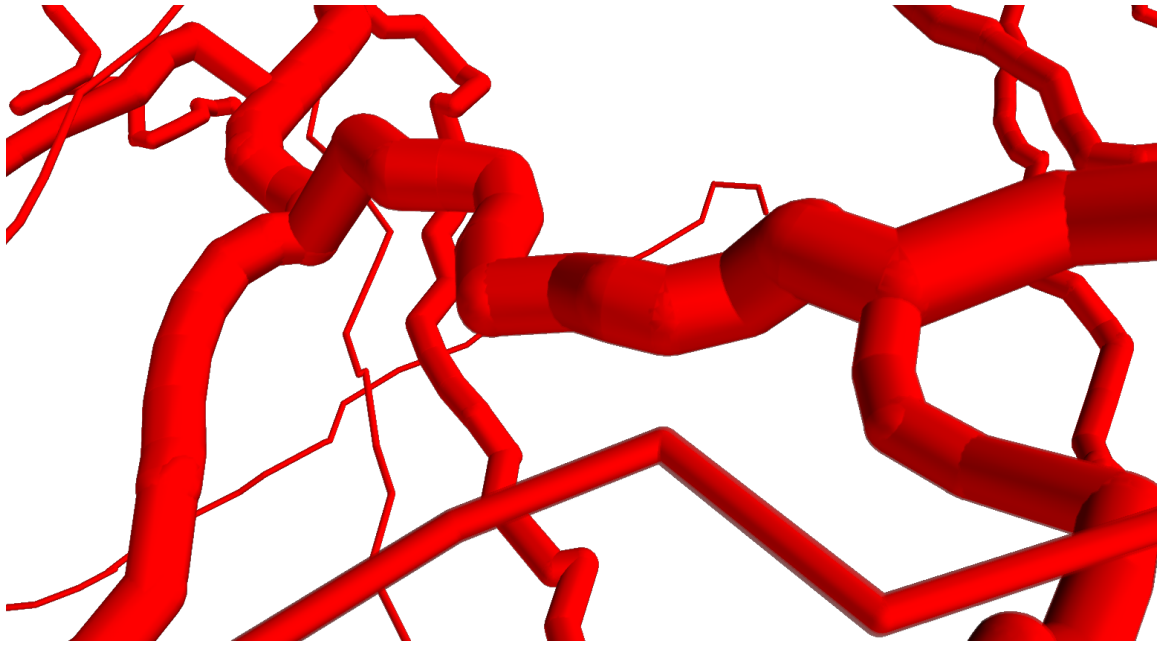


Figure C.3: Portion of a neuron rendered using capped frustums.

Appendix D

DERIVATION OF THE REACTION-DIFFUSION EQUATION

Consider a substance or substances on some domain \mathcal{D} , distributed with concentration $u(t, x)$ at time t and position x , where x is a vector in the domain. Suppose further that local reactions cause this concentration to increase at a rate $f(u, t, x)$, and that the substance diffuses at a constant rate D . Then assuming these are the only factors influencing the chemical distribution and assuming one additional hypothesis explained below, the concentration u is governed by the partial differential equation

$$\frac{\partial u}{\partial t} = D \Delta u + f(u, t, x). \tag{D.0.1}$$

This is a standard result, derived in any text on reaction-diffusion equations. The derivation that follows is based on [Britton 86].

The derivation requires the divergence theorem, which states that under certain assumptions the integral of the flux across the boundary ∂R of a region R is equal to the divergence of the flux over the entire region. That is,

$$\int_{\partial R} F \cdot dS = \int_R \nabla \cdot F \, dV. \tag{D.0.2}$$

The derivation also requires Fick's First Law, which is an empirical physics observation that for many substances, diffusive flux moves them from regions of high

concentration to regions of low conservation with the flux having magnitude proportional to the gradient. That is

$$J_{\text{diff}} = -D \nabla u. \quad (\text{D.0.3})$$

Exceptions to Fick's First Law are rare, and include diffusion across polymer films [Edwards 96].

Let $V \subset \mathcal{D}$ be an arbitrary region of the domain with boundary ∂V . The total amount of chemical m in this region at time t is the integral of the concentration; that is, $m(t) = \int_V u(t, x) dV$. The mass m changes over time due to the production (or loss) $f(u, t, x)$ within the volume and the diffusive flux $J(u, t, x)$ through the boundary ∂V . Thus,

$$\frac{d}{dt} \left[\int_V u(t, x) dV \right] = \int_V f(u, t, x) dV - \int_{\partial V} J(u, t, x) \cdot dS, \quad (\text{D.0.4})$$

where the sign convention is such that flux out of the region is denoted as positive.

Using the divergence theorem, equation (D.0.2), and assuming that all of the functions involved are sufficiently smooth, (D.0.4) becomes

$$\int_V [u_t(t, x) - f(u, t, x) + \nabla \cdot J(u, t, x)] dV = 0. \quad (\text{D.0.5})$$

Since V was arbitrary, it follows that

$$u_t(t, x) - f(u, t, x) + \nabla \cdot J(u, t, x) = 0, \quad (\text{D.0.6})$$

as 0 is the only function whose integral over every domain is 0. By Fick's First Law, it follows that

$$u_t(t, x) = \nabla \cdot (D \nabla u) + f(u, t, x). \quad (\text{D.0.7})$$

If D is constant, then the above becomes $u_t(t, x) = D \nabla^2 u + f(u, t, x)$, which is the same as equation (D.0.1) since $\nabla^2 = \Delta$, the Laplacian.